The measurement of the laminar flame speed of Dutch natural gas

Ali al Amery

Delft University of Technology

The measurement of the laminar flame speed of Dutch natural gas

An investigation on the burning characteristics of Dutch natural gas

By

Ali al Amery

in partial fulfilment of the requirements for the degree of

Master of Science
in Applied Physics

at the Delft University of Technology,
to be defended publicly on June 1st 2018

Supervisor:	Dr. Alexis Bohlin
	Dr. Johan Steimes
Thesis committee:	Dr. Arvind Gangoli Rao
	Dr. Andrea Sciacchitano

This thesis is confidential and cannot be made public until

TU Delft Delft University of Technology

Preface

I would like to first and foremost thank my super visor Dr. Alexis Bohlin for his continues support and invaluable guidance during the course of the research. I would also like to thank Dr. Johan Steimes for his help in designing a suitable experimental setup for this research. I would like to also thank Bart Hoek for his help in getting the right materials to design the Bunsen burner and for his help in the assembly of the experimental setup. I would like to further thank my parents for their moral support especially my father who inspired me to pursue a master's degree. Lastly I would like to thank my fellow students Vartan Margos and Shiva Hanuman for reading my thesis report and giving me their take on it.

Abstract

The characteristics of Dutch natural gas (DNG) have been quantified by measuring the laminar flame speed of a premixed Bunsen flame over a range of equivalence ratios ϕ, varied from φ=0.80 to φ=1.55. The laminar flame speed has been calculated from the OH* chemiluminescence images recorded with a high speed camera with an acquisition rate of 1 kHz. Both the semi-cone angle method and mass conservation method were used in deriving the magnitude of the laminar burning velocity. From the data it was shown that the laminar flame speed of DNG is consistently lower compared to natural gas from Pittsburgh, Abu Dhabi and Indonesia. Moreover the data has been compared using the laminar flame speed of methane mixtures to validate the experimental setup. This showed that the laminar flame speed of DNG was marginally lower than the laminar flame speed of methane. The uncertainty within the measurements has been quantified by deriving the probability density function of the data. Additional analysis has been performed on the variation of the laminar flame speed in the frequency domain. This analysis showed that a fundamental frequency was present in the data which was detectable due to the camera's high acquisition rate.

List of terms

Terms	Description
AFCU	Air flow control unit
AFM	Air flow measurement
D	Burner exit diameter
DFT	Discrete Fourier Transform
DNG	Dutch Natural Gas
f	Reaction rate
FFCU	Fuel Flow Control Unit
FFT	Fast Fourier Transform
FPS	Frames per second
FS	Full Scale or maximum of the device in ln/min.
ICCD	Intensified Charge Coupled Device
IQR	Inter Quartile Range
LDV	Laser Doppler Velocimetry
N	Sample size
n	Number of bins
PDF	Probability Density Function
PIV	Particle Image Velocimetry
Q	Heat in J
RD	Value displayed by the flow rate measurement device or Reading
RE	Relative Error
SE	Standard Error
T	Temperature in Kelvin (K)
W	Bin width

List of symbols

Symbol	Description
$\dot{V}_{air}$	Volumetric flow rate of air in m^3/s
$\dot{V}_{DNG}$	Volumetric flow rate of Dutch Natural gas in m^3/s
R_e	Reynolds number/ Reynolds number corresponding with the hydraulic diameter
$\dot{V}_{tot}$	Total Volumetric flow rate in l_n/min
$\bar{\nu}$	Average dynamic viscosity of the mixture in m^2/s
D_h	Hydraulic diameter in *mm*
l_e	Effective length in *mm*
U_{n_0}	Normal component of the unburned mixture w.r.t. the flame front in m/s
S_L^{sca}	Laminar flame speed using semi-cone angle in *cm/s*
S_L^{mc}	Laminar flame speed using mass conservation method in *cm/s*
S_L	Laminar flame speed in *cm/s*
U_0	Average exit velocity in *cm/s*
α	Semi-cone angle
A_e	Burner exit area
ρ_u	Density of the unburned mixture
M_a	Markstein number
ϕ	Equivalence ratio
FAR_{stoich}	Stoichiometric fuel to air ratio
FAR_{act}	Actual fuel to air ratio
V_{air}	Volume of air in litres
V_{DNG}	Volume of Dutch natural gas in litres
L_e	Lewis number
α	Thermal diffusivity
D	Mass diffusivity
λ	Thermal conductivity of gas in W/m.k
K_{a_L}	Local Karlovitz number
K_a	Karlovitz number
κ	Curvature in cm^{-1}
$\overline{u(r)}$	Average of the velocity distribution at the burner exit in *m/s*
ΔS_L^{sca}	Error in the laminar flame speed measurement using the semi-cone angle method
ΔS_L^{mc}	Error in the laminar flame speed using the mass conservation method
ΔS_L^{mc-sca}	Difference between the laminar flame speed from the mass conservation method and the semi-cone angle method
$\Delta\phi$	Error in the equivalence ratio
$\Delta S_{L_{SEM}}^{sca}$	Standard error of the mean at 95% confidence of the laminar flame speed estimated using the semi-cone angle method
$\Delta S_{L_{SEM}}^{mc}$	Standard error of the mean at 95% confidence of the laminar flame speed estimated using the mass conservation method
ρ_b	Burned gas density in kg/m^3
n_{fuel}	Moles fuel
n_{air}	Moles air

List of Figures

List of Tables

Summary

The quest for alternative fuels in aerospace has been the central topic in many modern aircraft and gas turbine designs. Natural gas is considered an alternative fuel that has been investigated for modern aircraft propulsion. Natural gas is currently employed in residential use, power generation and other industrial applications. There is a wide variety in natural gas composition. This variation in composition varies per region. Therefore additional experimental results are required to extend on the available data on the burning characteristics of natural gas. In here the emphasis is placed on determining the laminar flame speed of Dutch Natural Gas (DNG).

The characteristics of DNG have been quantified by means of measuring the laminar flame speed of a premixed Bunsen burner flame, over a range of equivalence ratio. The equivalence ratio has been varied from $\phi = 0.8$ to $\phi = 1.55$. The laminar flame speed has been calculated from the recorded OH chemiluminescence emission of the flame, using a high speed camera with an acquisition rate of 1 kHz. The fluctuation of the flow has been monitored and registered at 15Hz. Both the semi-cone angle and mass conservation method were used in deriving the magnitude of the laminar burning velocity.

From the results it was observed that the lean blow off region for DNG was at an equivalence ratio($\phi < 0.8$). This is the stability limit of the used Bunsen burner in this experiment for lean conditions. Moreover the laminar flames speed of DNG at lean conditions showed to be overall slightly higher than gas from Abu Dhabi, Pittsburgh and Indonesia. It was observed that the laminar flame speed of DNG is consistently lower compared to gas from Pittsburgh, Abu Dhabi, Indonesia at stoichiometric and rich mixtures. This has been thought to be caused by the high content of inert gas such as CO_2 and N_2 which is shown to be at 15% of the total volume. Comparison to the laminar flame speed of methane showed that the semi-cone angle consistently underestimated the laminar flame speed of DNG. The results of the mass conservation method showed comparable results to the laminar flame speed of methane in which the laminar flame speed of DNG was shown to be slightly lower than methane.

The semi-cone angle method was found to be more appropriate for a finely machined nozzle burner. For a Bunsen burner flame obtained from a straight tube burner, the velocity profile at the burner exit is not uniform and has to be corrected. This correction has been employed using the well-known velocity distribution of a Poiseuille flow. However, the semi-cone angle method after correction, underestimates the laminar flame speed by a maximum of 13.95% compared to the laminar flame speed obtained from the mass conservation method.

The uncertainty within the measurements has been quantified by obtaining the probability density function of the data which was shown to follow a Gaussian distribution. Additional analysis has been performed in the frequency domain. This analysis showed that a fundamental frequency was present in the measured laminar flame speed, which was detectable due to the high acquisition rate of the camera used in this experiment.

Table of Contents

Ch.1 Introduction

1.1 Motivation

The burning characterization of a fuel is typically determined empirically by the measurement of the laminar flame speed. The laminar flame speed is used in many turbulent flame models and chemical reaction kinetics of the combustion process. It is therefore a measure to the fuels burning rate and is a property of the mixture. In this case the laminar flame speed of Dutch natural gas (DNG) has been investigated.

It was observed from the published documentation, that the laminar flame speed measurements of natural gas in general, are few in number. Nevertheless some research has been conducted by Dirrenberger et al. [1] and Huang et al. [2]. In this investigation, it was observed that the laminar flame speed of natural gas has typically similar characteristics to methane. The laminar flame speed of methane on the other hand has been documented in abundance over the course of time and still remains an important fuel in combustion experiments. However, in order to obtain detailed information on the burning characteristics of a variety of natural gas compositions, additional measurements of the laminar flame speed are required.

For the determination of the laminar flame speed of DNG the Bunsen flame method is employed using the OH chemiluminescence technique. The laminar flame speed measurement using the Bunsen flame is typically obtained by means of the flame cone angle and mass conservation method using the flame area. In this research both techniques are employed to determine the laminar flame speed of DNG. The Bunsen flame method requires a simple experimental setup which has shown to give accurate approximation on the magnitude of the unstretched, 1 dimensional, laminar flame speed.

This research will further extend on the available laminar flame speed data of natural gas by measuring the laminar burning velocity of DNG. The data on the laminar flame speed of DNG obtained in this research can be employed to model other low calorific value fuels that have a comparable burning characteristic. Additionally, the variation of the laminar flame speed is investigated to observe the source of the unsteadiness. This will allow further insight on the uncertainty for the measurement of the laminar flame speed using the Bunsen flame method.

1.2 Dutch natural gas background

Natural gas is a natural mixture of mainly methane and to a smaller extent ethane and propane. Natural gas is currently applied in many applications such as in residents, generation of electric power, automobile industry etc. One of the reasons for the wide application of natural gas is the low carbon dioxide emission during combustion compared to petroleum fuels and coal [3]. As the demand for energy is increasing, natural gas has been considered as an alternative fuel for wider fields of applications such as aviation [4] [5]. Recent study in the gas market showed that the demand for natural gas has seen an increase of 48% between 2000 and 2007 in Europe [6]. This is expected to increase further in the future to 70% by 2020. This improves the position of natural gas as a strategic means for future energy supply.

Due to natural gas being a natural mixture of hydrocarbons, its composition differs per region [7]. This indicates a variation of the energy output in combustion of natural gas. Therefore natural gas is typically divided into a so called L-gas with a low calorific range value of (<10.5 kWh/m^3) and H-gas with a high calorific value ranging from (10.5kWh/m^3 to 12.8 kWh/m^3) in the Dutch classification system [8]. Dutch natural gas (DNG) is a variant of L-gas due to its energy per volume corresponding to its composition.

Dutch natural gas was initially discovered in 1940 in the Netherlands [9]. However, it was not until 1959 that the DNG was introduced in the European gas market. In 1959 a large gas field, which was considered to hold the 9th place in the world, was discovered in Groningen. The discovery of this gas field brought a significant boom to the position of the Netherlands in the North Western European gas market [8] [9] [10].The production of Dutch natural gas resumed in 1963, when the new gas transportation network was established.

The transportation of gas was significantly more expensive compared to oil and coal [9] at that time. However, Due to the geologically ideal layout of the land this was not the case for DNG. Large quantities of gas was produced and transported. This revolutionized the energy market as natural gas was the most clean hydrocarbon fuel in a civilization relying mostly on coal and oil. In 1974 the Dutch policy took place in which the large gas field in Groningen would no longer be used for gas production. This decision was taken to keep the large gas field as a strategic reserve. Instead, smaller gas fields would be capitalized in terms of natural gas production. The production of DNG was further limited after the stronger than usual earthquake witnessed in 2012 in the north-eastern part of the country [8] [10]. As such gas production from the Groningen gas field has been further reduced to avoid increase in seismic activity. To accommodate for this reduction, natural gas is imported to meet the demand. This imported gas is diluted using nitrogen to maintain the low calorific value of natural gas in the Netherlands. Due to this artificial addition of nitrogen the composition of DNG varies slightly over time.

1.3 Combustion and flame theory

1.3.1 Definition of the (laminar) flame speed

In combustion theory the term flame speed is unclear by itself. Since this term can have different meaning for different cases. There are typically 4 definitions given to clarify on what is meant with the flame speed in order to understand what is measured or to be measured. For each flame type the flame speed will refer to one of these 4 definitions or a combination thereof. The flame speed definition is therefore dependent on the propagation of the flame in the unburned mixture as perceived by the observer.

The first definition is the laminar flame speed, in which a steady, 1 dimensional, unstretched adiabatic flame propagates relative to the unburned gas velocity, in the direction normal to the flame surface [11]. The laminar flame speed of such an ideal flame is typically denoted by S_L^0 and is only dependent on the composition of the mixture, the temperature and pressure. The value of S_L^0 is often used as a reference value in many combustion studies and is typically the goal of many laminar flame speed measurements. The value of the laminar flame speed corresponds to the burning characteristics of a fuel. Hence this flame speed can be viewed as the fuel's eigenvalue.

Often in combustion experiments the conditions for adiabatic, fully steady flow and plane flame are not present. Hence the laminar flame speed definition is further elaborated by dividing the definition of the flame speed in 3 categories [11]. These categories are:

- Flame front speed relative to a fixed frame of reference (Absolute)
- Flame speed relative to the unburned mixture flow (Displacement)
- Speed at which the reactants are consumed (Consumption)

The notation of the flame speed definition is shown in Fig.1. In this figure the vector $\bar{n}$ is the normal of the flame surface and Θ_f is defined by the local gradient of the flame surface. If the flame thickness remains unchanged then the local flame velocity on the flame surface $\bar{w}$ must remain constant. The absolute flame speed is then given by the expression [11]:

$$S_a = \bar{w} \cdot \bar{n} \tag{1}$$

This flame speed is an indication to the propagation of the flame towards the unburned mixture in a fixed reference frame.

If now the unburned mixture has a finite velocity $\bar{u}$ towards the flame front, then the flame speed w.r.t. the unburned mixture indicates the displacement velocity S_d or the relative velocity. The relative velocity of the flame front is obtained by subtracting the flame speed from the unburned gas velocity $\bar{u}$. This results in the expression [11]:

$$S_d = (\bar{w} - \bar{u}) \cdot \bar{n} = S_a - \bar{u} \cdot \bar{n} \tag{2}$$

The final flame speed definition is the consumption speed which is an indication to the burning velocity. This speed denotes the rate at which the reactants are consumed during combustion and it is therefore not an indication to the flame propagation. This flame speed definition is mainly based on the reaction rate and is given by the expression [11] [12]:

$$S_c = \frac{1}{\rho_u\left(Y_k^b - Y_k^U\right)} \int_{-\infty}^{\infty} \omega_k \, dx \tag{3}$$

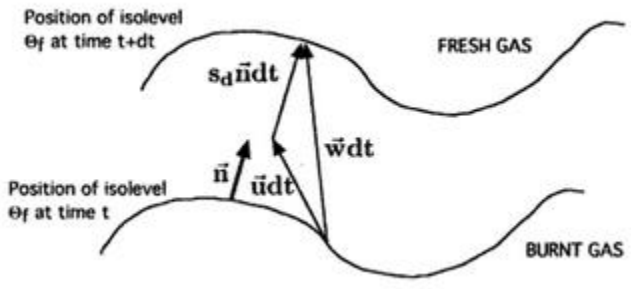

Fig.1: Flame propagation with the isolevel denoting the flame surface[11].

In this expression ρ_u is the unburned gas velocity, ω_k is the reaction rate of the k[th] species and Y_k^b, Y_k^U are the mass fractions of the k[th] species in the burned and unburned mixtures respectively. For the ideal case in which the flame propagates in a steady, adiabatic, unstretched and plane fashion, the value obtained from the absolute, relative and consumption flame speeds are equal to the reference laminar flame speed ($S_a = S_d = S_c = S_L^0$). The laminar flame speed is typically

presented in SI units in cm/s.

The burning velocity of the Bunsen burner flame for example, is the average consumption speed of the complete flame area [12]. However, from a different perspective, it can be noted that the absolute velocity of the Bunsen flame is zero $S_a = 0$ since the flame front is stationary w.r.t. to a fixed reference frame. Therefore it can be deduced that the displacement velocity is equal to the unburned mixture velocity component normal to the flame front with a direction opposite to the unburned mixture $S_d = -\bar{u} \cdot \bar{n}$. This is the case for any stationary flame subjected to a reacting flow at a certain velocity. However, the reference laminar flame speed S_L^0 is found to be equal to the consumption speed S_c for stationary, un-stretched flames of methane air mixtures [13]. This however, does not hold for regions in the flame where large curvature is present such as the Bunsen flame tip. Hence it can be stated for the case of a stationary, unstretched flame that the laminar flame speed is equal to the laminar burning velocity.

1.3.2 Premixed flame

Typically the laminar flame speed is determined from a premixed flame. This is the only type of flame in which flame propagation can be empirically determined [11]. In combustion research the use of premixed flames is essential. For instance [11]:

- It is one of the few cases where the numerical models can be verified accurately in experiments.
- It can be used to verify chemical reaction models.
- Many theoretical methods can be employed for laminar flames or to study various flame instabilities which can occur in the flame fronts.
- Premixed laminar flames are generally used in combustion models to simulate turbulent flows. It is the building block of many turbulent models.

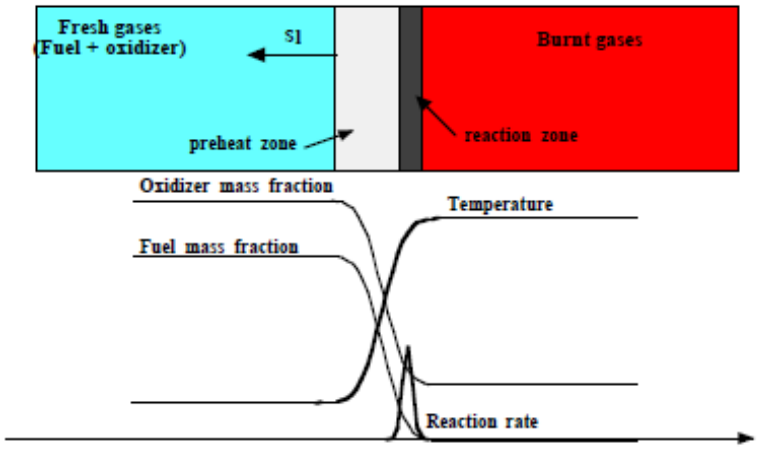

Fig.1.2: Typical premixed flame propagation [14].

A premixed flame is obtained from a mixture in which the fuel and oxidizer are mixed before combustion. A premixed flame is based on the assumption that the fuel and oxidizers are perfectly mixed before it enters the reaction zone [14]. A typical process for the establishment of a premixed flame is shown in Fig.1.2.

The flame front or the reaction zone is propagating towards the reactants at the displacement speed by a diffusion/reaction mechanism. If the reactants are at rest, then the relative and absolute flame speeds are equal. The reactants are then preheated due to

thermal diffusion until chemical reaction starts. The oxidizers and fuel are then converted into products after the flame front consumes the reactants at the reaction rate. The reaction rate increases exponentially with temperature. For conventional fuels the laminar flame speed typically ranges from 0.1 to 1m/s [14].

The burning efficiency of premixed flames is usually higher than their non-premixed counter part due to the prior mixing of fuel and oxidizer [14]. The burned gas temperature which is important for pollutant formation can be controlled by the amount of fuel mixed with the oxidizer. However, this is difficult to design since the amount of fuel to oxidizer ratio has to be well defined. In actual practical applications where high temperatures are present, non-premixed flames are encountered. This is due to safety concerns since a premixed mixture is combustible as soon as it is formed.

1.3.4 Flame front structure

For a reliable determination of the laminar flame speed it is necessary to have a deeper understanding on the general structure of the flame front. The flame front is the region where the chemical reaction of the reactants takes place. This region is detectable by the observer by its luminosity. The flame front either propagates or is stationary and has a finite thickness. The propagation of the flame front is a measure to the flammability of the mixture. The general temperature profile of a flame is shown in Fig. 1.3.

Generally two regions are recognized in the flame front. The preheat zone is the region between the cold reactants at temperature T_u and the location of the ignition temperature T_i. In this region the temperature of the reactants is rapidly increased mainly due to heat conduction and some heat convection from the reaction zone. This region is generally a heat sink indicated in Fig. 1.3 as a concave up ($\frac{\partial^2 T}{\partial x^2} > 0$), therefore no significant chemical reaction occur is this region. When the mixture reaches the ignition temperature T_i, chemical reaction occurs in which heat is generated. The temperature rises further which is shown in the graph by the concave down of the temperature profile ($\frac{\partial^2 T}{\partial x^2} < 0$). The temperature continues to rise until a final

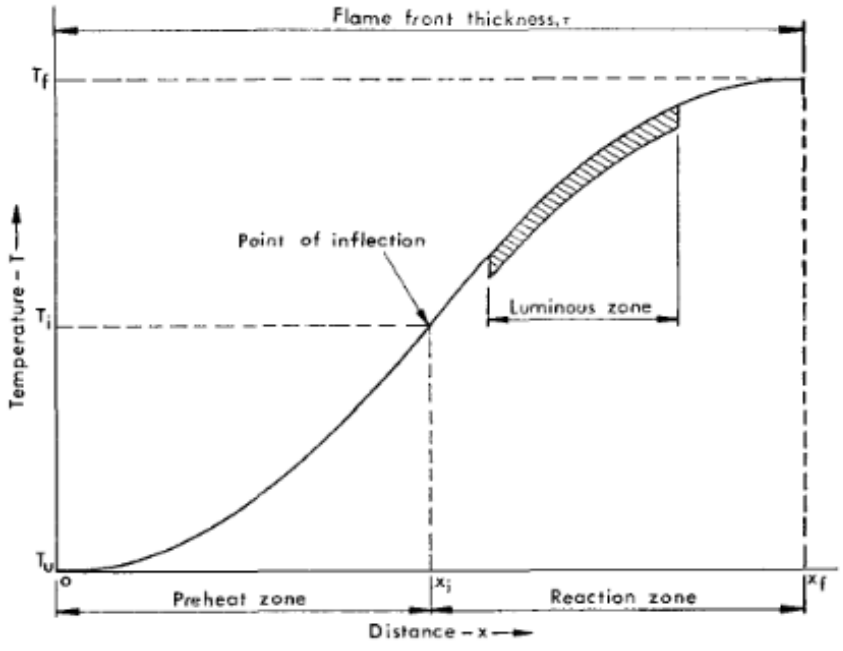

Fig. 1.3: Typical temperature profile of a flame and flame front structure [15].

equilibrium temperature is reached T_f. The region between the ignition temperature T_i and the final temperature T_f is called the reaction zone.

The reaction zone is further divided into two segments. Namely: The primary and secondary reaction zone. The primary reaction zone was shown by Fristrom et al. [16] to coincide with the luminous region of the flame front for a methane/oxygen mixture. This primary reaction region is normally used for the determination of the laminar flame speed. The secondary reaction zone is typically detected as a weak luminous region around the primary zone. The secondary reaction zone is formed by primarily the oxidation of CO particles [17]. The complete flame front is the combination of the pre-heat and the reaction zone. From Fig.1.3 observe that the temperature profile from the cold reactants T_u up until the final temperature T_f progresses asymptotically. The flame front thickness is estimated using this asymptotic behavior of the flame front to obtain the expression [11] [14] [15]:

$$\tau \approx 4.6 \frac{\bar{\lambda}}{\bar{c_p} \rho_u S_L^0} \tag{4}$$

In this expression $\bar{\lambda}$ is the average thermal conductivity of the mixture in W/mK , $\overline{C_p}$ is the average specific heat at constant pressure for the unburned mixture in Jkg/K, ρ_u is the unburned gas density in kg/m^3 and S_L^0 is the un-stretched laminar burning velocity in cm/s. This expression shows that the flame front thickness can become significant if the denominator becomes small i.e. if the laminar flames speed, unburned mixture density and/or average specific heat are reduced.

1.3.5 Laminar flame speed- flame temperature relation

Typically, the laminar burning velocity profile of a flame is of the form shown in Fig. 1.4. Observe that the velocity profile of the mixture near the reaction zone is similar to the temperature profile. This shows that the laminar flame speed and the flame temperature are correlated.

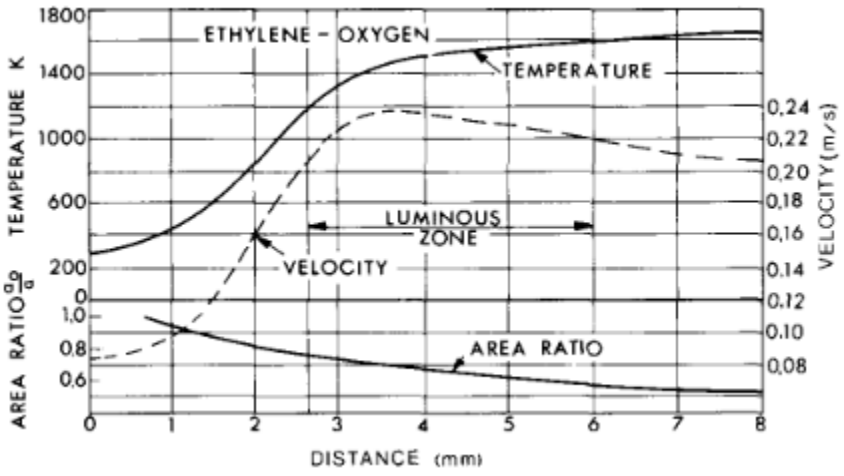

Fig.1.4: Flow velocity in a flame front compared to the flame temperature profile [15].

Several attempts have been made in relating the laminar flame speed to the flame temperature. However, this has been proven to be a complex problem. The most prominent of these attempts, is the analytical relation that has been proposed by Mallard and Le Chatelier. By assuming the ignition temperature of the gas to be a physical constant the relation was found to be of the form [18]:

$$S_L^2 = \frac{\lambda}{\rho_u^2 \overline{c_p}} \frac{T_b - T_u}{T_{ig} - T_u} f \tag{5}$$

In this expression λ is the heat conductivity of the gas in *W/m.K*, ρ_u is the unburned mixture density in *kg/m³*, T_b is the flame temperature in *Kelvin (K)*, T_u the unburned gas temperature in *(K)*, T_{ig} the ignition temperature in *(K)*, f the reaction rate in *(s^{-1})* and $\overline{c_p}$ the average specific heat in *J/kg.K* of the mixture at constant pressure. The relation proposed by Mallard and Le Chatelier relates the laminar flame speed to the flame temperature. It shows that if the flame temperature reduces then the laminar flame speed will also decrease. Similarly if the burning temperature increases then the laminar flame speed will increase.

Note that this expression is in general quite crude; it has been rarely shown to agree with experiments. This is due to the underlying assumption that the ignition temperature is a universal constant which in practice is not the case. However, this is a useful relation that can be used to explain certain observations from experiments.

1.3.6 Flame stretch

Flame stretch occurs due to non-uniform unburned flow velocities. It is therefore an aerodynamic effect that influences the flame front structure and flame front area. In the early measurements of the laminar flame speeds the aerodynamic effects were not accounted for. This caused a large scatter in the obtained laminar flame speed measurements [19].

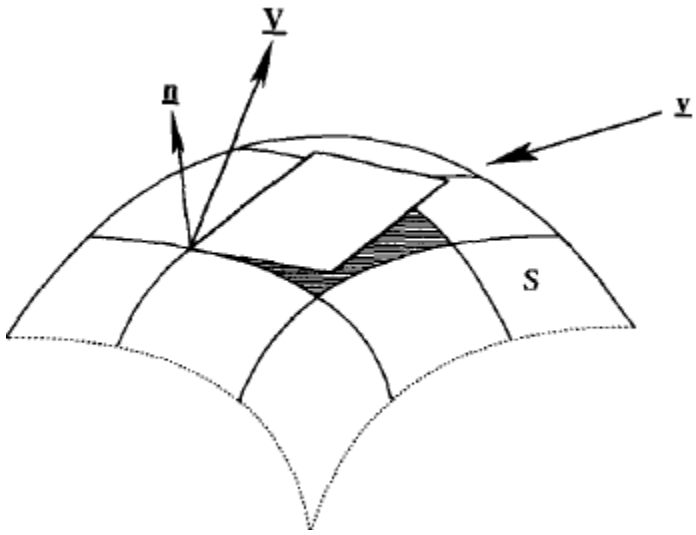

Fig.1.5: Flame surface propagation in unburned gas [19].

The concept of stretch is based on the motion and change of the surface in a non-uniform flow and has the unit s^{-1}. This is described by the general stretch equation, representing the time derivative of the logarithm of an infinitesimal area of this surface [19]:

$$K = \frac{1}{A}\frac{dA}{dt} \tag{6}$$

In the case of a flame the surface represents an isotherm moving in a fluid with a velocity $\underline{V}$ in m/s w.r.t. the unburned mixture at a velocity $\underline{v}$ in m/s. This is represented in Fig.1.5. The tangential motion of the boundary of this surface element moves towards the tangential component of the fluid velocity $\underline{v_t}$ in m/s. The expression for the stretch rate can therefore be written in terms of the flow velocity as [19]:

$$K = \underline{\nabla_t} \cdot \underline{v_t} + \left(\underline{V} \cdot \underline{n}\right)\left(\underline{\nabla} \cdot \underline{n}\right) \tag{7}$$

With:

$$\underline{\nabla_t} \cdot \underline{v_t} = \underline{\nabla} \cdot \left[\underline{n} \times \left(\underline{v} \times \underline{n}\right)\right]$$

In this expression $\underline{\nabla_t}$ is the differential operator for the tangential component of the fluid velocity and $\underline{n}$ is the normal vector of the surface directed towards the unburned mixture. The first right hand term of the equation $\underline{\nabla_t} \cdot \underline{v_t}$ is the non-uniformity of the velocity of the unburned mixture. The second term represents the non-stationary term of the flame through $\underline{V}$. Finally the term $\underline{\nabla} \cdot \underline{n}$ describes the curvature of the surface. The stretch induced effects can therefore be separated into the aerodynamic straining, flame motion and flame curvature.

In literature often times the flame stretch is derived w.r.t. other parameters such as the one used by Candel and Poinsot [20]. In which the expression was written in terms of the displacement flame velocity. The concept of stretch is however the same. For the Bunsen burner flame, the flame stretch has been found by using Eq.7. In the derivation of this equation it was assumed that the unburned mixture velocity is uniform and does not change along the length of the flame. Moreover, the flame is considered stationary. From these assumptions the flame stretch of the Bunsen burner flame is found to be [19] [21]:

$$K = -\frac{U_0 \sin(2\alpha)}{2R_f} \tag{8}$$

In this expression $U_0$is the uniform unburned gas velocity, α is the cone angle and R_f is the flame radius along the flame length. This shows that the Bunsen flame is negatively stretched.

The influence of the flame stretch on the laminar flame speed has been thoroughly investigated by Chen et al. [22] and Choi et al. [23]. For a curved flame front the laminar flame speed is given by the empirically determined expression [22]:

$$S_L = CS_L^0 - \mathcal{L}K \tag{9}$$

In this expression $\mathcal{L}$ is the Markstein length, C is a constant usually set to unity and K is the flame stretch. This expression is only suitable for weakly stretched flames where the Lewis number is close to unity [19]. This expression relates the stretched laminar flame speed to the un-stretched reference laminar flame speed. Usually this expression is normalized by the un-stretched laminar flame speed S_L^0 combined with the introduction of the flame thickness τ leading to the expression [23] [24]:

$$\frac{S_L}{S_L^0} = 1 - \frac{\mathcal{L}K}{S_L^0}\frac{\tau}{\tau}$$

$$\frac{S_L}{S_L^0} = 1 - M_a K_a \tag{10}$$

In this expression M_a is the Markstein number defined as $M_a = \frac{\mathcal{L}}{\tau}$ and $K_a = \frac{K\tau}{S_L^0}$ is the Karlovitz number in which τ is the flame thickness.

1.3.7 Equivalence ratio

The laminar flame speed of a premixed flame is dependent on the mixture composition. The amount of air mixed with fuel affects the laminar flame speed. The quantity of fuel and air in a mixture is defined by the fuel to air ratio (*FAR*).

A certain amount of fuel combined with air causes a complete combustion of the fuel. Complete combustion occurs if all the fuel particles are oxidized [25]. This fuel to air ratio is commonly referred to as the stoichiometric fuel to air ratio or stoichiometry in short. At stoichiometry the product species generated from the chemical reaction is at its minimum. In the case of hydrocarbons these are mainly CO_2 and H_2O. One may recognize that the enthalpy release of the fuel is at its maximum at stoichiometry. Indicating that the flame temperature and hence the laminar flame speed will reach its theoretical maximum at this FAR. This stoichiometric fuel to air ratio is determined by solving a chemical equilibrium for hydrocarbons equation given by [25]:

$$C_\alpha H_\beta O_\gamma + \left(\alpha + \frac{\beta}{4} - \frac{\gamma}{2}\right)(O_2 + 3.76N_2) \rightarrow \alpha CO_2 + \frac{\beta}{2}H_2O + 3.76\left(\alpha + \frac{\beta}{4} - \frac{\gamma}{2}\right)N_2 \qquad (11)$$

From this equation the number of moles of oxygen required to fully combust a certain hydrocarbon fuel can be determined. The stoichiometric fuel to air ratio can be found by volume or by mass. The end result of the calculation will be the same regardless which of the 2 methods are used. Here only the volumetric based $FAR_{stoich.}$ is discussed. The expression for the volumetric based stoichiometric fuel to air ratio is given by Eq.12.

$$FAR_{stoich} = \frac{V_{fuel}}{V_{air}} \qquad (12)$$

In this equation V_{air} is unit volume air and V_{fuel} is the unit volume of fuel. Using the ideal gas model one can rewrite Eq.12 in terms of moles [26]. Given that the pressure and temperature of the two gases are equal. The ideal gas model for gaseous fuels and air is given by Eq.13a and Eq.13b respectively.

$$PV_{fuel} = n_{fuel}\bar{R}T \rightarrow V_{fuel} = \frac{n_{fuel}\bar{R}T}{P} \qquad (13a)$$

$$PV_{air} = n_{air}\bar{R}T \rightarrow V_{air} = \frac{n_{air}\bar{R}T}{P} \qquad (13b)$$

In this expression $\bar{R}$ is the universal gas constant in J/mol.K, n_{fuel} is the mole of fuel, n_{air} is the mole of air, P is the pressure in Pascal and T is the temperature in Kelvin. Substituting these expressions in Eq.12 results in:

$$FAR_{stoich} = \frac{V_{fuel}}{V_{air}} = \frac{n_{fuel}}{n_{air}} \qquad (14)$$

In practice it is usually beneficial to relate the actual fuel to air ratio (FAR_{act}) to the stoichiometric fuel to air ratio (FAR_{stoich}). This ratio is referred to as the equivalence ratio and denoted as [25]:

$$\phi = \frac{FAR_{act}}{FAR_{stoich}} \tag{15}$$

The equivalence ratio relates the actual or present fuel to air ratio to the stoichiometric fuel to air ratio. It is a measure to how far or close one is to stoichiometry. If the equivalence ratio is less than $1(\phi < 1)$, then a lean mixture is achieved indicating excess air. Similarly, if $(\phi > 1)$ then a rich mixture is obtained indicating excess fuel. If $(\phi = 1)$ then the mixture is equal to stoichiometry and complete combustion is achieved.

1.4 Measurement of the laminar flame speed

The burning velocity of a flame became an important parameter after the chemist Sir Benjamin Thompson discovered in his experiments, that heat is related to the motion of the particles in 1798 [27]. This allowed for the development of a kinetic theory of gasses that gave an understanding on the energy aspect of combustion. In mid-19th century the determination of the burning velocity became a fundamental aspect in understanding theories regarding combustion mechanisms.

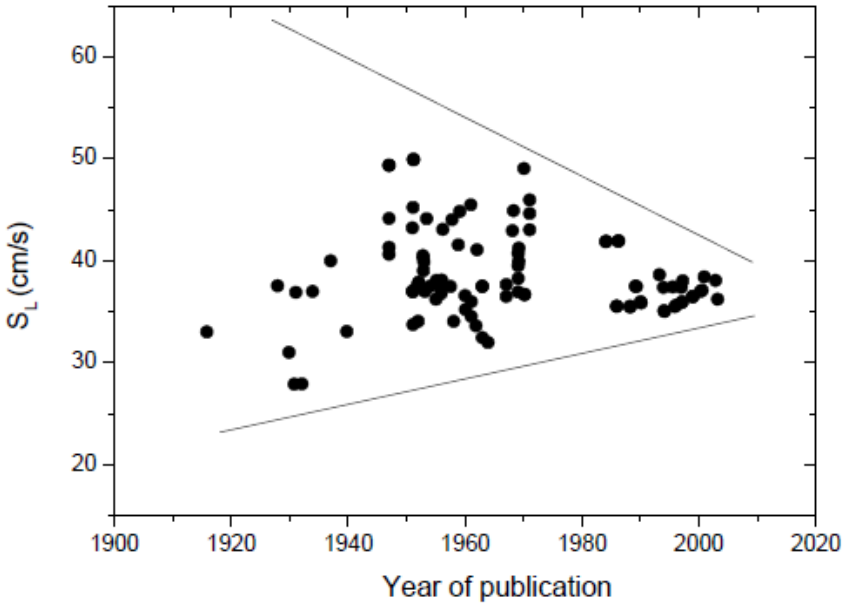

Fig. 1.6: History of the determination of the laminar flame speed of methane for $\phi = 1.0$ [31].

Among the first who measured the laminar flame speed were Lewis and Von Elbe [28] for ozone/oxygen mixtures using spherically propagating flame in 1934. From then on the measurements of the laminar flame speeds of fuels were continuously investigated. The main emphasis was placed on the determination of the laminar flame speed of gaseous fuels such as methane, propane, ethylene etc. The laminar flame speed is an appealing parameter for experimental quantification since it can be for instance visually determined from the flame geometry if the unburned flow velocity is known.

The Bunsen flame geometry was one of the early flames to be used in the determination of the laminar flame speed. This was mainly due to the simplicity of the burner design [29] [30] and the geometry of the flame which was generally conically shaped. As the experimental methods used in the determination of the laminar flame speed improved, the accuracy of the measurement increased [31]. The laminar flame speed measurement over time for methane at equivalence ratio $\phi = 1$ is shown in

Fig. 1.6. In addition to the improvement on the laminar flame speed measurement techniques, the earlier determination of the laminar flame speed did not account for aerodynamic effects. This caused a large scatter in the laminar flame speed measurements which is shown in the early publications of the laminar flame speed measurement in Fig.1.6.

This figure shows a converging trend in the measurement of the laminar flame speed of methane/air mixtures. This trend shows that the measurements of the laminar flame speed for methane air mixtures are converging to 35~37cms/s at stoichiometric conditions.

1.5 Laminar flame speed measurement of Bunsen flame

The Bunsen burner flame still remains a prominent flame geometry encountered in many combustion studies in determining the laminar flame speed. The Bunsen burner flame is generally axisymmetric and is conical in shape and is stabilized on a cylindrical burner rim. This indicates that the Bunsen burner flame is not the ideal 1 dimensional flame required to obtain the reference laminar flame speed S_L^0. This is due to the effect of strong curvature present in an axisymmetric flame which influences the measured laminar flame speed. Nevertheless, it was shown in literature [22][32] that the flame curvature at the tip of the Bunsen burner flame is the most prominent and that the laminar flame speed of the Bunsen flame should give a good approximation of the reference laminar flame speed S_L^0. Therefore in many combustion researches such as the investigation of Natarajan et al. [33], deal with a Bunsen burner flame in which the flame height is large compared to the burner exit diameter. This is performed to limit the influence of the flame stretch on the laminar flame speed measurement to only the flame tip.

The Bunsen burner is known to maintain a stable flame for a wide range of operational conditions in terms of pressure, temperature and equivalence ratios. In addition the burner itself is simple to manufacture. Hence it is more accessible in many combustion research facilities. Therefore, The Bunsen burner flame remains important flame geometry in combustion research due to its reliability and robustness. Typically two types of Bunsen burner are used in combustion experiments. These are the tube type Bunsen burners and an aerodynamically tailored nozzle burners.

A tube type Bunsen burner is a simple tube that ensures a fully developed laminar flow is maintained at the burner exit for a wide range of flow rates. The aerodynamically tailored nozzle burner or nozzle burners are burners that have a carefully designed contracting diameter along the length of the burner. These nozzle burners lead to a generally uniform velocity distribution at the burner exit. Additionally the effect of the boundary layer on the flame curvature at the flame base is reduced by reducing this boundary layer thickness. This generates a near conical flame with the flame stretch to be effectively only present at the flame tip.

The measurement of the laminar flame speed has proven to be rather challenging despite its quite straight forward definition. Typically two methods are used to determine the laminar flame speed of a Bunsen burner flame. Namely: the flame cone or semi-cone angle method and the mass conservation method. Both of these methods are of interest and are discussed.

1.5.1 Semi-cone angle method

The semi-cone angle method or the flame angle method relies on the geometric cone angle of the Bunsen burner flame. This method is explained by means of geometry of the flame shown in Fig.1.7. The Bunsen flame is typically illustrated as a conical flame by omitting the curved sections at the flame base and flame tip. A stable Bunsen burner flame is obtained at the burner rim if the reactant flow velocity is larger than the laminar flame speed of the mixture. In this method, the flow velocity is assumed to be uniform along the radius of the burner. This is typically achieved by means of a contoured nozzle. The use of such a nozzle reduces the influence of the boundary layer at the flame base. This leads to a flame that has almost no curvature at the flame base, hence the only main curved section of the flame is at the flame tip. However, often times a Bunsen burner flame is obtained from a straight burner tube. This straight tube Bunsen burners are typically more accessible in many combustion experiments compared to the contoured nozzle Bunsen burners.

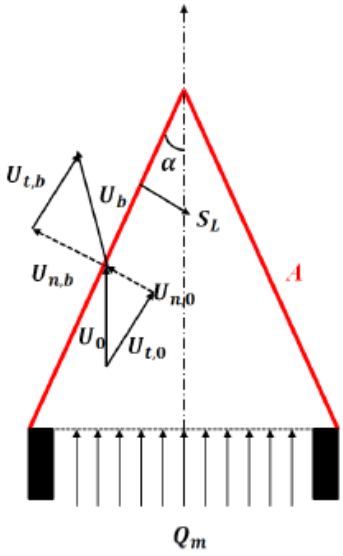

Fig. 1.7: laminar flame speed using the flame cone method [12].

Observing Fig.1.7 the uniform reactant flow is moving towards the flame front at a certain velocity U_0. The tangential velocity along the flame contour U_{t_0} is not affected by the gas expansion and remains unchanged [12].

As was discussed earlier the flame velocity is defined to be normal to the flame front with a direction towards the unburned mixture given in Fig.1.7 as S_L. Since the Bunsen burner flame is stationary, the unburned flow velocity normal to the flame front U_{n_0} must be equal to the laminar flame speed S_L. This can be mathematically written as [12]:

$$S_L = U_{n_0} = U_0 \sin(\alpha) \tag{16}$$

The main drawback of this method is that the laminar flame speed has to be corrected for stretch effects if dealt with a flame height that is close to the burner diameter.

1.5.2 Mass conservation method

The second method often used in determining the laminar flame speed, is the mass conservation method. The mass conservation method states that the mass flow rate through the flame front must be equal to the mass flow rate through the burner exit. This gives an overall average laminar burning velocity across the complete flame area. This technique has been shown to give a close approximation to the ideal 1D flame if the flame height is larger than the burner exit diameter [33]. The mass conservation of a conical flame can therefore be described as [33]:

$$S_L^0 \approx S_L = \frac{\dot{m}_{total}}{\rho_b A_f} \tag{17a}$$

In this expression $\dot{m}_{total}$ is the total mass flow rate in kg/s, ρ_b is the burned gas density in kg/m^3 and A_f is the flame area in mm^2. From the 1D flame the mass conservation reads [33]:

$$S_L^0 = \frac{\rho_u}{\rho_b} S_u^0 \qquad (17b)$$

In which ρ_u is the unburned gas velocity in kg/m^3 and S_u^0 is the mixture velocity in cm/s close to the reaction zone. Substitution of expression 17b into 17a results in the equation [33]:

$$S_u^0 \approx S_L = \frac{\dot{m}_{total}}{\rho_u A_f} = \frac{\dot{V}_{total}}{A_f} \qquad (18)$$

In this expression $\dot{V}_{total}$ is the total volumetric flow rate of the unburned mixture in cm^3/s. This method however raises a question, after all the flame front is not a two dimension entity since it has a finite thickness. This flame front thickness is especially relevant if it is significant compared to the flame dimension. For thin reaction zones which are typically the case for light molecule fuels such as methane, the reaction zone is in the order of 10^{-3}mm [16].The question that needs to be answered is where in the flame front should the flame area be determined? This question has been heavily debated in the community since each optical technique gives a different region in which the flame area is detected as shown in Fig.1.8. The general consensus is that any location in the flame front where the values of the density and the mass flow rate can be determined is acceptable [15]. Ideally, the flame area should be determined from the region where the first temperature rise can be detected. This however is very difficult to determine in experiments since the temperature profile of the flame is asymptotic in nature.

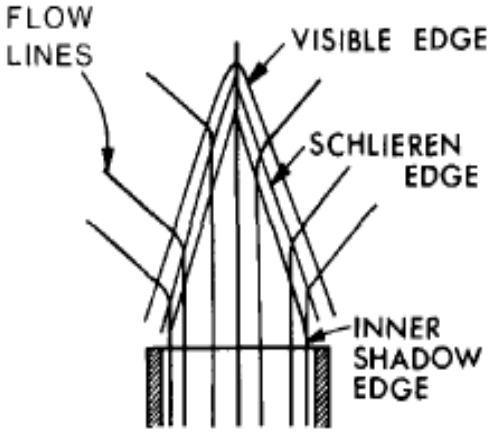

Fig.1.8: Variouse optical regions of the flame front [15].

The visible edge of the flame is often used in earlier work since its natural luminosity is easily detectable using simple photography. However, the luminous region has been shown to be some distance away from the location of the first temperature rise in the unburned mixture. Therefore the location of this luminous zone is generally not representative to the region where the initial chemical reaction starts. This is especially significant if the flame front thickness is considerable ($\tau \geq 1mm$) [15]. This region is not suitable to measure the flame area at conditions lower than atmospheric pressures. However with the analysis of the light of the flame at a limited spectrum this region showed to yield good estimations of the laminar flame speed. The inner shadow edge is close to the initial rise in temperature, if the distance of the flame and the photo detection device is small. Due to its dependence on the distance between the photo detector and the flame which lead to difficult reproducible results, this method was abandoned [15]. The outer shadow edge which is equivalent to the Schlieren edge is on the other hand independent on the distance between the flame and the photo detector. This variation in the location of

the shadow graphic method is therefore unreliable. The Schlieren method is considered one of the best techniques to determine the flame area. The location of the Schlieren edge is obtained from the maximum intensity of the temperature slope ($\frac{1}{T^2}dT/dx$) which is easily located. For conical flames, the Schlieren edge is much closer to the location of the first temperature rise required to determine the laminar flame speed.

1.6 Laminar flame stability

Flame stability of a premixed laminar flame is when the combustion of the reactants is self-sustained at the burner exit. Therefore the flame stability is dependent on the mixture composition, burner design and bulk flow velocity. The topic of flame stabilization is a complex problem in burner design, especially when lean mixtures are used. Typically there are three criteria's for the stability of a laminar premixed flame. These are [34]:

- Flammability limit of the mixture which is mainly affected by the fuel composition requires a minimum amount of oxygen to sustain chemical reaction. For instance the level of dilution in the fuel impacts the flammability of the mixture and is therefore a flammability limit concern.
- Quenching distance which is the loss of heat to a wall that reduces the reaction rate and in turn negatively impacts the sustainability of the chemical reaction.
- Mixture flow relation with the laminar flame speed. This stability limit is a direct relation between the bulk flow and the laminar flame speed of the mixture which includes the onset of turbulence, blow off, flash back limits etc. these are stabilization problems encountered in real experimental situations.

Here the emphasis is placed on the flammability limit of the fuel and the mixture flow relation with the laminar flame speed.

1.6.1 Flammability limit

The lean flammability limit is directly related to the fuel composition. It is the limit in which the fuel/air ratio is exactly correct to still support a self-sustaining reaction. This limit is at the maximum lean equivalence ratio and the maximum rich equivalence ratio which still allows for a self-sustaining chemical reaction [34]. The primary factor that determines the flammability limit of a mixture is the competition between the heat generation of the reaction, which is governed by the reaction rate and the heat release of the reaction at the mixture limit, and the rate of heat loss of the flame to the ambient. The addition of diluents to the fuel such as N_2 or CO2 changes the flammability limit negatively. Each of these

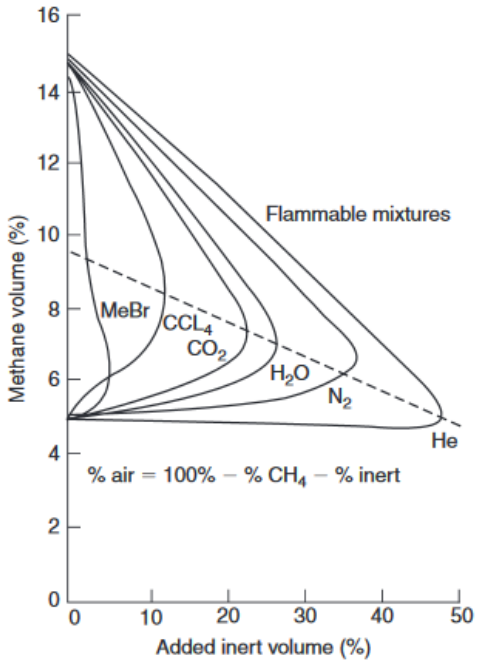

Fig. 1.9: Flamability limit of methane mixture [35].

diluents has a different strength on the extinction of the flame. The order of the extinction power of common diluents is $CO_2 > N_2 > Ar(or\ He)$. This means that the addition of CO_2 has a stronger negative effect on the flammability of the mixture than for instance Argon. The effect of the addition of diluents is indicated by the specific heat of the gas. If a gas has a high specific heat, then the final flame temperature will be reduced. This reduces the heat release of the fuel and in turn the loss of the sustainability of the reaction. This effect of additives was investigated by Zebatakis [35] who derived the diagram shown in Fig.1.9 for methane.

This diagram is for the combustibility limit of fuel mixtures at atmospheric pressure and a temperature of 298K. This figure shows that the addition of each diluent effect on the minimum required air in order to achieve a self-sustaining chemical reaction. For instance this diagram shows that the maximum amount of CO_2 that can be present with a mixture of 7.5% methane in order to obtain a stable flame is approximately 25%. Similarly the effect of other diluents on the flammability limit of methane can be estimated.

1.6.2 Flame stability

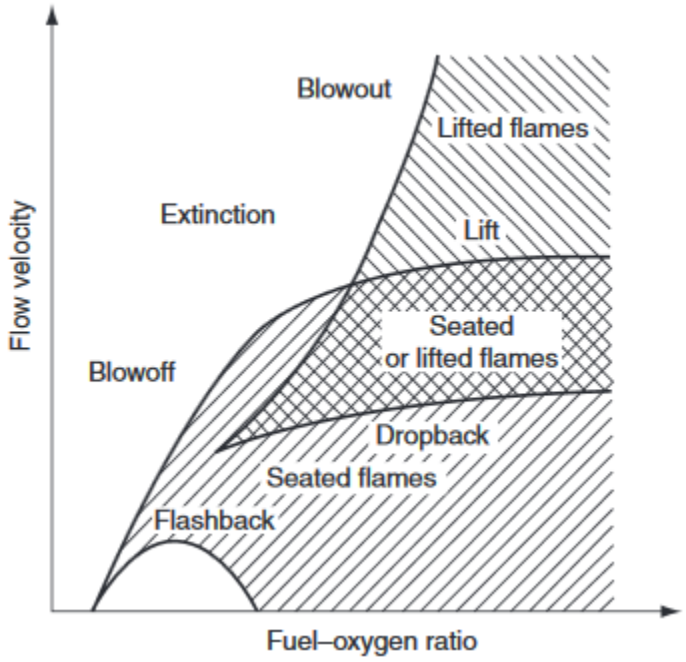

Fig. 1.10: Bunsen flame stability limit diagram [34].

When a flame is introduced in a stationary mixture, it propagates along the cold unburned mixture at the laminar flame speed. If the stationary mixture would be given a velocity equal to the laminar flame speed of the reaction zone within for instance a tube, then a stationary flame is achieved. Increasing the velocity of the mixture beyond the laminar flame speed will push the reaction zone back. This scenario is what is actually happening with stabilizing a flame on a burner. For the case of a tube Bunsen burner, the burner acts as a heat sink in order to achieve a burner stabilized flame. If the mixture velocity is increased further a conical shape of the flame is formed at the exit of the tube. The cone angle of the flame reduces with increasing flow velocity. The unburned mixture velocity component normal to the flame front is here equal to the laminar flame speed which creates a stationary Bunsen flame.

However the velocity near the burner rim is lower than at the center of the burner tube. This causes an equalizing effect between the laminar flame speed at the burner rim and the unburned mixture velocity. This equalizing effect anchors the flame to the burner rim. Due to the short distance between the flame and the burner exit, the laminar flame speed of the flame close to the burner is governed by the heat loss to this burner rim [34]. If the mixture velocity is increased further, then the flame will move further

downstream allowing for air to entrain to the flame base causing the mixture to be diluted. This dilution of the mixture at the flame base causes a reduction in the flame speed and the blow off of the flame is realized.

In a similar fashion, if the flow velocity of the mixture is reduced then the laminar flame speed of the flame will be higher than the unburned mixture velocity. This causes the Bunsen flame to collapse into the burner. This tendency of the flame to move upstream into the burner is referred to as flash back of the flame. From this discussion it can be deduced that a certain limit is present where a stationary Bunsen burner flame can be established. This stability of the Bunsen flame has been investigated by Cheng et al. [36] to determine the effect of buoyancy on lean premixed flames. The stability diagram of a Bunsen flame is given in Fig. 1.10.

It shows the stability limit of the combination of the bulk flow velocity and the fuel to air ratio of the mixture. This diagram is important in burner design. In this figure a seated flame indicates a flame stabilized at the burner rim. If the unburned mixture velocity is further increased for a fuel rich mixture then a lifted flame is observed. This is a flame detached from the burner exit and is stabilized further downstream. Finally if the rich mixture velocity is increased further, the chemical reaction can no longer be sustained due to dilution of the mixture caused by the entrained air, which results in a flame blow out.

1.7 Chemiluminescence

1.7.1 Chemiluminescence background

The measurement of the laminar flame speed of a fuel has been investigated continuously. A wide array of experimental setups has been developed over the course of time, to tackle the problem of determining the magnitude of this parameter. One of the techniques commonly employed in the experimental determination of the laminar burning velocity is the chemiluminescence method.

The determination of the burning velocity was mainly determined from the flame luminosity. In this, the Bunsen burner flame was the main flame geometry of investigation. Mainly due to the simplicity of the burner and the geometry of the flame which was commonly simplified to a conical flame. This flame allowed for an insight on fundamental flame structures. The use of the flame luminosity to determine the laminar flame speed, introduced the application of spectroscopy and in turn, experimental setups involving optical observation techniques.

This rise in optical observation of the flame allowed for the development of the chemiluminescence technique. The chemiluminescence of a chemical reaction occurs by the de-excitation of radicals generated during this reaction in the form of electromagnetic radiation. The concept of chemiluminescence was fully defined since the early 1900s [37]. However, the application of this method in combustion research was employed later on as early as 1958 [38]. The concept of chemiluminescence technique in combustion research allowed for an in depth understanding on the chemical reaction of a fuel. For hydrocarbon fuels, the general radical species contributing to the chemiluminescent light are OH*, CH* and C_2*. It is common practice to depict an excited molecule with

an asterix. These radical species are generally responsible for the most visible and ultra violet light of a flame corresponding to hydrocarbon fuels [39]. The chemiluminescence technique has several advantages such as [40]:

- The measurement of the radiation does not interfere with the reaction region.
- Remote sensing is possible by means of fiber optics.
- The transient species can be easily identified.
- In its most basic form the observers eye is the only tool required in the setup.

Due to these advantages chemiluminescence is often considered for the analysis on the flame characteristics in combustion research. Combined with the currently advanced detection devices, that cover a wide light spectrum ranging from ultra violet to infrared, the chemiluminescence technique becomes a powerful tool in species detection.

Besides species detection, flame chemiluminescence allows for the detection of the reaction zone location. This provides the means for a precise observation of the flame geometry which in turn contributes to a reliable deduction of the laminar flame speed.

1.7.2 Principle of chemiluminescence

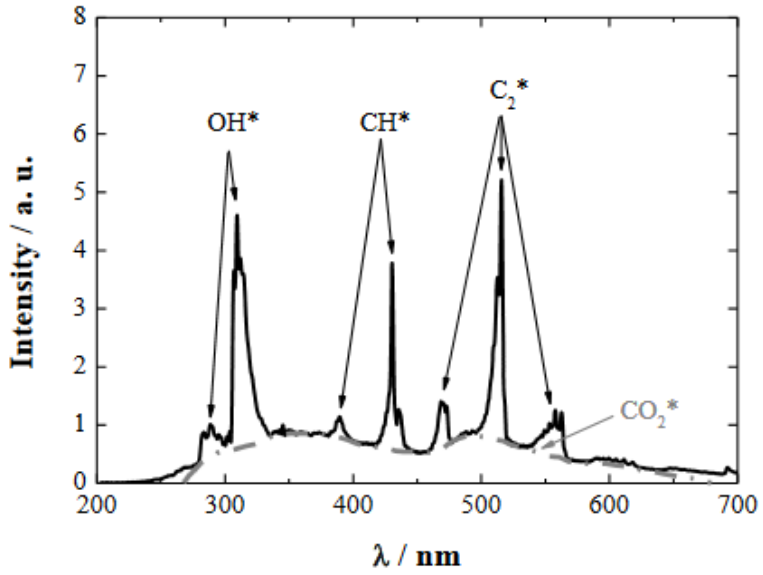

Fig.1.11: Typical swan band of the flame light emission spectrum [41].

The idea of chemiluminescence has been shown to have a long history. However, the principle still remains a valuable asset in combustion research. Generally for hydrocarbon fuel combustion, OH*, CH*, C_2* and CO_2*are the prominently present excited particles. General chemiluminescence emission spectrum of OH*, CH*, C_2*, and CO_2* of methane/air mixture combustion is shown in Fig.1.11. The radicals OH* and CH* has been extensively researched while the investigation on CO_2* and C_2* are scarce in comparison [41] since the OH* and CH* are more commonly found in the chemical reaction encountered during the combustion of hydrocarbon fuels.

The reaction mechanics for the formation of OH*, CH* are different. However, the principle of chemiluminescence is the same. Therefore in this research the discussion on chemiluminescence is limited to only the OH* species. In depth description of chemiluminescence in combustion is given by

Bozkurt [41]. However, a short explanation on the principle of chemiluminescence will be given in this section to understand the origins of the chemiluminescent light during combustion of hydrocarbons.

The emission of a chemiluminescence signal is an attribute of a combustion process. Hence the heat release and the equivalence ratio are affecting the intensity of the chemiluminescence signal [39] [42]. Typically a chemiluminescence reaction occurs independently from the main reaction process. This is due to the population of the chemiluminescent particles being several orders of magnitude smaller than the population of the ground state molecules.

The formation of OH* radicals are for instance obtained from the chemical relation:

$$CH + O_2 \rightarrow OH^* + CO \tag{19}$$

Note that this is one of such reaction in which OH* is formed. Nevertheless, this reaction is generally accepted to be the prominent way in which OH* is generated [43]. This reaction indicates the formation of an excited state diatomic OH particle and a ground state CO particle. The de-excitation of the OH* particle is then achieved by releasing the energy in the form of a photon. The radiation reaction of the excited molecule OH* is described by:

$$OH^* \rightarrow OH + hv \tag{20}$$

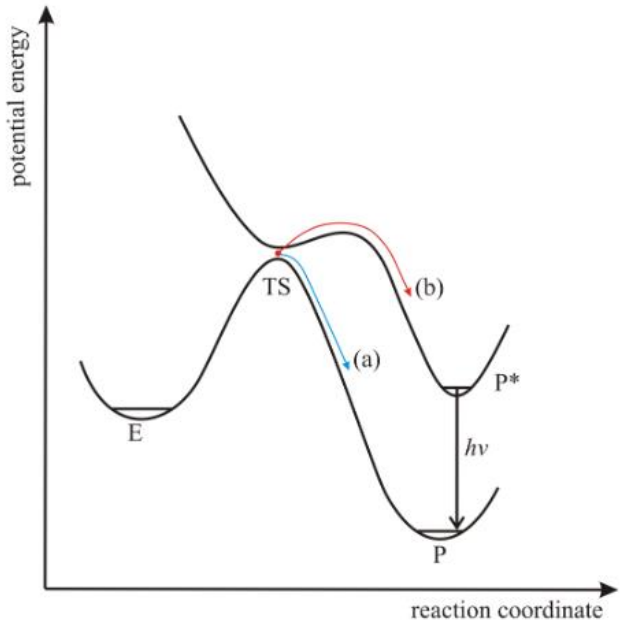

Fig. 1.12: Schematic principle of the normal (a) and chemiluminescent reaction (b) [41].

In this expression the energy released in the form of a photon is equal to the Plank constant *h* in *(J*s)* and the frequency of the light ν. For the OH* the wave length of the light is shown in Fig.1.11 to be in the order of 300 nm. The quantum level of the electron in its excited state determines the wavelength of the photon during de-excitation. The time of this de-excitation is virtually instantaneous after the OH* particle is produced. However, one has to realize that not all the energy obtained during excitation is converted to radiation. Most of the energy of the excitation is absorbed by the collision of the molecules and is therefore not emitted in the form of electromagnetic radiation. This is referred to as quenching [44].

For the purpose of this research, the discussion is only limited to the de-excitation of the OH* particle by electromagnetic radiation. However, it is worth to note that not all energy of the excited particle is emitted in the form of radiation. This is important for chemiluminescence modeling as has been performed by Haber et al. [43] [45]. This principle of energy release can be graphically shown using the qualitative potential energy surface diagram in Fig.1.12.

For a normal chemical reaction the energy of the particle will remain in the ground state throughout the chemical reaction. That is, the species at ground state energy level (E) will undergo excitation due to the thermal activation from the chemical reaction, raising the particles to the transition state (TS). The de-excitation of the particles will then occur by the formation of the products from the chemical reaction at the new energy level (P). This procedure follows the direction as pointed out by the arrow (a). This is usually referred to as an adiabatic reaction. However, when chemiluminescence reaction occurs, the chemical reaction will no longer follow the energy level of the particle's ground state. Instead, the activated reaction of the particles at (TS) will be transferred to the energy level of the excited state of the particle which follows the path (b). This results in products that are at a higher energy level compared to their ground state. To return to their ground state, the energy obtained during excitation is released through radiation or by quenching. Indeed, the energy of the radiation is therefore $h\nu = E_2 - E_1$. This indicates that the energy of the photon and hence the photon wave length is equal to the difference of the energy levels between the excited state E_2 and the ground state E_1.

1.7.3 Flame front detection using (OH*) chemiluminescence

The OH chemiluminescence emission has been shown to occur during the de-excitation of charged particles. The generation of such particles occurs due to the chemical reaction in the flame front. As such one can use the chemiluminescence radiation of OH* particles to study the structure of the reaction zone. Chemiluminescence was used commonly in the determination of the flame front structure of a premixed turbulent flame [46].

However, this method can be extended in the study of a premixed laminar flame. The intensity of the OH* radicals has been investigated by Kojima et al. [47] in the reaction zone. In this research the OH chemiluminescent emission was determined for a laminar flame of methane air mixture at an equivalence ratio 1.1. In the 1 dimensional analysis of the reaction zone, it was found that the maximum OH*, CH*and C_2* emission is located at the luminous region. This gives an indication on the location of the reaction zone. This allows for a detailed flame front structure analysis using a relatively simple experimental setup. This has been employed often in complex flame front structure analysis such as by Meier et al. [48].

It should be noted that the chemiluminescence technique is a line of sight method. This indicates that the chemiluminescence signal is line integrated in the final image if the object is three dimensional such as a Bunsen burner flame. This may cause difficulty in the analysis of the flame front such as determining the flame front thickness. Often times a correction is used by means of Abel inversion of the image to remove the line of sight effect [49].

1.7.4 Experimental application of (OH*) chemiluminescence

The chemiluminescence technique has shown a wide field of application in experimental studies of combustion. The CH chemiluminescence method was employed by Fernando et al. [50] in his experimental setup to determine the laminar flame speed of methane air mixture. In this experimental setup a Bunsen burner was used. The laminar flame speed was determined from the semi-cone angle. Similarly the laminar flame speed of hydrogen carbon monoxide mixture using the chemiluminescence method was determined by Natarajan et al. [51]. In this experimental setup a knife edge is used to

improve the detection of the chemiluminescence emission of the Bunsen burner flame tip. The laminar flame speed was then determined from the mass conservation method.

In similar investigation on the burning characteristics of methane flames enriched with oxygen and addition of water vapor, a chemiluminescence setup was chosen by Maza et al. [44]. In this Experimental setup a Bunsen burner flame was used. The laminar flame speed of the mixture was then determined from the semi-cone angle method. This shows that the chemiluminescence of a flame is commonly accepted as an indicator for the flame front. A more advanced approach to the laminar flame speed measurement using chemiluminescence of the flame was employed by Kojima et al. [47]. In this experiment cassagrain optics was used to relay the chemiluminescence signal to the photo detector. In this setup a slot burner was used to obtain a 2 dimensional flame. The flame geometry in this case took the form of a prism in which the laminar flame speed was obtained in a similar fashion to the semi-cone angle. A further investigation on the chemiluminescence signal was performed by the same group [52]. In this experiment the chemiluminescence radiation was spatially resolved by means of a cassagrain mirror system. The chemiluminescence light emission was obtained from a Bunsen burner flame. In this investigation it was found that the OH*/CH* are a good indication markers on the local flame stoichiometry of the reaction zone. This finding was shown earlier by Roby et al. [53], by employing chemiluminescence in the determination of the temperature of a laminar and turbulent flame in a combustion chamber. This is achieved by correlating the chemiluminescence signal intensity to the local temperature and equivalence ratio.

The effect of the equivalence ratio on the chemiluminescence signal was investigated further by Muruganandam et al. [54] for a more practical application. In this investigation, the intensity of the OH*/CH* chemiluminescence signal of natural gas combustion was related to the equivalence ratio. It was known that when the equivalence ratio approached stoichiometric conditions the chemiluminescence signal would increase. This finding inspired the idea of introducing a chemiluminescence system in gas turbines for equivalence ratio and temperature monitoring. In their research it was again found that the OH*/CH* radicals were a good indication for the equivalence ratio of natural gas. Similar approach in the application of this method was considered by Nori et al. [39].

The influence of the pressure on the OH* chemiluminescence intensity was researched by Higgins et al. [55]. In this experiment a Bunsen burner was placed in a pressure vessel. The Bunsen burner was observed from the outside of the vessel through a quartz window. From the experiment it was found that the chemiluminescence intensity of the flame diminishes with increasing pressure. The increase of the mass flow rate on the other hand increased the chemiluminescence intensity. The emission of the OH* chemiluminescence was found to increase linearly with increasing the mass flow rate.

From this overview one can observe the versatility of the technique in determining important combustion parameters. It has been shown that the OH/CH chemiluminescence emission can be used as an indicator for the flame front. In addition the light emissions of these radicals are correlated to the mixture composition and temperature.

1.8 Research Objective

It was found that the laminar flame speed measurements for natural gas are generally lacking in documentation. This research is therefore aimed to obtain the burning characteristics for Dutch natural gas to extend on the existing data of natural gas. To quantify the burning characteristics of Dutch natural gas, the laminar flame speed has to be experimentally determined. The presented data of the laminar flame speed of DNG in this report will provide additional information that can be used for the modeling of the combustion of low calorific natural gas.

Therefore the objective of this research is:

- Determine the laminar flame speed of Dutch Natural Gas over a large span of equivalence ratios using the OH chemiluminescence emission of a premixed Bunsen burner flame, by means of the mass conservation method and flame cone angle method.

From this objective the following main question is stated:

- What is the influence of the equivalence ratio on the laminar flame speed of DNG?
- Is there a difference between the laminar flame speed using the mass conservation method and the flame cone angle method if so, what is this difference?

The following sub-questions are required to be answered based on the observations in the experiment and analysis:

- What is the precision and accuracy of the OH chemiluminescence method in the determination of the laminar flame velocity of DNG using the mass conservation method and semi-cone angle method?
- How does the increase of the mass flow rate influence the laminar flame speed measurement using the semi-cone angle and mass conservation method?
- How does the laminar flame speed of Dutch natural gas compare to gas from other regions?
- What is the influence of the unsteadiness of the flame on the laminar flame speed measurement?
- How can the source of the uncertainty of the laminar flame speed measurement be identified?
- What is difference between the laminar flame speed measurements using Bunsen flame method compared to other measurement techniques?

Ch.2 Experimental setup

2.1 Experimental design requirements

The goal of this experiment is to obtain the laminar flame speed of DNG using the OH* emission of the premixed Bunsen burner flame. Therefore the experimental setup needs to have the necessary equipment, in order to accurately determine the reaction zone location and measure the magnitude of the flow rate of the unburned mixture. In addition the air and DNG flow rates needs to be accurately controlled in order to obtain the required equivalence ratios. Therefore the requirements for the experimental setup are as follows:

- A stationary and stable Bunsen burner flame needs to be established for a wide range of equivalence ratios.
- To locate the reaction zone, OH* emissions of the Bunsen burner flame has to be recorder.
- The air flow and fuel flow rate is required to be measured and controlled in order to vary the equivalence ratio of the mixture
- Air and DNG must be fully mixed before combustion in order to obtain a premixed Bunsen burner flame.
- To determine the steadiness of the Bunsen flame multiple images has to be recorded for each equivalence ratio.

For these requirements the experimental setup shown in Fig.2 is designed and employed. For this experiment the flame resides in atmospheric conditions and room temperature (approximately 293K).

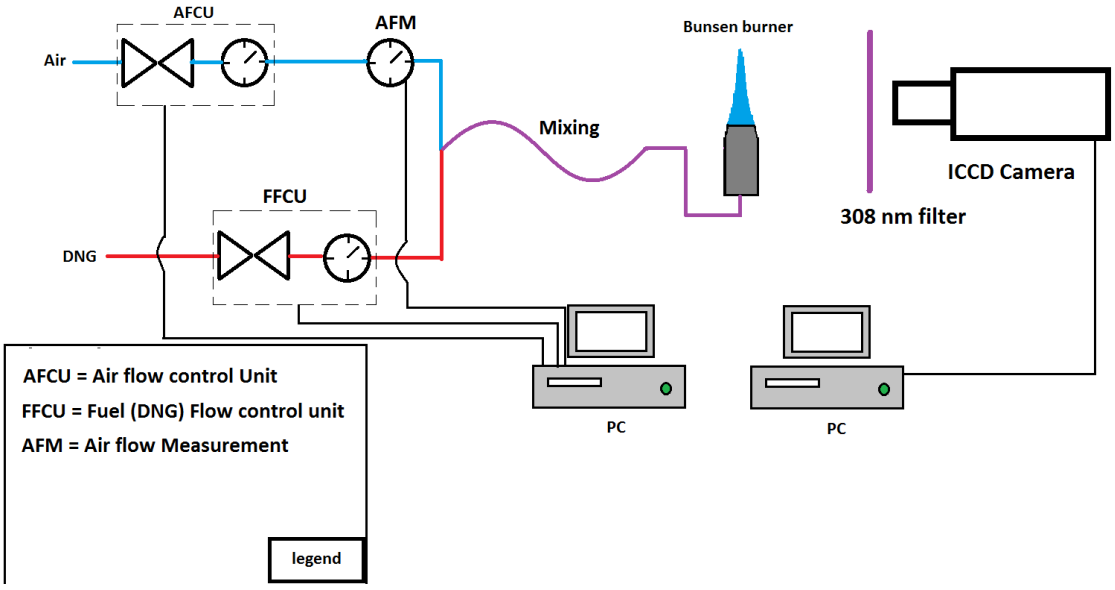

Fig. 2: Schematic of the experimental setup employed in this research.

2.2 Apparatus

In this experimental setup the flow of DNG and air is governed by LABVIEW. LABVIEW provides a graphical user interface (GUI) to easily control the flow rates of both air and fuel. This software also registers the fluctuations of the flow rates at an acquisition rate of 15Hz, during the recording of the OH* emission of the Bunsen burner flame.

Similar to the flow control units, the camera is governed by a separate computer using the software provided by Optronis. In this experiment an Intensified Charge Coupled Device (ICCD) camera from Optronis is used to record the OH* emission of the Bunsen burner flame. It was shown that the OH* emission ranges in the optical spectrum between 300~310 nm. Therefore to omit the other light spectrums a 308nm filter is used. This optical filter is placed on the camera lens and acts as a band pass filter. The images of the Bunsen burner flame recorded from this setup will mainly show the OH* emission of the flame.

The images are recorded at a resolution of 1280x512. To assess the variation of the Bunsen burner flame in time, 1000 images are taken at an acquisition rate of 1 kHz. This is the maximum FPS the camera can provide at the given image resolution. The camera exposure time was set to 400 microseconds and the intensifier gain was set to 2200, in order to clearly visualize the OH* emission of the Bunsen burner flame on the recorded images. These settings yielded the best image quality and were determined during the experiment. The camera settings and specifications are tabulated in Table 1.

Table 1: Image data used in the analysis and the camera settings.

The image Specifications and acquisition rate	Values
Image resolution	1280x512
CMOS chip pixel size	14 μm X 14 μm
Image acquisition rate	1000 frames per second (FPS)
Exposure time	400 μsec
Intensifier gain	2200

In this table the exposure time indicates the time that the camera photo detector is exposed to the flame radiation. If a short exposure time is used the flame will appear dim in the recorded image. If a long exposure time is used then the flame will appear bright and blurred. A short exposure time is used here to avoid oversaturation of the recorded OH* emission of the flame. Additionally the contrast of the recorded OH*emission of the flame is improved, by fast registration of the unsteadiness in the Bunsen flame. The intensifier gain is a feature of the ICCD camera which multiplies the original photons collected from the flame radiation before they are detected by the CMOS chip. This increases the flame brightness on the recorded image while avoiding oversaturation. These settings remain constant throughout the experiment.

Table 2: The data on the operational range of the volumetric flow rate controllers and measurement devices in the experiment

Volumetric flow rate controllers and measurement devices	Operational range in l_n/min from minimum to Full Scale (FS) (or maximum)
FFCU	0.6 l_n/min. to 30 l_n/min.
AFCU	0.6 l_n/min. to 500 l_n/min.
AFM	0.6 l_n/min to 48 l_n/min

The flow rate of DNG is measured and controlled by the fuel flow control unit (FFCU) provided by Bronkhorst. The measurement is shown in the LABVIEW GUI in real time and given in normal liters per minute (nl/min). This indicates that the measured volumetric flow rate is calculated back to normal conditions and presented. The normal condition is defined as the condition of the fluid (in this case DNG and air) at 0 degrees Celsius and 1 bar atmospheric pressure [56]. The flow rate of air is controlled by the air flow control unit (AFCU) provided by the same manufacturer. Due to the large operational range of the AFCU the measurement of the air flow cannot be accurately detected. Therefore an additional air flow measurement (AFM) device is added in series at the air flow line as shown in Fig.2. This additional Air flow measurement unit has a shorter operation range and is therefore more accurate in the measurement of the volumetric air flow rate.

All the used flow control units and measurement devices were calibrated by Bronkhorst for each flow type. The limits of the AFCU, FFCU and AFM are shown in Table 2. The operational range of FFCU and AFM are required for the determination of the accuracy of the measured volumetric flow rates of DNG and air.

2.2.1 Bunsen burner design

The purpose of the Bunsen burner is to achieve a stable laminar Bunsen flame at the burner tip over a wide range of equivalence ratios. For the manufacturing of this burner a stainless steel tube is used. The dimensioning of the burner is obtained from the following additional requirements:

- The unburned mixture must have a fully developed laminar flow at the burner exit.
- The Bunsen burner must be simple to manufacture.
- The interaction of the burner rim with the flame must be kept at a minimum to minimize the heat transfer from the flame and flow irregularities.

To obtain a fully developed laminar flow the Reynolds number of the unburned mixture may not exceed 2000 **[57].** This requirement gives an indication on the diameter of the burner. Consider the definition of the Reynolds number for a circular tube given as:

$$R_e = \frac{U_0 D_h}{\bar{\nu}} \tag{21}$$

In this equation D_h is the hydraulic diameter in millimeters, U_0 is the average velocity in m/s the tube and $\bar{\nu}$ is the average dynamic viscosity of the mixture in m^2/s. The average dynamic viscosity of the

mixture is obtained from the dynamic viscosity of Dutch natural gas and air as given in literature [58] [59] respectively. The hydraulic diameter is the diameter of the wetted area of the tube. The average velocity in the tube is given by the definition of the total volumetric flow rate $\dot{V}_{total}$:

$$U_0 = \frac{\dot{V}_{total}}{A_e} \tag{22a}$$

In this expression A_e is the burner exit area in mm^2. If the tube is a circular shape then the hydraulic diameter is equal to the geometric diameter $D_h = D$. Therefore the equation for the burner exit area can be written in terms of the hydraulic diameter as:

$$A_e = \frac{\pi}{4} D_h^2 \tag{22b}$$

Substitution of Eq.22b into Eq.22a and subsequently in Eq.21 gives the expression of the Reynolds number in terms of the total volumetric flow rate:

$$R_e = \frac{4}{\pi} \frac{\dot{V}_{total}}{D_h \bar{\nu}} \leq 2000 \tag{23}$$

The Reynolds number required to maintain a laminar flow of the unburned mixture shows that this equation must be lower or equal to 2000. For each chosen volumetric flow rate a series of diameters can be obtained that satisfies this condition. To simplify the manufacturing process of the burner, the calculated diameter must be equal to one of the standard dimensions of a stainless steel pipe.

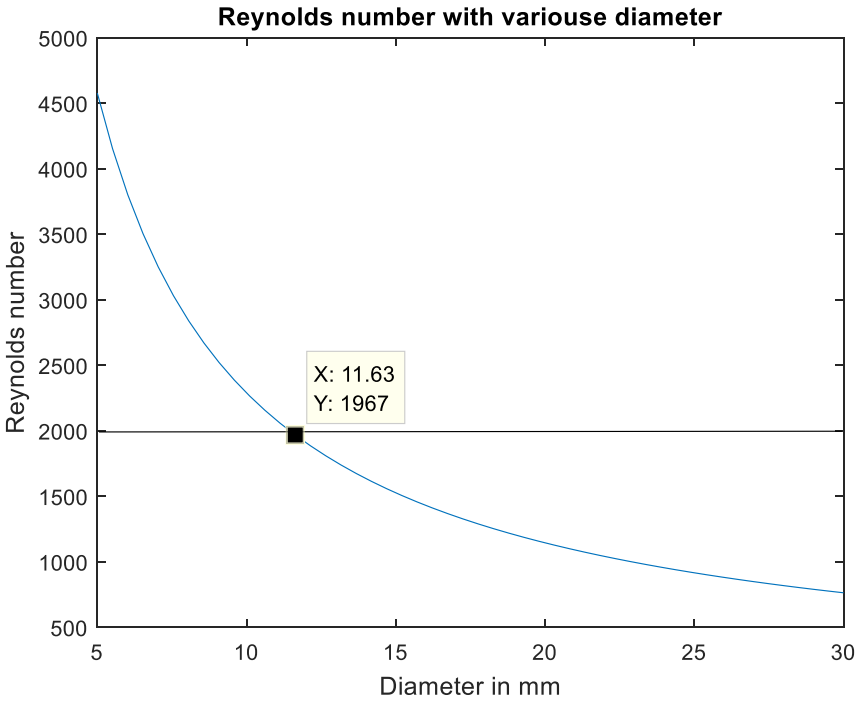

Fig.2.1: Variation of the Reynolds number with variouse diameters at constant flow rate of 16 liter/min

For the dimensioning, a total volumetric flow rate is assumed based on similar experiments performed by Hu et al. [60]. This experiment showed that a typical total volumetric flow rate of a stable Bunsen burner flame used to determine the laminar flame speed is approximately 8 l/min. This is an indication to the stability range of a typical flame corresponding to a hydrocarbon fuel. In order to improve the range of volumetric flow rates of the burner in which a fully

developed laminar flow is maintained, this value is multiplied by a factor of 2. Using Eq.23 in combination with the total volumetric flow rate and varying the diameter of the tube, results in the graph shown in Fig.2.1. From this figure the diameter that satisfies the Reynolds number condition is shown to be 11.6 mm. However, this dimension does not satisfy the standard pipe dimension constraint. Therefore the diameter is rounded up to 12mm which satisfies the Reynolds number and the manufacturing constraint. The diameter of a tube type Bunsen burner for any hydrocarbon fuel that satisfies the flame stability is usually in the order of 10 mm [34]. Therefore, it is expected that this design also satisfies the flame stability conditions discussed earlier.

The final dimension is the burner length which is determined from the empirical relation [57]:

$$\frac{L_e}{D_h} \approx C_1 + C_2 R_e \tag{24}$$

In this expression L_e is the effective tube length defined by the location of the flow entry until the location where the flow starts to fully develop, C_1 and C_2 are constants typically set to 0.5 and 0.05 respectively. This empirical expression relates the ratio of the tube length and diameter to the Reynolds number. From the definition of the effective length it is clear that to obtain a fully developed flow the tube length must be larger than the effective length. As such from the Reynolds number corresponding to a tube diameter of 12mm, an effective length of 0.9m is obtained. Thus the length of tube must be larger than 0.9m to achieve a fully developed laminar flow, hence a nominal tube length of 1m is chosen.

From this analysis a Bunsen burner is designed that satisfies the first burner requirement. The second requirement requires the minimization of the interaction of the flame and the burner rim. To satisfy this requirement the burner rim has to be modified. From the investigation of Ishida [61] it was found that the heat transfer of the flame to burner rim can be lowered by introducing a tapered burner rim. By

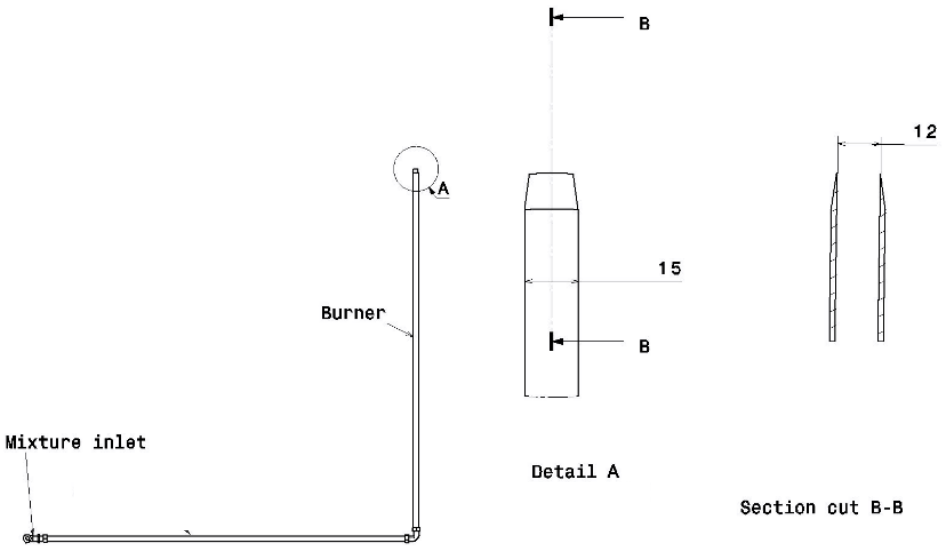

Fig. 2.2: Schematic of the burner employed in the experiment.

introducing a tapered burner rim, the heat extraction of the flame is reduced. In addition introducing taper reduces the flow irregularities that may influence the steadiness of the flame. However, introducing taper reduces the flame stability due to the reduction in the recirculation zone at the burner rim compared to an un-tapered burner [62]. It should be noted that the effect of introducing a taper is minimal to the stability of the flame. To ensure that the Bunsen burner flame remains stationary and the flow irregularities at the burner rim are at a minimum, a taper is introduced at the burner exit. To allow for this modification an outer diameter of 15 mm is chosen. With this final modification to the burner rim, the burner is fully defined. The schematic of the Bunsen burner is shown in Fig.2.2.

2.3 Experimental reliability and accuracy

The error that is involved in this experiment is inherited by the inaccuracy of the used components in the experimental setup. In this experiment one of the sources of the errors that are involved that influence the laminar flame speed measurement and the equivalence ratio, are the volumetric flow rates of air and DNG. The inaccuracies of the volumetric flow rate components are given by the manufacturer Bronkhorst to be of the form:

$$\Delta\dot{V} = 0.5\%\ RD + \ 0.1\%\ FS \tag{25}$$

In this expression *RD* is the actual read out of the measurement from the volumetric flow rate meter and *FS* is the maximum flow rate commonly referred to as the full scale of this component. The value for the maximum range of the volumetric flow measurement units (FFCU) and (AFM) were given in Table 2. The read out is what has been measured for the volumetric flow rates to obtain the required equivalence ratios.

Note that the method involved in determining the equivalence ratio range is discussed in the methodology chapter. In here the emphasis is placed on the determination of the inaccuracy of the equivalence ratio.

2.3.1 Inaccuracy of the equivalence ratio

The error propagation of a relation $f(x_1, x_2, x_3, \dots, x_n)$ relying on independently measured quantities $(x_1, x_2, x_3, \dots, x_n)$, with each having an absolute measurement error Δx_i , can be determined by the following general equation [63] [64]:

$$\Delta f(x_1, x_2, x_3, \dots) = \sqrt{\left(\frac{\partial f}{\partial x_1}\Delta x_1\right)^2 + \left(\frac{\partial f}{\partial x_2}\Delta x_2\right)^2 + \left(\frac{\partial f}{\partial x_3}\Delta x_3\right)^2 + \cdots + \left(\frac{\partial f}{\partial x_n}\Delta x_n\right)^2} \tag{26}$$

The absolute error in the measurement of the volumetric flow rate of air and DNG influence the equivalence ratio. Recall the expression for the equivalence ratio given in Eq.15. This equivalence ratio is dependent on 2 independently measured parameters namely the volumetric flow rate of air and the volumetric flow rate of DNG. Therefore, by applying Eq.26 the equation of the absolute error in the equivalence ratio can be determined. This absolute error equation is given by:

$$\Delta\phi = \sqrt{\left[\left(\frac{\partial\phi}{\partial\dot{V}_{DNG}}\Delta\dot{V}_{DNG}\right)^2 + \left(\frac{\partial\phi}{\partial\dot{V}_{air}}\Delta\dot{V}_{air}\right)^2\right]} \quad (27)$$

From this expression the absolute error in the equivalence ratio is found to be:

$$\Delta\phi = \frac{1}{FAR_{stoich}}\sqrt{\left[\left(\frac{\Delta\dot{V}_{DNG}}{\dot{V}_{air}}\right)^2 + \left(\frac{\dot{V}_{DNG}}{\dot{V}_{air}^2}\Delta\dot{V}_{air}\right)^2\right]} \quad (28)$$

For the derivation of this equation the reader is referred to Appendix A. In this equation $\dot{V}_{DNG}$ is the volumetric flow rate of DNG, $\dot{V}_{air}$ is the volumetric flow rate of air, $\Delta\dot{V}_{DNG}$ is the absolute error in the measurement of the volumetric flow rate of DNG and $\Delta\dot{V}_{air}$ is the absolute error in the measurement of the volumetric flow rate of air.

Dividing the absolute error of the equivalence ratio to the exact equivalence ratio $\frac{\Delta\phi}{\phi}$ gives the relative error. A maximum relative error of 4.92% and a minimum relative error of 3.07% are present in the equivalence ratios employed in this experiment. A detailed value of the relative error for the equivalence ratios realized in this experiment is tabulated in Table 3.

Table 3: The relative error in % of the equivalence ratio due to the inaccuracy of the flow controllers

ϕ	0.80	0.88	0.93	1.00	1.06	1.15	1.20	1.36	1.41	1.45	1.50	1.53	1.55
$\dot{V}_{air}$	7.14	7.14	7.19	7.09	7.11	6.97	6.97	6.96	6.87	6.81	6.78	6.77	6.77
$\dot{V}_{DNG}$	0.68	0.75	0.79	0.85	0.89	0.95	0.99	1.12	1.15	1.17	1.21	1.23	1.25
$\frac{\Delta\phi}{\phi}$%	4.92	4.55	4.32	4.13	3.91	3.74	3.61	3.28	3.24	3.20	3.13	3.09	3.07

Note that the equivalence ratio is increasing in a non-linear fashion. This will be discussed in the next section.

Ch.3 Methodology

The variation of the laminar flame speed w.r.t. equivalence ratio is required to be measured in order to answer the main questions of this research. Therefore the equivalence ratio range has to be determined. In addition, the total unburned gas velocity that corresponds to a stable Bunsen burner flame has to be obtained. Recall that the total volumetric flow rate is an indication to the total unburned gas velocity by the relation $\dot{V}_{total} = A_e U_0$ in which U_0 is the unburned mixture velocity. Therefore the total volumetric flow rate was used instead to achieve a stable Bunsen burner flame. This is due to the readily available measurements for the fuel and air flow in the experimental setup.

For the determination of the total volumetric flow rate an initial test was conducted. In this test the stability limit of the Bunsen burner was investigated for a fuel lean mixture. This test will indicate the lower limit of the equivalence ratio span that still allows for a Bunsen flame for this burner where no blow off occurs. This equivalence ratio was found to be $\phi = 0.80$. Once this equivalence ratio was determined, the volumetric flow rate of air and fuel was increased, such that this equivalence ratio was maintained by minimizing its variation, until blow off of the flame was observed.

The total volumetric flow rate was then determined from the equation:

$$\dot{V}_{total} = \dot{V}_{DNG} + \dot{V}_{air} \tag{29}$$

From this test the total volumetric flow rate for a stable Bunsen burner flame corresponding to the lower limit of the equivalence ratio span was found. This total volumetric flow rate obtained from this test was found to be 7.82nl/min.

Ideally in the experiment to determine the laminar flame speed of DNG, the total volumetric flow rate should remain constant for each equivalence ratio. However, maintaining the total volumetric flow rate constant is difficult in practice. Therefore, the variation of the total volumetric flow rate for each equivalences ratio was kept at a minimum during the experiment.

3.1 Determining the equivalence ratio span

In order to obtain the required equivalence ratio the volumetric flow rate for air and DNG is varied, such that the variation in the total volumetric flow rate was kept at a minimum. Through this method, the laminar flame speed will be mainly affected by the change in the constituents of the mixture. To determine the equivalence ratio span, the stoichiometric fuel to air ratio for DNG has to be computed. This requires knowledge about the fuel composition of DNG. The composition of DNG is given in Table 4.

Table 4: The composition of Dutch Natural Gas according to Derrenberger et al. [21]

Species	CH_4	C_2H_6	C_3H_8	$i-C_4H_{10}$	N_2	CO_2
Volumetric fraction in %	81.3	2.9	0.4	0.2	14.3	0.9

The equivalence ratio is calculated using Eq.15. The stoichiometric fuel to air ratio is obtained from employing Eq.14 for the species in DNG. Using the species given in Table 4 it was found that $\alpha = 0.900$, $\beta = 3.478$ and $\gamma = 0.018$. Solving the chemical equilibrium for DNG using the values for α, β and γ, the moles of air required for complete combustion is found. This resulted in $n_{air} = 8.38$ which is comparable to what was documented in literature [65]. Note that in the combustion community the composition of air is typically accepted to consist of 79% N_2 and 21% O_2 [25]. For the complete derivation to obtain the moles of air required for the complete combustion of DNG, the reader is referred to Appendix A.

The volumetric based stoichiometric fuel to air ratio is then found from Eq.14 which results in:

$$FAR_{stoich} = \frac{n_{fuel}}{n_{air}} = \frac{1}{8.38} = 0.119$$

The actual fuel to air ratio (FAR_{act}) is determined from the ratio between the volumetric flow rate of DNG $\dot{V}_{DNG}$ and the volumetric flow rate of air $\dot{V}_{air}$:

$$FAR_{act} = \frac{\dot{V}_{DNG}}{\dot{V}_{air}} \tag{30}$$

The range of the equivalence ratio can now be determined. For this research a wide range of equivalence ratio is required in order to cover a broad spectrum of mixture qualities. For this purpose the equivalence ratio for the lean blow off limit which was found to be $\phi = 0.80$, was used as the starting point and increased gradually with a step size of 0.05 until an equivalence ratio of 1.55 was reached. In practice, maintaining this step size constant appeared to be difficult therefore some variation were allowed. The equivalence ratios used in this experiment, while keeping the variation of the total volumetric flow at a minimum are shown in Table 5.

Table 5: The equivalence ratio obtained from the volumetric flow rate of DNG and air.

Equivalence ratio ϕ	Total volumetric flow rate in l_n/min $\dot{V}_{tot}$	Volumetric flow rate of DNG in l_n/min $\dot{V}_{DNG}$	Volumetric flow rate of air in l_n/min $\dot{V}_{air}$
0.80	7.82	0.68	7.14
0.88	7.89	0.75	7.14
0.93	7.99	0.79	7.19
1.00	7.94	0.85	7.09
1.06	8.01	0.89	7.11
1.15	7.92	0.95	6.97
1.20	7.97	0.99	6.97
1.36	8.09	1.12	6.96
1.41	8.02	1.15	6.87
1.45	7.98	1.17	6.81
1.50	7.99	1.21	6.78
1.53	8.00	1.23	6.77
1.55	8.02	1.25	6.77

3.2 Image analysis algorithms

For each equivalence ratio, 1000 images are taken from the corresponding OH* emission of the Bunsen flame. Additionally the fuel and air flow rates are registered and stored simultaneously during the recording of the flame at an acquisition rate of 15Hz. The data is then analyzed using a MATLAB algorithm to obtain the laminar flame speed of DNG.

Two methods are commonly used in which the laminar flame speed of a Bunsen burner flame can be obtained. Namely:

- The semi-cone angle method
- The mass conservation method using the flame front area.

In the analysis of the images, both methods are employed in the algorithms to obtain the laminar flame speed. The average of the laminar flame speed obtained from the images is then presented. The principle of the MATLAB algorithm employed to obtain the semi-cone angle and the flame surface area are discussed.

3.2.1 Image analysis algorithm semi-cone angle method

The semi-cone angle method used to determine the laminar flame speed of a conic flame is given by Eq.16. In this expression the laminar flame speed is determined using the average bulk velocity obtained from Eq.22a and the semi-cone angle of the Bunsen flame.

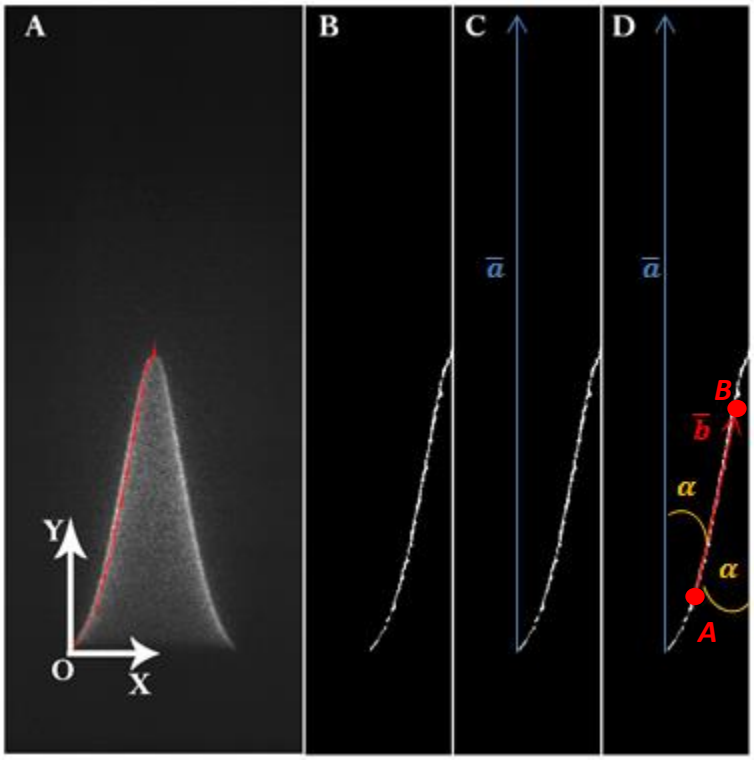

Fig. 3a, b, c and d: The visual process of the MATLAB algorithm to determine the semi-cone angle of the Bunsen flame.

The semi-cone angle of the Bunsen flame is determined from the maximum OH* emission recorded in the images. The process of this algorithm is shown in Fig.3. The program considers half the image by employing the symmetrical property of a Bunsen burner flame.

The original image as shown in Fig.3a is first converted into a binary image for 1 half of the flame as shown in Fig.3b. In here the left half of the flame is considered. Next, a direction vector $\bar{a}$ is defined along the y-axis at the edge of the flame base as shown in Fig.3c. In the same way a direction vector $\bar{b}$ is defined at the flame contour as shown in Fig.3d. This vector is fixed at 30% of the flame height at point ***A*** and is directed towards point ***B***. Point ***B*** is

positioned on the flame contour at 80% of the flame height.

The semi-cone angle can then be derived from the definition of the dot product given by:

$$\bar{\boldsymbol{a}} \cdot \bar{\boldsymbol{b}} = |\bar{\boldsymbol{a}}||\bar{\boldsymbol{b}}| \cos(\alpha) \tag{31}$$

Rearranging this equation and solving for the semi-cone angle α the following expression is obtained:

$$\alpha = \cos^{-1}\left(\frac{\bar{\boldsymbol{a}} \cdot \bar{\boldsymbol{b}}}{|\bar{\boldsymbol{a}}||\bar{\boldsymbol{b}}|}\right) \tag{32}$$

Note that vector $\bar{\boldsymbol{b}}$ is defined w.r.t. the flame height. Hence the flame height has to be determined in order to use this algorithm. The flame height is found from the OH* emission of the Bunsen flame recorded in the image along the symmetry axis, extracted from top of the image to the location of the flame base. The process is shown in Fig.3.1a. The normalized brightness distribution of the OH* emission obtained from this method is shown in Fig.3.1b. The flame tip location is readily found at the inflection point. The flame height can then be determined from the equation:

$$h = H - T - B \tag{33}$$

In this expression *H* is the total image height, *T* is the distance to the flame tip from the upper boundary of the image, and *B* is the location of the flame base from the lower boundary of the image as shown in Fig.3.1a.

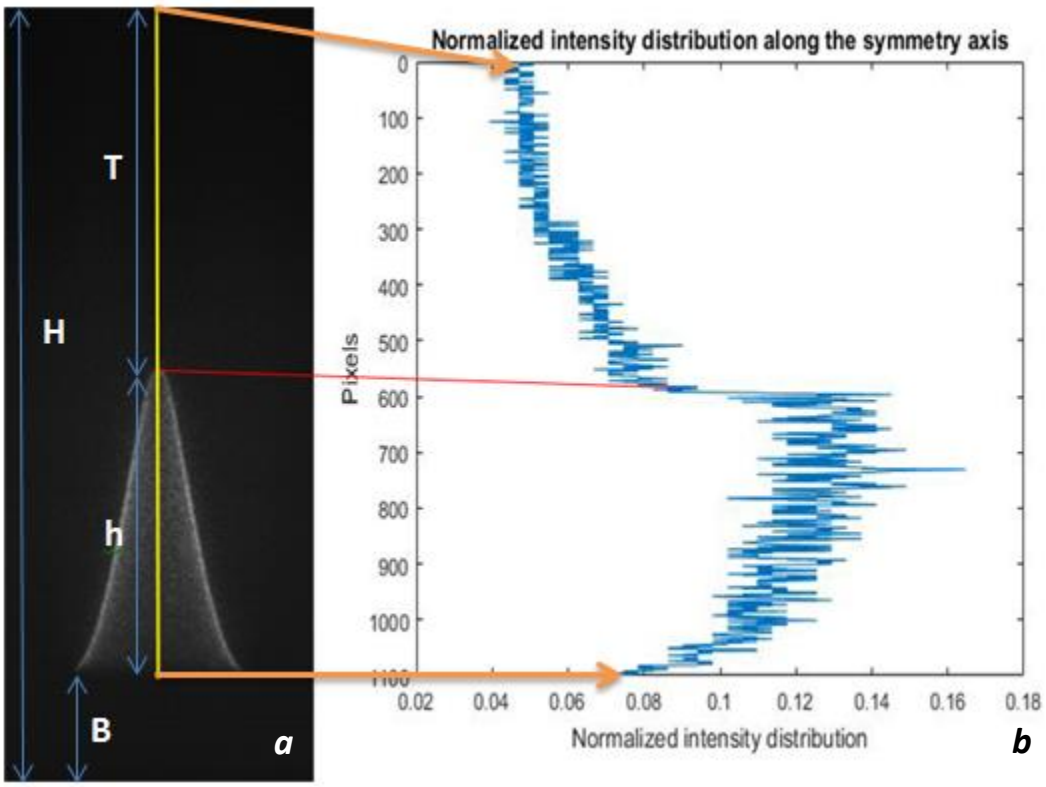

Fig. 3.1a and 3.1b : The determination of the flame height in the image using the brightness distribution along the symmetry axis.

Note that there are cases in which the flame tip of the Bunsen flame is not present due to local extinction this phenomenon is called tip opening. It is clear that this method will not be suitable for determination of the flame height in such a situation. Therefore an exception is made in the algorithm for the case in which tip opening is present. In this exception the value of the flame height is hard coded, in which the flame height was manually determined.

3.2.2 The algorithm of the mass conservation method

This method is based on the conservation of mass equation given in Eq.18. In this equation the total volumetric flow rate through the system is known. However, the flame area has to be determined from the OH* emission of the flame.

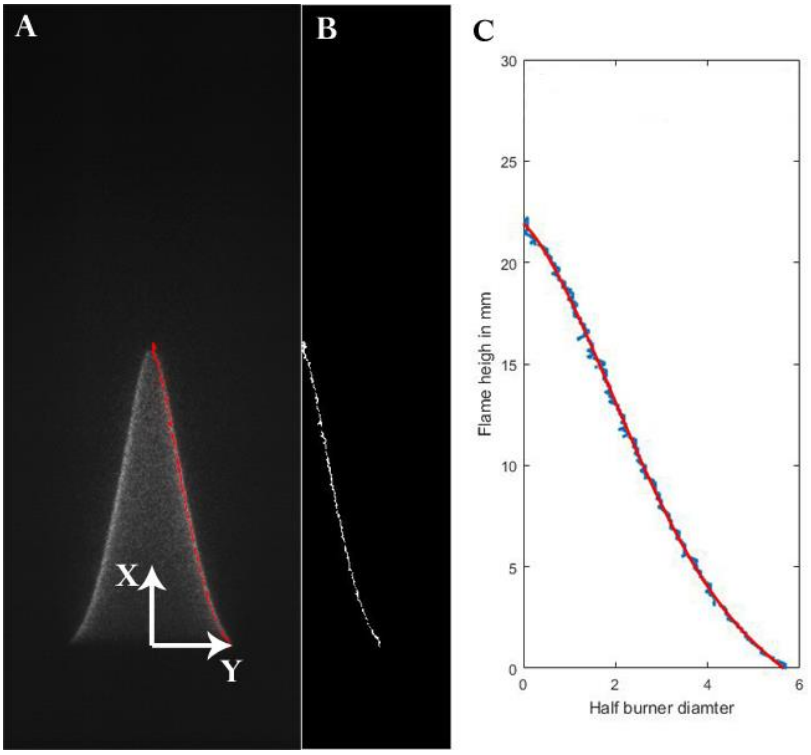

Fig. 3.2 a, b and c: The visual process of determining the flame area of the Bunsen flame.

There are many approaches in which the flame area can be determined. Such as the method used by Souflas et al. [66], in which the flame area was obtained from a CAD remodeling by extracting the maximum OH* emission of the flame. However, this method is unsuitable for this case since a large number of images have to be analyzed.

A more often encountered method is based on the axisymmetric property of the Bunsen burner flame. Observing half the Bunsen burner flame, the shape of this half represents a function $f(x)$. The maximum OH* emissions can then be viewed as data points that describe the flame contour. The area of an axisymmetric shape, with its contour represented by a function $f(x)$ can be found from the expression [67]:

$$A_f = 2\pi \int_a^b f(x) \sqrt{1 + \left(\frac{df(x)}{dx}\right)^2}\, dx \qquad (34)$$

This expression gives the area of a revolved surface around the x-axis, with is contour described by the function $f(x)$. Hence, in order to use this equation, a function $f(x)$ must be found that describes half the flame contour, this process is shown in Fig.3.2. This method is employed in many experiments in order to obtain the flame area [33] [68] [69] [70]. In this method it was found to be analytically convenient to define the axis system as shown in Fig.3.2a.

In some experiments it was noted that the recorded OH* emission of a Bunsen flame is Abel inverted to eliminate the effect of the line of sight techniques. The Abel inverted image is then used to obtain the flame contour of the Bunsen flame. However, it was shown by Bouvet et al. [29] that the Abel inversion of the recorded OH* emission of the Bunsen flame had almost no influence on the extracted flame contour. Therefore in this experiment where a large number of images have to be analyzed, the Abel inversion of the Bunsen flame has been omitted to reduce the calculation time of each image using this algorithm.

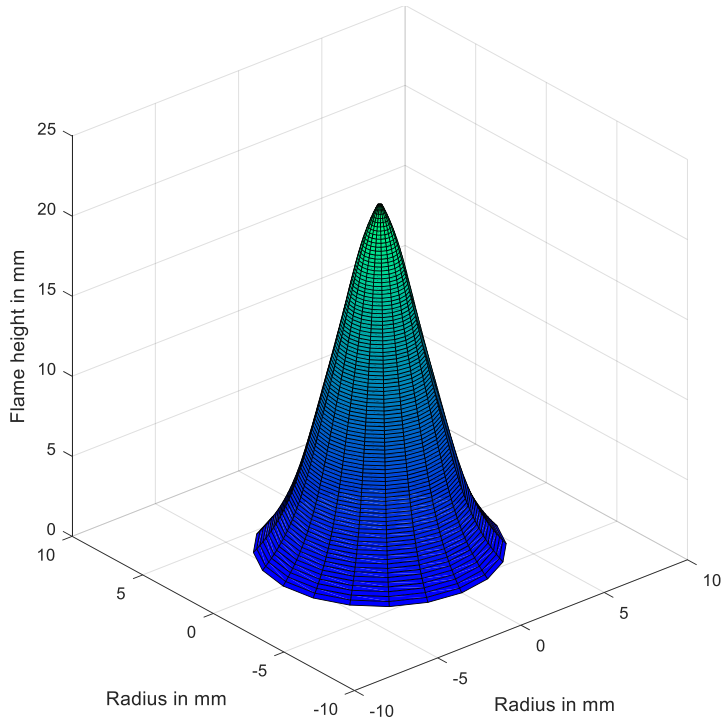

Fig. 3.3: The Bunsen flame reconstructed using the revolved surface area method for$\phi = 1.06$.

From the original image shown in Fig 3.2a half the flame is converted to a binary image depicted in Fig.3.2b by extracting the maximum trace of the OH* emission. To obtain the flame area in spatial dimensions, the digital resolution is used.

The digital resolution of the image is obtained by using an object with a known spatial dimension in that image. In the derivation of the digital resolution of the image the burner exit diameter is used. Recall that the burner exit diameter was known to be 12mm. This burner exit diameter is equal to the length of the flame base in the image. Taking the length of the flame base in number of pixels, the digital resolution was obtained by dividing this value with the burner exit diameter. The digital resolution of the image is found to be 24 pixels per millimeter for this case. Using this digital resolution, the flame dimension in the image is converted to spatial dimensions as shown in Fig.3.2c.

From this plot the function to describe the flame contour was obtained using the Polyfit package in MATLAB. In here a 5th order polynomial was used given in the form:

$$f(x) = y = a_0x^5 + a_1x^4 + a_2x^3 + a_3x^2 + a_4x + a_5 \quad (35)$$

In this expression the scales a_0 to a_5 are curve fitting constants. This curve fit is plotted in Fig.3.2c. This shows that a 5th order polynomial is indeed sufficient to describe the flame contour.

The derivative of this equation is given by:

$$\frac{df(x)}{dx} = \frac{dy}{dx} = 5a_o x^4 + 4a_1 x^3 + 3a_2 x^2 + 2a_3 x + a_4 \quad (36)$$

Substituting Eq.35 and Eq.36 in Eq.34 and subsequently evaluating the integral will result in the value of the flame area. In the algorithm the integral was evaluated using the trapezoid rule, a numeric integration method. The surface area of the premixed Bunsen flame with its contour described by Eq.35, revolved around the x-axis as depicted in Fig.3.3 is given by the Eq.34.

3.3 Accuracy and reliability of the algorithms

The accuracy and the reliability of the algorithms are investigated by identifying key elements used to determine the semi cone angle and the flame area. The key element in each algorithm is that the Bunsen burner flame is symmetric. Obviously in reality this is not necessarily true since the flame tip position can vary slightly in time due to unsteadiness. This introduces an error in the determination of the flame area and the semi-cone angle if the assumption of symmetry is used. Therefore the consequence of the assumption of symmetry needs to be quantified. In addition the determination of the semi-cone angle is based on 2 points defined on the un-curved section of the Bunsen flame. The points were defined at 80% and 30% of the flame height. However, one can use any set of combination of two points on the un-curved section to obtain the semi-cone angle in theory. In practice this does not have to be the case and should be verified. Therefore the effect of using a different combination to obtain the semi-cone angle has to be investigated.

3.3.1 The robustness of the semi-cone angle method algorithm

The semi-cone angle of the Bunsen burner flame was determined using two points of the flame contour at 30% and 80% of the flame height. These two points are selected such that the largest straight (un-curved) region of the flame contour is covered. The influence of the flame height percentage can be investigated, in which the two points are varied to observe the effect on the laminar flame speed. This has been performed on 5 different settings. The results on the average laminar flame speed are shown in Fig. 3.4. Note that the notation (x, y) here, depicts the location in percentage of the flame height (x) for the first point on the flame contour (*point **A***) and (y) of the second point (*point **B***) as was shown in Fig.3.

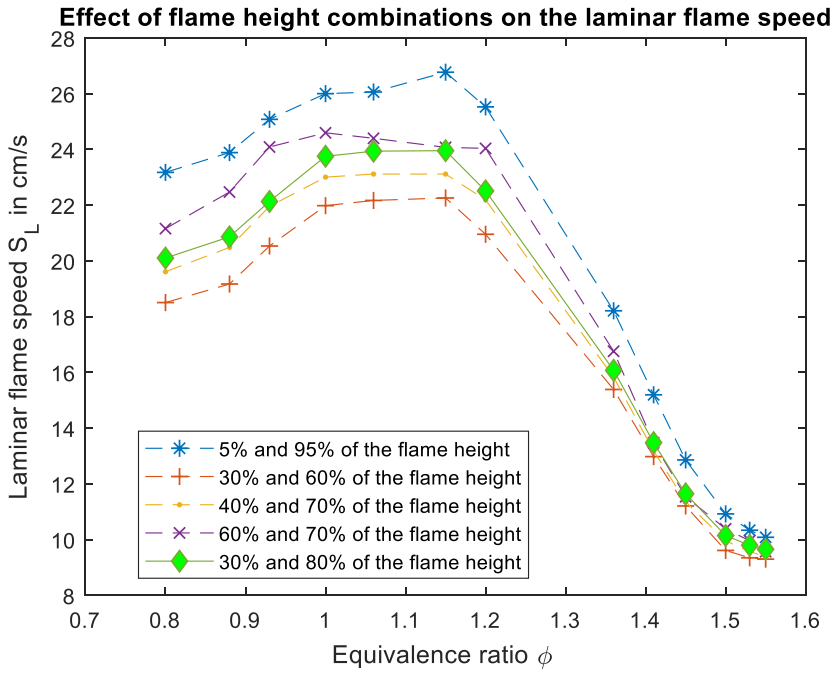

Fig. 3.4: The average laminar flame speed variation with using different combination for the two points on the flame contour as a percentage of the flame height.

Observe that the laminar flame speed magnitude changes when (5, 95) is used. This is due to the fact that the semi-cone angle is overestimated due to the misrepresentation of the flame cone as shown in Fig.3.5. The used points are no longer in the un-curved region of the Bunsen flame hence the laminar flame speed is overestimated.

A combination of (60, 70) shows a slight deviation from the proposed (30, 80) at near stoichiometric conditions. It shows that the laminar flame speed is well within the approximation given by the combination (30, 80).The combinations: (30, 80), (30, 60) and (40, 70), shows comparable results. The magnitude of the laminar flame speed corresponding with the combinations (30, 80) and (40, 70), is measured to be higher than the combination (30, 60). However, the discrepancy between these combinations is still close to or within the error margin of the combination (30, 80), this is shown in Fig.3.6.

In Fig.3.6 the laminar flame speed measurement according to the combination (30, 80), (40, 70), (60, 70) and (30, 60) is shown, including the uncertainty range of the measurement corresponding with the combination of (30, 80). Observing Fig.3.6 shows that the uncertainty of the combination (30, 80) indicated by the error bars, covers a large portion of the scatter band. This shows that a large portion of the uncertainty due to variation of the flame height in the semi-cone angle determination algorithm is in general implicitly included in the uncertainty of the combination (30, 80).

The variation of the laminar flame speed, between each combination w.r.t. the reference laminar flame speed $S_{L_{ref}}$ obtained from (30, 80) is shown in Table 6. Note that reference laminar flame speed $S_{L_{ref}}$ should not be confused with the upstretched laminar flame speed S_L^0 which is the laminar flame speed of an ideal flame. From this it can be concluded that a large portion of the un-curved section of the Bunsen flame should be covered to obtain the semi-cone angle. In this case this is provided by the combination (30, 80).

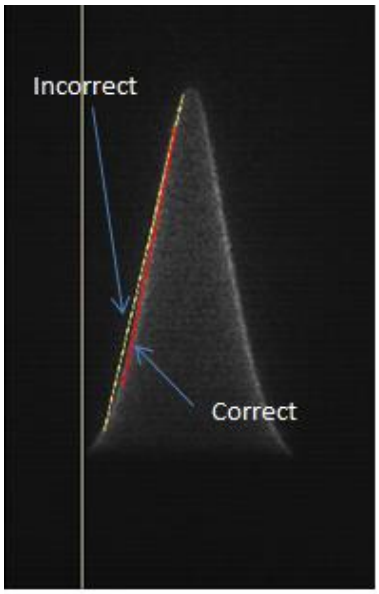

Fig. 3.5: Misrepresentation of the semi-cone angle using (5, 95).

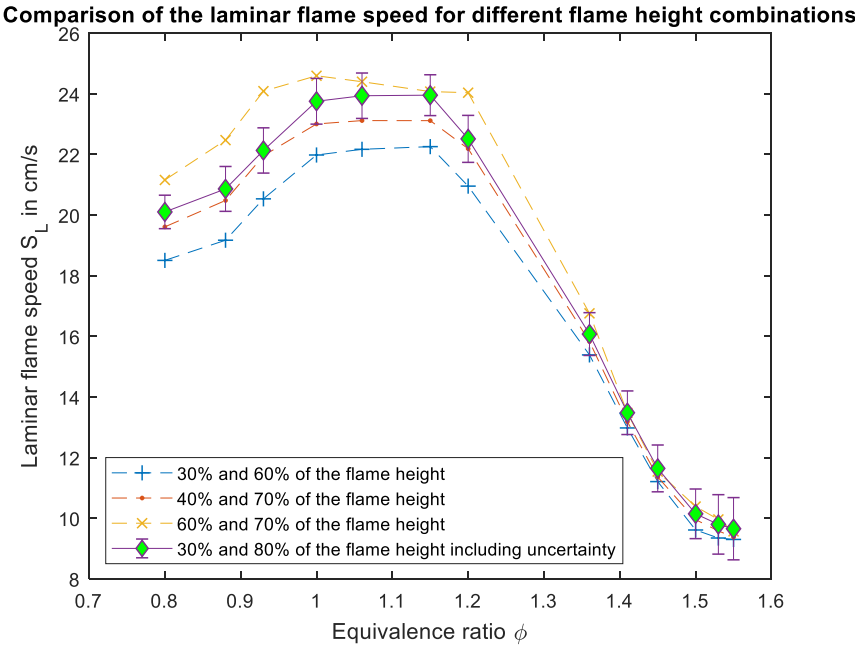

Fig. 3.6: The laminar flame speed behavior with equivalence ratio for combinations (30, 80), (40, 70), (30, 60) and (60, 70).

Table 6: The absolute variation of the laminar flame speed using different sets of points on the un-curved flame contour in percent

ϕ	0.80	0.88	0.93	1.00	1.06	1.15	1.20	1.36	1.41	1.45	1.50	1.53	1.55
$\frac{\Delta S_{L(40,70)}}{S_{L_{ref}}}$	2.45	1.83	0.78	3.15	3.43	3.51	1.44	1.54	2.18	2.43	1.90	2.20	2.89
$\frac{\Delta S_{L(30,60)}}{S_{L_{ref}}}$	7.95	8.11	7.21	7.46	7.38	7.08	6.92	4.28	3.72	3.73	5.26	4.58	3.67
$\frac{\Delta S_{L(60,70)}}{S_{L_{ref}}}$	5.24	7.71	8.84	3.54	1.93	0.50	6.76	4.25	0.04	0.89	2.37	1.66	0.90

3.3.2 Consequence of symmetry assumption

The algorithm for the measurement of the semi-cone angle and the flame surface area relies on the fundamental assumption that the Bunsen flame is symmetric. As was stated earlier, in practice the Bunsen flame does not necessarily have to be perfectly symmetrical. Since a perfectly symmetrical Bunsen flame corresponds to the ideal fully stationary flame. A fully stationary flame in practice is difficult to realize since the Bunsen flame will be influenced by surrounding drafts due to the air currents of the environment. Additionally the flow control valves of air and fuel may vary slightly in time which affects the flame. This variation and environmental air currents influences, the flame causing it to become slightly asymmetrical. Hence the consequence of the assumption of symmetry has to be taken into account. For this purpose the semi-cone angle has been determined from both halves of the flame and compared. Similarly the flame area has been computed for both halves of the flame. The relative

error is calculated w.r.t. the value of the semi-cone angle and flame area of the left hand side of the flame. The results are shown in Table 7 and Table 8 for the semi-cone angle and the flame area respectively. The subscript LHS stands for left hand side indicating that the value of the semi-cone angle and the flame area is obtained from the left hand side of the flame image.

Table 7: The effect of symmetry assumption on the semi-cone angle w.r.t. the cone angle of the LHS of the flame in %

ϕ	0.80	0.88	0.93	1.00	1.06	1.15	1.20	1.36	1.41	1.45	1.50	1.53	1.55
$\frac{\Delta\alpha}{\alpha_{LHS}}$	1.50	1.37	0.64	3.42	2.30	2.38	1.17	10.35	12.67	13.25	7.98	14.74	11.26

Table 8: The effect of symmetry assumption on the flame area w.r.t. the flame area of the LHS of the flame in %

ϕ	0.80	0.88	0.93	1.00	1.06	1.15	1.20	1.36	1.41	1.45	1.50	1.53	1.55
$\frac{\Delta A_f}{A_{f_{LHS}}}$	1.52	0.21	3.03	2.70	3.39	4.10	4.48	0.01	2.52	0.99	4.58	0.19	1.74

Comparing the tables, it can be deduced that the symmetry assumption has a more significant impact on the semi-cone angle compared to the flame area. The flame area is a surface, therefore if the flame is slightly asymmetric the flame area will not be significantly affected. The cone angle on the other hand depends on the un-curved section of the flame. Therefore if the flame is slightly asymmetric the cone angle estimated from 1 half of the flame is always larger than the other. It was observed that the difference between the average half flame cone angles obtained from the two flame halves can vary up to a maximum of 0.9 degrees.

For this reason, the average semi-cone angle is obtained from using both halves of the OH* emission of the Bunsen flame and subsequently, taking the average of the two results to determine the semi-cone angle. Similarly the flame area is determined from both halves of the flame and subsequently taking the average value of the two halves.

3.4 Uncertainty in the laminar flame speed

The uncertainty in the laminar flame speed is determined based on the random error. The random error is the error that occurs independently of the used equipment if the experiment is repeated. Therefore each measurement session will result in different value of the laminar flame speed. The source of the random error is generally thought to be the lack of observer precision. Due to the random nature of this type of error there is an equal chance that a measured value will be lower or higher than the mean value.

For instance the flame area and the semi-cone angle determination using the algorithms will lead to different value for each image. This value is independent on the previous value and appears to fluctuate randomly. These random errors are determined employing statistical methods by repeating the experiment multiple times and using the standard deviation (STD) to quantify its range. The standard

deviation is determined from the number of images (sample size) for each equivalence ratio. The uncertainty of the estimation of the laminar flame speed is given by the STD and presented as ΔS_L.

Additionally, the average laminar flame speed may vary for each experiment; therefore the average laminar flame speed should be documented with a certain confidence level. The uncertainty of the average laminar flame speed estimation is determined with 95% confidence. It is known that if large samples are taken (n ≥ 30); any series of measurements will have a probability density function (PDF) that resembles a Gaussian distribution [71]. This will be verified later on by deriving the PDF of the measurements. The error in the measurements of the average laminar flame speed is then given using a 95% confidence interval. The 95% confidence interval for a Gaussian distribution is given by [71]:

$$\Delta S_{L_{SEM}} = \pm Z \frac{\sigma}{\sqrt{n}} \tag{37}$$

In this expression σ is the standard deviation of the measurements, n is the sample size which is equal to 1000 in this experiment, and Z is the critical value. For a 95% confidence interval the critical value Z is given by the Normal distribution table in Appendix B and is found to be equal to 1.96. All the average laminar flame speed measurements presented in this report are given at 95% confidence.

Ch.4 Results & discussion

The laminar flame speed of DNG is determined using the semi-cone angle and mass conservation method. The variation of the laminar flame speed is indicated by the change in the flame height. This is shown in Fig.4.

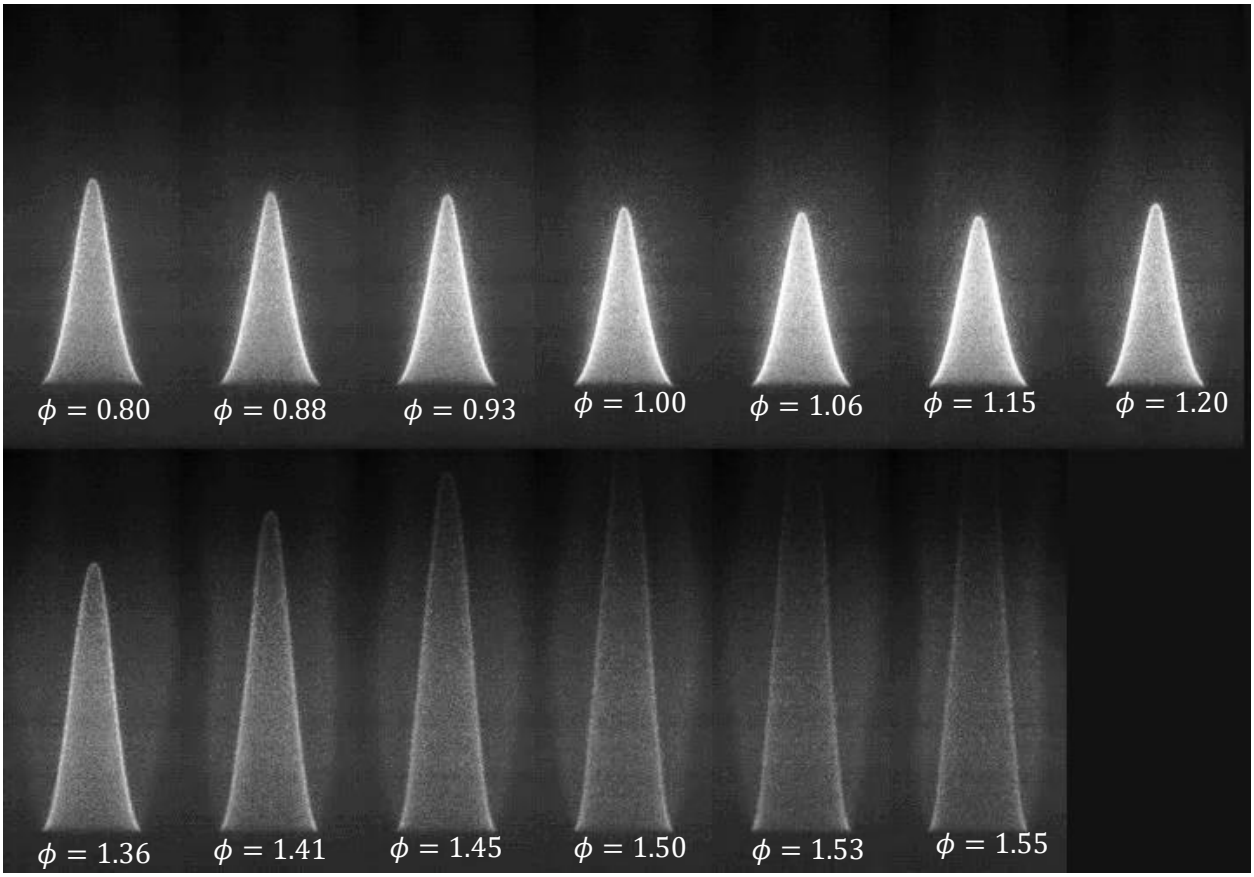

Fig. 4: Flame height variation with the equivalence ratio.

Observing the variation of the flame height as the mixture composition changes from lean to rich, it shows that the flame height reduces as the fuel to air ratio in the mixture approaches stoichiometry. Moreover the intensity of the chemiluminescence is shown to increase as the fuel to air ratio of the mixture approaches stoichiometry. The flame height and the chemiluminescence intensity, decreases as the mixture composition is increased beyond stoichiometry into the rich region.

This variation of the flame height influences the semi-cone angle and the flame area of the Bunsen burner flame. From this observation one can state that the semi-cone angle increases as the mixture composition approaches stoichiometry. If the mixture composition becomes rich in fuel then the semi cone angle decreases. For the flame area the opposite is true. The flame area decreases as the mixture composition approaches stoichiometry while the flame area increases if the mixture composition

becomes rich in fuel. This in turn influences the laminar flame speed of Dutch natural gas and is an indication for the flame velocity.

4.1 Laminar flame speed of DNG

In this experiment the equivalence ratio ranges from the point of lean blow off at $\phi = 0.80$ to rich $\phi = 1.55$ to cover a wide range of equivalence ratios for the determination of the laminar flame speed. The process of the experiment in order to obtain the laminar flame speed of DNG follows this direction from lean mixture to rich. The laminar flame speed is than obtained by using the flame cone method and the mass conservation method. The results using the semi-cone angle method and the mass conservation method is shown in Fig.4.1

The laminar flame speed obtained using both techniques are shown in Table 9 and Table 10 respectively. The laminar flame speed estimation according to the mass conservation method and semi-cone angle method is given by the super script *mc* and *sca* respectively. The standard error (S.E.) of the average laminar flame speed estimation from each method, indicated by the super script, is given by $\Delta S_{L_{SEM}}$.The uncertainty of the laminar flame speed corresponding with each method, indicated by the super script, is given by ΔS_L.The difference between the two methods is tabulated in Table 11 in percent w.r.t. the mass conservation method denoted as S_L^{mc}. In Table 11 the difference between the laminar flame speed of the mass conservation method and the semi cone angle method is given by the relation $\Delta S_L^{mc-sca} = S_L^{mc} - S_L^{sca}$.

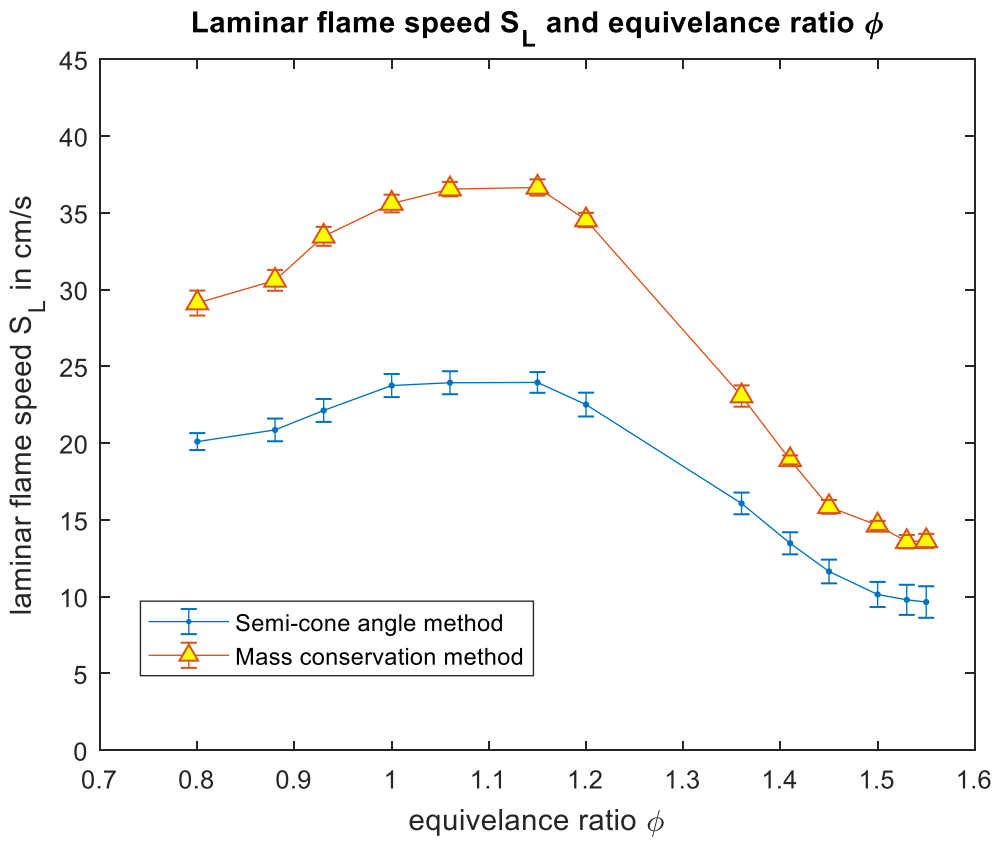

Fig. 4.1: The laminar flame speed as a function of the equivalence ratio using the semi cone angle method.

Table 9: The laminar flame speed according to the semi-cone angle method

Equivalence ratio ϕ	Mean laminar flame speed S_L^{sca} in cm/s	The mean laminar flame speed S.E. $\frac{\Delta S_{L_{SEM}}^{sca}}{S_L^{sca}}$ in %	Uncertainty of the laminar flame speed $\frac{\Delta S_L^{sca}}{S_L^{sca}}$ in %
0.80	20.1	0.19	2.74
0.88	20.86	0.24	3.55
0.93	22.13	0.22	3.37
1.00	23.75	0.21	3.17
1.06	23.93	0.20	3.13
1.15	23.95	0.19	2.81
1.20	22.51	0.22	3.44
1.36	16.07	0.29	4.39
1.41	13.48	0.34	5.33
1.45	11.64	0.47	6.63
1.50	10.14	0.57	8.07
1.53	9.79	0.69	10.00
1.55	9.65	0.71	10.63

Table 10: The laminar flame speed according to the mass conservation method

Equivalence ratio ϕ	Mean laminar flame speed S_L^{mc} in cm/s	The mean laminar flame speed S.E. $\frac{\Delta S_{L_{SEM}}^{mc}}{S_L^{mc}}$ in %	Uncertainty of the laminar flame speed $\frac{\Delta S_L^{mc}}{S_L^{mc}}$ in %
0.8	29.12	0.17	2.79
0.88	30.60	0.14	2.22
0.93	33.47	0.11	1.84
1.00	35.61	0.10	1.62
1.06	36.54	0.08	1.29
1.15	36.65	0.09	1.44
1.20	34.53	0.08	1.36
1.36	23.07	0.19	3.00
1.41	18.91	0.09	1.54
1.45	15.85	0.17	2.84
1.50	14.64	0.12	2.00
1.53	13.58	0.20	3.23
1.55	13.63	0.21	3.39

Table 11: difference between the laminar flame speed of the semi-cone angle and the mass conservation method in percent

ϕ	**0.80**	**0.88**	**0.93**	**1.00**	**1.06**	**1.15**	**1.20**	**1.36**	**1.41**	**1.45**	**1.50**	**1.53**	**1.55**
$\frac{\Delta S_L^{mc-sca}}{S_L^{mc}}$	30.97	31.83	33.88	33.29	34.50	34.65	34.81	30.32	28.72	26.56	30.73	27.87	29.19

Observe that the laminar flame speed obtained from the semi –cone angle shows a different magnitude compared to the mass conservation method. A maximum difference of 34.81% is observed from Table 11. The discrepancy found between the laminar flame speed analysis using the semi-cone angle and mass conservation method, is due to the fact that the equation for the determination of the laminar flame speed with the semi-cone angle method assumes a uniform flow distribution at the burner exit. This however, is only true for carefully machined nozzle burners as has been employed by Bouvet et al. [29] and Guiberti et al. [72].

For a tube type Bunsen burner similar to the one used in this experiment, the velocity profile at the burner exit is not constant. This non-uniform flow induces flame curvature that alters the laminar flame speed. The laminar flame speed obtained from the semi-cone angle method does not account for this non uniform flow distribution. Therefore the aerodynamic effect on the laminar flame speed has to be evaluated separately.

4.1.1 Accounting for the aerodynamic effect

For a burner that does not have the characteristics of a nozzle, the velocity is not constant along the radius of the burner exit. Moreover, observe that at the flame base the flame is curved. This is due to the boundary layer effect in a normal straight tube burner, similar to the one used in this experiment. Indeed this boundary layer is also present for an aerodynamically tailored nozzle burner although, the effect of this on the flame has been reduced by reducing the boundary layer thickness. This generates a straight flame sides in a Bunsen flame which reduces the flame curvature, restricting the flame curvature to effectively only to the flame tip. The semi-cone angle method is therefore typically used in a nozzle type Bunsen burner. However, a nozzle type Bunsen burner is known to be sensitive to experimental uncertainties. Therefore the use of tube Bunsen burner is more desirable in experiments. Thus an attempt is made here in order to correct for this non-uniformity of the velocity distribution of the unburned mixture.

The following method is proposed by means of which the laminar flow velocity profile of a fluid within a tube is described by a Poiseuille flow [73]. The Poiseuille flow is well documented and understood and is one of the fundamental flow velocities in aerodynamic studies. This was shown to be a valid description of the velocity profile of a tube type Bunsen burner by Hu et al. [60].The radial velocity profile distribution can be described using the uniform flow average velocity by the following equation [73]:

$$u(r) = 2U_0\left(1 - \left(\frac{r}{R}\right)^2\right) \tag{38}$$

In this expression r is the radial coordinate along the burner exit diameter with r=0 indicating the center of the burner exit and R is the burner radius. The flow velocity described by the Poiseuille flow is shown in Fig.4.2.

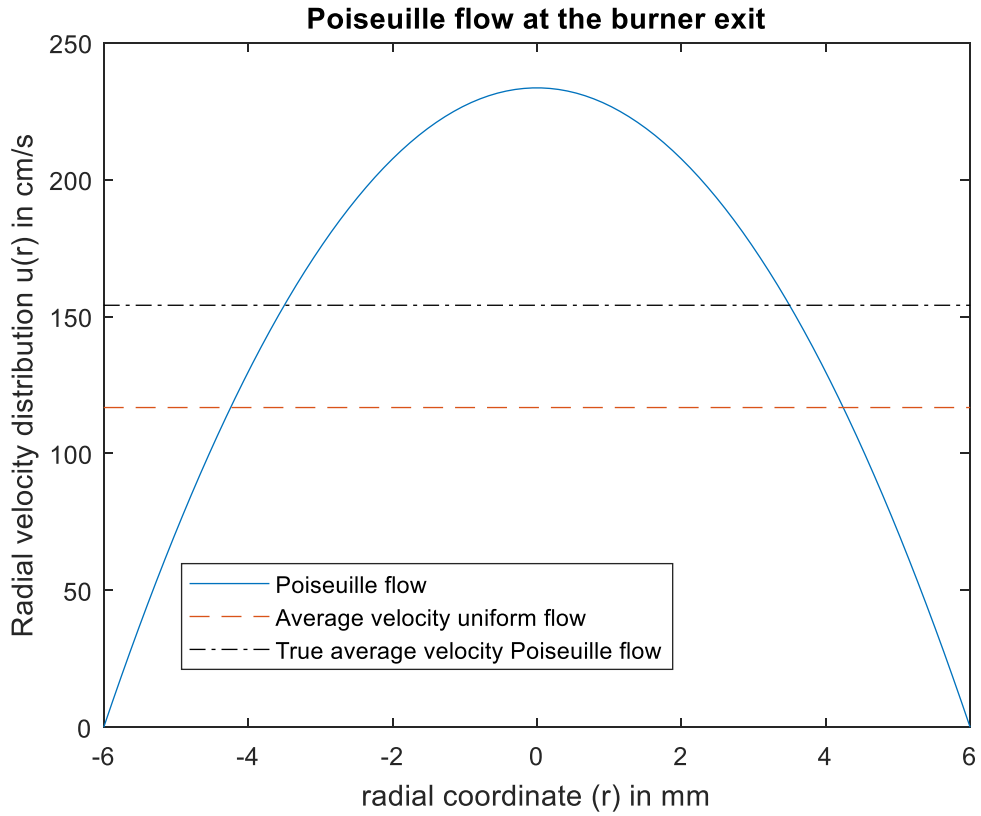

Fig.4.2: The radial velocity distribution at the burner exit according to Poiseuille flow.

This form of the radial velocity distribution in a tube is commonly used in practical applications since the average velocity is readily obtained using the volumetric flow rate definition given previously in Eq.22a. In this figure the true average velocity corresponding with a Poiseuille flow is shown to have a higher magnitude compared to the average velocity corresponding with a uniform flow. For the derivation of the average laminar flame speed the Bunsen flame is assumed to be fully conical as shown in Fig. 4.3.This is based on the observation from Fig.4 that the curved section of the Bunsen flame at the flame base and flame tip are small compared to the flame height. Moreover the Poiseuille flow is assumed to be axisymmetric at the burner exit.

For a 2D analysis of the flame, the flame speed is defined normal to the flame front. Since the bulk flow velocity is not constant, the laminar flame speed varies along the radius of the burner. Since the Bunsen flame is stationary it indicates that the normal component of the unburned mixture velocity w.r.t. the flame front must be equal to the flame speed. The laminar flame speed on any location r of the Bunsen flame can be found by the expression:

$$S_L(r) = u(r)\sin(\alpha) \tag{39}$$

This is graphically depicted in Fig. 4.3. Note that the laminar flame speed is in the opposite direction to the perpendicular component of the unburned mixture velocity w.r.t the flame front by definition.

The average laminar flame speed is then given by the expression:

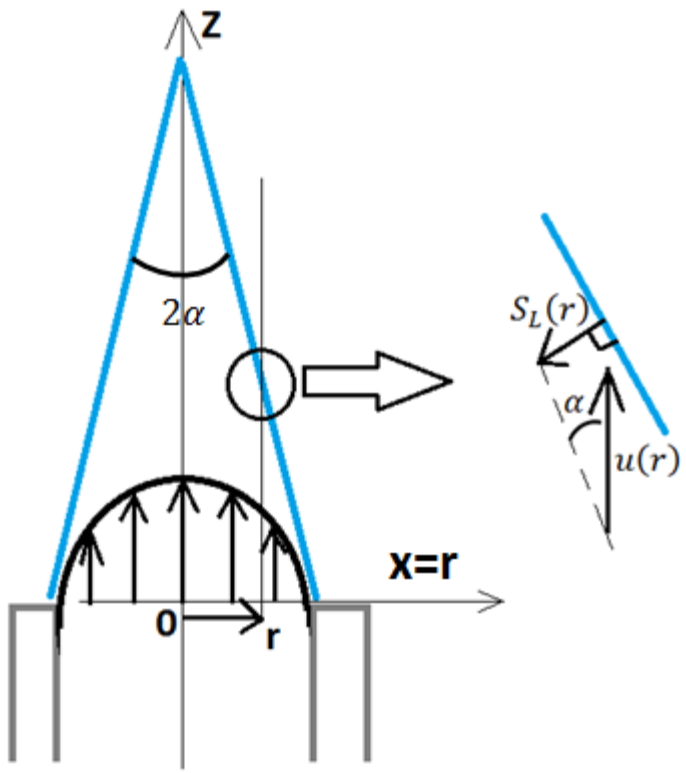

Fig. 4.3: The laminar flame speed of a bunsen flame for a non uniform unburned bulk flow.

$$\overline{(S_L(r))} = S_L = \overline{u(r)\,\sin(\alpha)} \qquad (40)$$

Since α is assumed to be constant everywhere on the conical flame, the average laminar flame speed can be simplified to:

$$\overline{(S_L(r))} = S_L = \overline{u(r)}\,\sin(\alpha) \qquad (41)$$

This expression appears to be similar to the original equation given in Eq.16.

The velocity profile in this case is well approximated by the Poiseuille flow. The Poiseuille flow can be recognized to be a parabolic function. The average value of a function $\overline{f(x)}$ of an interval (a, b) is given by the equation [67]:

$$\overline{f(x)} = \frac{1}{b-a}\int_a^b f(x)\,dx \qquad (42)$$

This equation can be used to determine the average velocity at the burner exit. In here $x = r$ which results in the following expression:

$$\overline{f(r)} = \frac{1}{b-a}\int_a^b f(r)\,dr \qquad (43)$$

The expression for the Poiseuille flow given in Eq.38 is used in Eq.43 with $\big(f(r) = u(r)\big)$ which gives the following equation:

$$\overline{u(r)} = \frac{1}{b-a}\int_a^b u(r)\,dr \qquad (44)$$

Where in *a=-6* and *b=6* are the limits which corresponds to the diameter of the burner exit and the boundary in which the velocity is equal to zero. Solving this integral result in the equation:

$$\overline{u(r)} = \frac{4}{3}U_0 = constant \qquad (45)$$

The evaluation of the integral is detailed in Appendix A and the value of Eq.45 was shown in Fig.4.2 as the true average velocity of the Poiseuille flow. Substituting the expression found in Eq.45 in Eq.41 will result in the following expression for the laminar flame speed using the semi-cone angle method:

$$S_L = \frac{4}{3} U_0 \sin(\alpha) \tag{46}$$

In this equation the value 4/3 is a correction to the average velocity accounting for the velocity profile due to aerodynamic effects. Recall that the uncorrected laminar flame speed using the semi-cone angle was given by $S_L^{uc} = U_0 \sin(\alpha)$, so that Eq.44 can be written in terms of the uncorrected laminar flame speed as:

$$S_L^c = \frac{4}{3} S_L^{uc} \tag{47}$$

In this equation the superscript *c* and *uc* denotes the corrected and uncorrected laminar flame speed respectively. This suggests that the magnitude of the laminar flame speed is higher by 4/3 compared to the uncorrected laminar flame speed for a Bunsen flame subject to non-uniform velocity profile.

The magnitude of the laminar flame speed using the corrected semi-cone angle method is shown in Table 12.The results are shown in Fig.4.4 for the laminar flame speed using the corrected, the uncorrected and the mass conservation method.

Comparing the results to the mass conservation method shows that the rich region from $\phi = 1.36$ to $\phi = 1.55$ are closely approximated using the correction with the error being overall less than 8%. The error in the stoichiometric region $\phi = 1.06$ is reduced to 13.7% while the overall maximum difference is found to be 13.95% between the mass conservation and the corrected semi-cone angle method. Comparing the lean region between $\phi = 0.8$ to $\phi = 0.93$ it shows a maximum difference of 12.74%. The minimum difference between the mass conservation method and the corrected semi-cone angle method is found to be 3.07%. The detailed difference in percent of the corrected semi-cone angle method w.r.t. the mass conservation method is shown in Table 13. For the remainder of this discussion when the results obtained using the semi-cone angle is used, it refers to the corrected semi-cone angle method.

Recall the empirical relation given in Eq.10 which indicates the influence of stretch on the laminar flame speed, and noting that the laminar flame speed of the mass conservation method is approximately equal to the reference laminar flame speed $S_L^{mc} \approx S_L^0$ [33]. It can be shown that the difference between the stretched flame and the reference flame is given by the Markstein number M_a times Karlovitz number K_a:

$$M_a K_a \approx 1 - \frac{S_L^{sca}}{S_L^{mc}} \approx \frac{(S_L^{mc} - S_L^{sca})}{S_L^{mc}} \approx \frac{\Delta S_L^{mc-sca}}{S_L^{mc}} \tag{48}$$

This relation is shown in Table 13 which quantifies the effect of omitting the flame curvature at the flame base and flame tip. It can therefore be concluded that the effect of omitting the curved section of the flame at the flame base and flame tip, results in an underestimated laminar flame speed. This becomes more significant for a shorter flame which is shown in Table 13 that the value of $M_a K_a$ increases as the flame approaches stoichiometry.

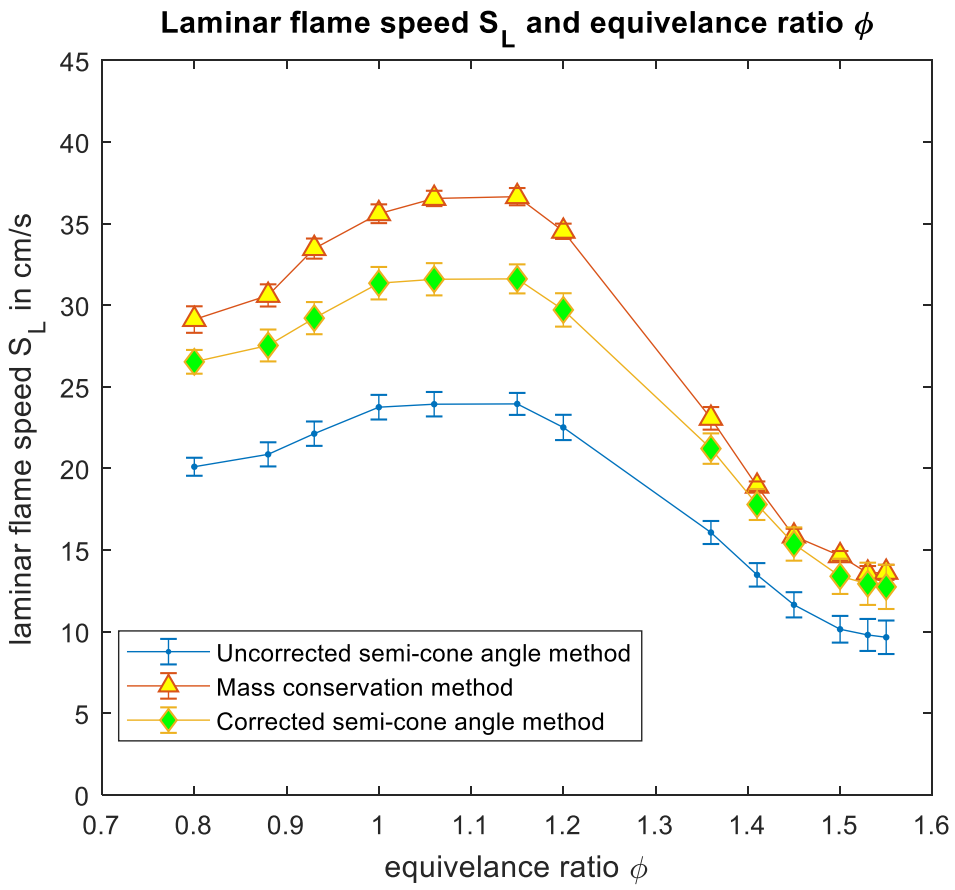

Fig. 4.4: Laminar flame speed measurement of the mass conservation, semi-cone angle and the corrected semi-cone angle method.

Table 12: The laminar flame speed according to the corrected semi-cone angle method

Equivalence ratio ϕ	Mean laminar flame speed S_L in cm/s	S.E. laminar flame speed $\frac{\Delta S_{L SEM}}{S_L}$ in %	Uncertainty in the laminar flame speed $\frac{\Delta S_L}{S_L}$ in %
0.80	26.53	0.19	2.74
0.88	27.53	0.24	3.55
0.93	29.21	0.22	3.37
1.00	31.35	0.21	3.17
1.06	31.59	0.20	3.13
1.15	31.61	0.19	2.81
1.20	29.71	0.22	3.44
1.36	21.22	0.29	4.39
1.41	17.79	0.34	5.33
1.45	15.37	0.47	6.63
1.50	13.39	0.57	8.07
1.53	12.93	0.69	10.00
1.55	12.74	0.71	10.63

Table 13: The difference of the corrected semi-cone angle method w.r.t. the mass conservation method in % and Markstein Karlovitz number of the flame

ϕ	0.80	0.88	0.93	1.00	1.06	1.15	1.20	1.36	1.41	1.45	1.50	1.53	1.55
$\frac{\Delta S_L^{mc-sca}}{S_L^{mc}}$	8.89	10.02	12.74	11.95	13.55	13.74	13.95	8.00	5.92	3.07	8.58	4.80	6.54
$M_a K_a$	0.089	0.100	0.127	0.119	0.135	0.137	0.139	0.080	0.059	0.030	0.086	0.048	0.065

4.1.2 Laminar flame speed from rich to lean

The results presented earlier are obtained by varying the equivalence ratio from a lean mixture to a rich mixture. To test the reproducibility of this experiment, the process is reversed. Here the equivalence ratio is varied from rich to lean. The laminar flame speed obtained from this process was evaluated using the mass conservation method and the semi-cone angle method.

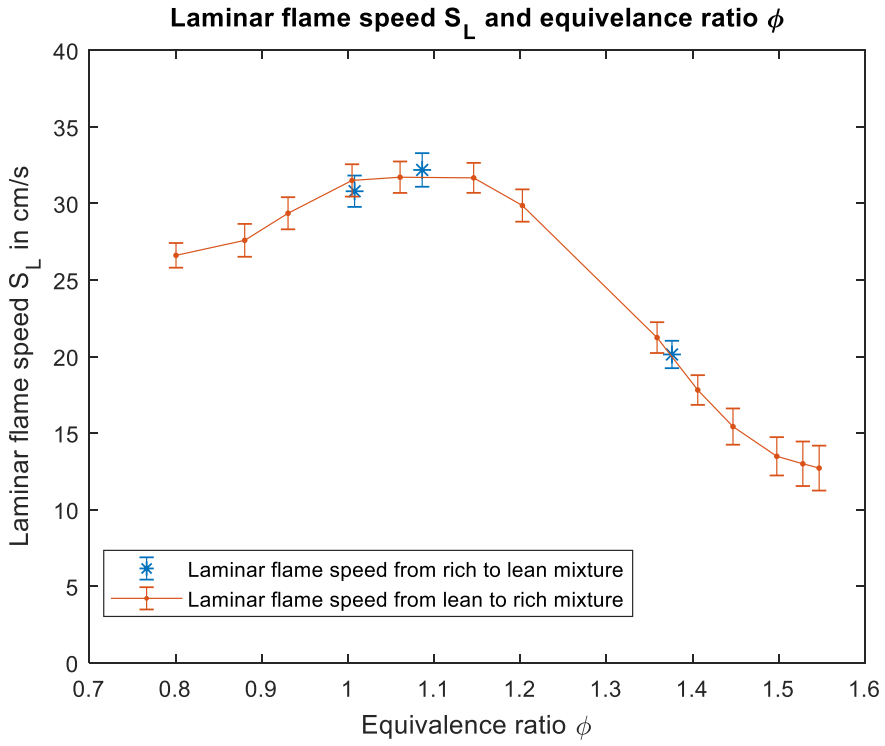

Fig. 4.5: The laminar flame speed obtained by reversing the process from lean to rich using the semi-cone angle method.

This results in the additional points shown in Fig.4.5 using the semi-cone angle method. This figure shows that the laminar flame speed obtained by reversing the direction of the process results in a value that follows the same curve as the sequence from lean to rich. However, according to the mass conservation method, reversing the direction, results in slightly different values for the laminar flame speed at $\phi = 1.38$. This is shown in Fig. 4.6. However the difference between the values of the lean to rich and rich to lean process is found to be less than 5%. This indicates that reversing the direction of the experiment has small influence on the obtained data. The equivalence ratio used for this test is shown in Table 14 and Table 15. The corresponding laminar flame speed using the semi-cone angle method and the uncertainty in the equivalence ratio is included in Table 14. Similarly for the laminar flame speed using the mass conservation method is given in Table 15.

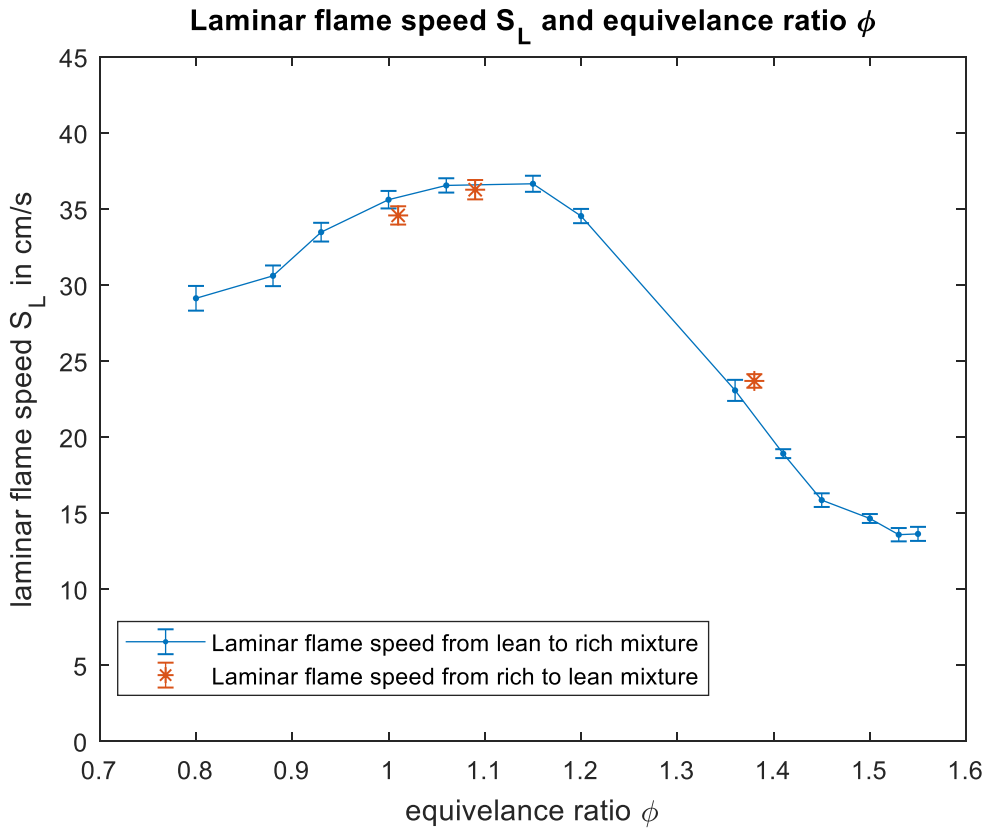

Fig. 4.6: The laminar flame speed obtained by reversing the process from lean to rich using the mass conservation method

Table 14: Laminar flame speed from rich to lean mixture using the semi-cone angle method

$\boldsymbol{\phi}$	**1.38**	**1.09**	**1.01**
$\boldsymbol{\Delta\phi/\phi}$ in %	3.28	3.81	4.01
$\boldsymbol{S_L^{sca}}$ in cm/s	20.14	32.02	30.80
S.E. $\boldsymbol{\Delta S_{L_{SEM}}^{sca}/S_L^{sca}}$ in %	0.27	0.21	0.20
Uncertainty $\frac{\boldsymbol{\Delta S_L^{sca}}}{\boldsymbol{S_L^{sca}}}$ in %	4.44	3.40	3.32

Table 15: Laminar flame speed from rich to lean mixture using the mass conservation method

$\boldsymbol{\phi}$	**1.38**	**1.09**	**1.01**
$\boldsymbol{\Delta\phi/\phi}$ in %	3.28	3.81	4.01
$\boldsymbol{S_L^{mc}}$ in cm/s	23.69	36.26	34.57
S.E. $\boldsymbol{\Delta S_{L_{SEM}}^{mc}/S_L^{mc}}$ in %	0.12	0.11	0.11
Uncertainty $\frac{\boldsymbol{\Delta S_L^{mc}}}{\boldsymbol{S_L^{mc}}}$ in %	1.89	1.76	1.74

4.2 The laminar flame speed of DNG compared to other natural gas variations

Comparing the results from this experiment with the laminar flame speed obtained using the heat flux method, will indicate the viability of the process used here to determine the laminar flame speed. However, no data was found on the laminar flame speed of DNG to use as a reference. It was shown by Dirrenberger et al. [1] and Huang et al. [2] that the laminar flame speed of natural gas closely resembles the laminar flame speed of methane. Therefore, methane can be used to approximate the validation of the experimental results and setup.

The laminar flame speed of DNG is further compared with gas from Indonesia, Abu-Dhabi and Pittsburgh that was investigated by Dirrenberger et al. [1]. The method that they used to obtain the laminar flame speed was the heat flux method. The heat flux method is a different technique to determine the laminar flame speed. It is used to directly determine the adiabatic, un-stretched, 1D laminar flame speed. Therefore the laminar flame speed obtained from this method is equal to the reference laminar flame speed S_L^0 defined earlier. Additionally the laminar flame speed measurement of natural gas obtained by Huang et al. [2] was used, which was obtained from the expanding sphere method.

4.2.1 Laminar flame speed comparison of DNG with methane

For the validity of the data presented in this research a reference laminar flame speed of DNG is required. However, no experimental results were found in which the laminar flame speed of DNG has been measured. Therefore to approximate the validation of the data, the laminar flame speed of methane is used instead. It was shown earlier that the laminar flame speed of natural gas in general is similarly affected by the variation of the equivalence ratio as methane.

To the contrary of the available data on the laminar flame speed of DNG, the laminar flame speed of methane has been extensively measured and documented. The laminar flame speed of DNG obtained using the mass conservation method and the semi-cone angle method is plotted in Fig.4.7. Additionally the laminar flame speed of methane documented in literature [1] [74] [75] [76] [77] is shown in this same figure.

It should be noted that the methods employed to measure the laminar flame speed in each of the mentioned references differ. It was already mentioned that Dirrenberger et al. [1] employed the heatflux method to determine the laminar flame speed of natural gas and here methane. Halter et al. [74] employed a spherical expanding flame. Similarly Hassan et al. [75], Beekman et al. [76] and Varea et al. [77] determined the laminar flame speed in the same fashion. Therefore this comparison will also indicate the effectiveness of the Bunsen flame method compared to the expanding sphere method to estimate the laminar flame speed.

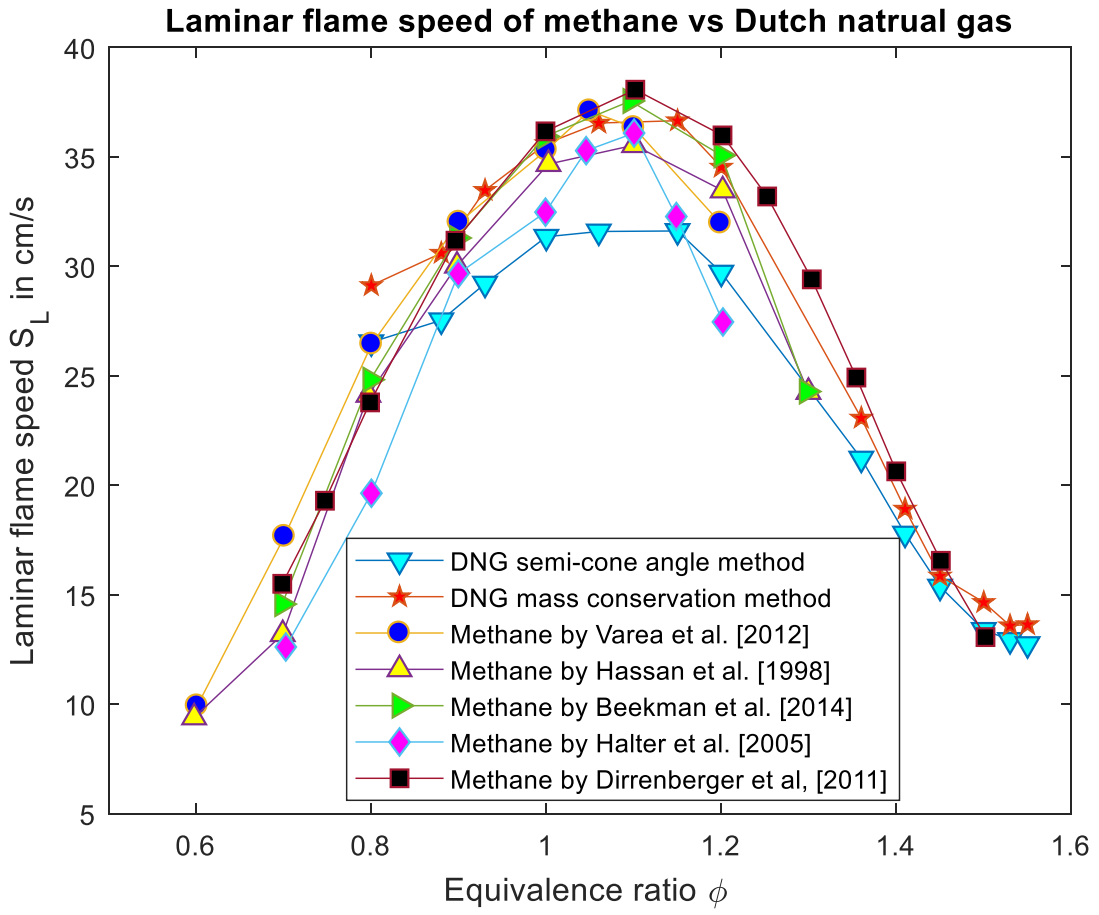

Fig.4.7: Comparison of the laminar flame speed of DNG vs. methane as presented in the literature [9] [74] [75] [76] [77].

The laminar flame speed of methane recorded in the literature shows a narrow scatter band of approximately 5 cm/s. The laminar flame speed of DNG using the mass conservation method and the semi-cone angle method are shown to be close or within this scatter band. This figure shows that the laminar flame speed of DNG obtained from the mass conservation method is close to the laminar flame speed of methane using the heatflux method. The overall absolute difference between the laminar flame speed of methane presented in literature [1] [75] [76] [77] and the laminar flame speed of DNG obtained using the mass conservation method, is shown to be approximately less than 10% for $0.8 < \phi < 1.20$. Similarly the laminar flame speed of DNG using the semi-cone angle method is shown to be approximately less than 20% for $0.8 < \phi < 1.20$.

The laminar flame speed using the semi-cone angle method of DNG at near stoichiometric conditions is underestimated. Therefore it can be conclude that the laminar flame speed measurement by means of a Bunsen burner flame is more accurate using the mass conservation method. However, the semi-cone angle method gives acceptable results for the lean and rich regions of the equivalence ratio spectrum. The detailed difference in percent, between the laminar flame speed of DNG using the mass conservation method and semi-cone angle method w.r.t. the laminar flame speed of methane is shown in Table 16 and Table 17 respectively. Moreover from this observation it can be concluded that the

values obtained from the Bunsen flame method are within the scatter band of the expanding sphere method and heat flux method, indicating that a comparable result can be obtained from a less sophisticated experimental setup such as the one used in this experiment.

Table 16: Difference between the laminar flame speed of DNG using the mass conservation method and various laminar flame speed measurements of methane in %

ϕ	$\frac{\Delta S_{L Varea}}{S_{L DNG}}$ in %	$\frac{\Delta S_{L Hassan}}{S_{L DNG}}$ in %	$\frac{\Delta S_{L Beekman}}{S_{L DNG}}$ in %	$\frac{\Delta S_{L Halter}}{S_{L DNG}}$ in %	$\frac{\Delta S_{L Dirrenberger}}{S_{L DNG}}$ in %
0.80	9.32	16.17	14.48	32.63	17.93
0.88	-1.9	4.59	1.07	7.49	1.62
0.93	1.4	5.58	1.39	7.96	0.99
1.00	0.85	2.83	-1.04	8.67	-1.66
1.06	-1.75	2.72	-2.08	1.6	-3.23
1.15	7.4	4.32	-1.12	12.34	-2.57
1.20	7.47	2.87	-1.6	20.16	-4.37
1.36	-	-	-	-	-5.72
1.41	-	-	-	-	-4.48
1.45	-	-	-	-	-4.81
1.50	-	-	-	-	9.96
1.53	-	-	-	-	17.4
1.55	-	-	-	-	27.55

Table 17: Difference between the laminar flame speed of DNG using the semi-cone angle method and various laminar flame speed measurements of methane in %

ϕ	$\frac{\Delta S_{L Varea}}{S_{L DNG}}$ in %	$\frac{\Delta S_{L Hassan}}{S_{L DNG}}$ in %	$\frac{\Delta S_{L Beekman}}{S_{L DNG}}$ in %	$\frac{\Delta S_{L Halter}}{S_{L DNG}}$ in %	$\frac{\Delta S_{L Dirrenberger}}{S_{L DNG}}$ in %
0.80	0.47	7.98	6.13	26.06	9.92
0.88	-13.26	-6.03	-9.95	-2.81	-9.34
0.93	-13	-8.2	-13	-5.48	-13.46
1.00	-12.61	-10.36	-14.76	-3.73	-15.46
1.06	-17.7	-12.53	-18.08	-13.83	-19.41
1.15	-7.36	-10.92	-17.23	-1.63	-18.92
1.20	-7.54	-12.88	-18.07	7.21	-21.29
1.36	-	-	-	-	-14.96
1.41	-	-	-	-	-11.05
1.45	-	-	-	-	-8.12
1.50	-	-	-	-	1.51
1.53	-	-	-	-	13.24
1.55	-	-	-	-	22.48

4.2.2 Laminar flame speed of DNG compared to natural gas from Pittsburgh, Abu-Dhabi and Indonesia

The results for the laminar flame speed of natural gas from Pittsburgh, Abu Dhabi and Indonesia was presented by Dirrenberger et al. [1] other variations of natural gas has been investigated and presented by Huang et al. [2]. The origin of the natural gas used by Huang et al. [1] was however not mentioned. The composition of the natural gas used by Huang et al. [2] and Dirrenberger et al. [1] is shown in Table 18 and 19 respectively. The composition of DNG as presented by Dirrenberger et al. [1] is added in Table 18 for a complete overview.

The laminar flame speed of the natural gas given in Table 18 and 19 are compared to DNG obtained using the semi-cone angle and mass conservation method. The results are shown in Fig.4.8.

Table 18: The composition of natural gas from Pittsburgh, Abu Dhabi and Indonesia according to Dirrenberger et al. [1] in percent (%) volume

	CH_4	C_2H_6	C_3H_8	$i-C_4H_{10}$	$n-C_4H_{10}$	$i-C_5H_{12}$	N_2	CO_2
Pittsburgh	85	14	-	-	-	-	1	-
Abu Dhabi	82.07	15.86	1.89	-	0.06	-	0.05	-
Indonesia	89.91	5.44	3.16	1	0.75	0.03	0.04	-
The Netherlands	81.3	2.9	0.4	0.2	-	-	14.3	0.9

Table 19: The natural gas composition used by Huang et al.[2] given in percent (%) volume.

Items	CH_4	C_2H_6	C_3H_8	N_2	CO_2	**Others**
Volumetric fraction (%)	96.16	1.096	0.136	0.001	2.54	0.067

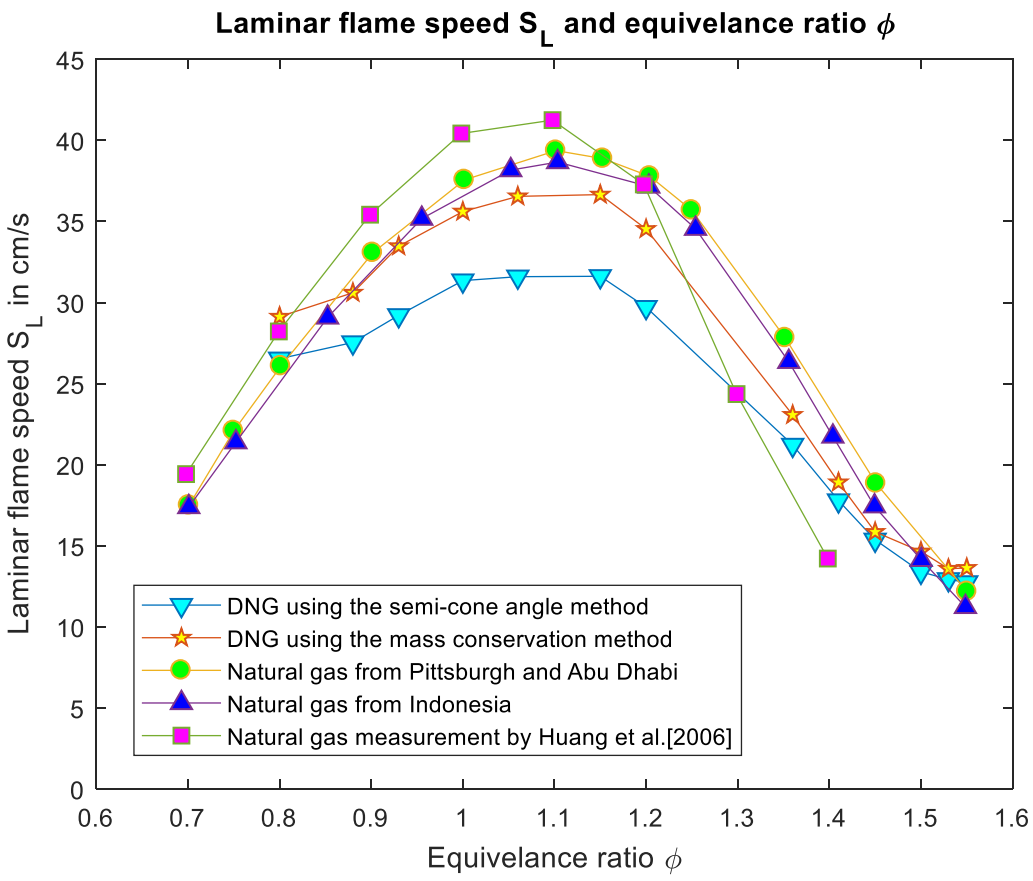

Fig. 4.8: The laminar flame speed of natural gas with varying composition.

From this figure it can be observed that the laminar flame speed of natural gas shows a wide spectrum. Ranging from; 16*cm/s* to 20*cm/s* at $\phi = 0.7$ and 15 *cm/s* to 28*cm/s* at $\phi = 1.4$. The width of this spectrum shows to be larger at $\phi = 1.1$ which corresponds to the maximum laminar flame speed ranging from 31 *cm/s* to 41 *cm/s*.

It is important to emphasize that the comparison here is based on the laminar flame speed measurement of natural gas obtained from different experimental techniques. Therefore the estimated laminar flame speed difference reported here between the natural gas from other regions is largely influenced by this. However, it can be observed that the laminar flame speed from the mass conservation method is in general closely related to the laminar flame speed measurement of methane obtained from the heat flux method employed by Dirrenberger et al. [1] as was shown in Fig.4.7. Hence it can be deduced that the mass conservation method from the Bunsen flame indeed approximates the ideal laminar flame speed S_L^0. Therefore the difference between the laminar flame speed of natural gas from Pittsburgh, Abu Dhabi and Indonesia with DNG presented here, is mainly due to the individual composition of the natural gasses.

This figure shows that the laminar flame speed obtained using the corrected semi-cone angle method underestimates the laminar flame speed at stoichiometry by a maximum of approximately 20 %. The

laminar flame speed obtained from the mass conservation method shows to coincide with the results obtained from literature. However, the laminar flame speed of the semi-cone angle is within the spectrum of the reported laminar flame speed of natural gas for lean and rich regions of the equivalence ratio spectrum.

Continuing the comparison of the results with the laminar flame speed of natural gas from Pittsburgh and Abu Dhabi, it shows that the peak of the laminar flame speed is indeed close to $\phi = 1.1$. This stoichiometric equivalence ratio is also the maximum of all the other natural gas compositions shown in this figure. This confirms the results that the maximum laminar flame speed obtained from the experiment occurs at $\phi = 1.1$. The stoichiometric laminar flame speed of DNG is shown to be lower than the natural gas from Pittsburgh and Abu Dhabi by 5.32%. The laminar flame speed of DNG is higher by 10.84 % compared to the natural gas from Pittsburgh and Abu Dhabi for $\phi = 0.8$. However, the absolute difference is less than 5.5 % for $\phi = 0.88, 0.93\ and\ 1.00$, hence the burning velocity of DNG is near identical to the natural gas of Pittsburgh and Abu Dhabi for the lean region. The laminar flame speed of DNG in the rich region $(\phi > 1\ .1)$ is shown to be lower by a maximum of 19.43% compared to the natural gas of Abu Dhabi and Pittsburgh. Similar behavior can be observed when comparing DNG with the natural gas from Indonesia. Although it shows that the laminar flame speed of DNG is estimated to be closer to the laminar flame speed of natural gas from Indonesia.

Comparing the laminar flame speed of DNG with the laminar flame speed of natural gas presented in literature [2] shows that at $\phi = 0.80$, the laminar flame speed of DNG is estimated higher by 2.89%. However, the overall comparison of the laminar flame speed of DNG from $\phi = 0.88\ to\ \phi = 1.20$ shows a lower value by a maximum of 13.66%. In the rich region $\phi > 1.3$ the laminar flame speed of DNG appears to be slightly higher than what was reported in literature [2]. It should be noted that the expanding sphere technique was used to determine the laminar flame speed of natural gas by Huang et al. [2]. Therefore the difference between the results is strongly influenced by the difference in the employed methods in this research and in literature [2].

Further observation of Fig.4.8 shows that the laminar flame speed of DNG decreases rapidly beyond $\phi \approx 1.20$. In addition, the laminar flame speed of DNG is in general lower than the variant from Abu Dhabi, Pittsburgh and Indonesia. This is the consequence of the high dilution of the DNG containing high concentration of N_2 and CO_2. At $\phi = 1.5$ the laminar flame speed is comparable with the results found in literature [1]. From this observation it can be deduced that the results for the DNG are comparable with gases from Pittsburgh, Abu Dhabi and Indonesia, for lean equivalence ratios $0.86 \leq \phi < 1.20$. However, the laminar flame speed of DNG at rich region of the equivalence ratio spectrum shows to be consistently lower than natural gas from Pittsburgh, Abu Dhabi and Indonesia. However, due to the lower concentration of ethane in natural gas from Indonesia, the laminar flame speed of this gas is closer to the estimated laminar flame speed of DNG.

The difference between the laminar flame speed of DNG compared to the gases shown in Table 18 and 19 is shown in Table 20. In this table only the laminar flame speed obtained from the mass conservation method is considered due to the better approximation of the laminar flame speed of DNG. It shows that the results obtained using this method is closer in comparison with the laminar flame speed of natural

gas presented in the literature while the semi-cone angle method results in a consistently lower laminar flame speed estimation. In this table the minus sign indicates that the laminar flame speed of DNG is lower in comparison.

Note that the equivalence ratio for the lean blow off is shown to be at a higher equivalence ratio compared to natural gas from Abu Dhabi, Pittsburgh and Indonesia. The lean blow off limit is here affected by the burner design as was discussed earlier. The laminar flame speed presented by Dirrenberger et al. [1] is based on the heat flux method and the laminar flame speed present by Huang et al. [2] is based on a propagating sphere method. Therefore, the Bunsen burner is not suitable for the determination of the flammability limit of DNG and may require to be investigated further.

Table 20: The difference in percentage, between the laminar flame speed of DNG using the mass conservation method and the gases used in literature

Equivalence ratio ϕ	$\frac{\Delta S_{L_{Indonesia}}}{S_{L_{DNG}}}$ in %	$\frac{\Delta S_{L_{Pittsburgh.\&\ A.bu\ Dhabi}}}{S_{L_{DNG}}}$ in %	$\frac{\Delta S_{L_{Huang}}}{S_{L_{DNG}}}$ in %
0.80	13.65	10.84	2.89
0.88	-1.17	-3.62	-11.68
0.93	-1.37	-3.4	-11.53
1.00	-3.63	-5.32	-13.66
1.06	-4.76	-6.8	-13.24
1.15	-4.92	-6.17	-9.57
1.20	-7.91	-9.77	-7.32
1.36	-12.48	-17.38	27.09
1.41	-11.74	-18.89	26.45
1.45	-9.66	-19.43	4.78
1.50	3.39	-2.71	-
1.53	8.36	2.99	-
1.55	18.39	10.62	-

4.3 Maximum laminar flame speed and tip opening

Observing Fig.4.7 shows that the flame velocity increases as it approaches stoichiometry $\phi = 1$. However the maximum is seen to be beyond this point. This is contradicting the statement of earlier that the maximum enthalpy release of the fuel is at stoichiometry $\phi = 1$. This is due to the increase of the temperature at which the products of the combustion process are changed from typically a triatomic species in to a diatomic species [78]. This phenomenon is known as dissociation. Dissociation is an equilibrium process by which the products of the reaction achieve the minimum of the Gibbs function [79]. Another phenomenon that was observed in this experiment is the tip opening of a Bunsen flame at $\phi = 1.50$. Tip opening is when local extinction of the flame occurs at the flame tip. This phenomenon is typically undetectable using the light in the visible spectrum $(400 < \lambda < 700)$ of the flame as was visually observed during the experiment.

4.3.1 Dissociation effect on the laminar flame speed

Dissociation of the products of combustion is when a triatomic species is reduced to a diatomic species by separating the bond to one of its atoms typically oxygen. This phenomenon occurs at high temperatures and increases exponentially with increasing temperature [80]. The effect of dissociation is therefore prominent at stoichiometric conditions in which the theoretical maximum heat release is achieved. The effect of dissociation is important for pollution study. However, this topic is outside the scope of this current research. Although, the principle of dissociation and its effect on the laminar flame speed at stoichiometry is elaborated.

The products of combustion at stoichiometry were earlier shown to be primarily carbon dioxide and water vapor. Due to dissociation these molecules reduce to carbon mono-oxide CO and hydrogen H_2 by separating from oxygen. Note that other species are also present at such high temperature such as NOx [79]. However, for the explanation here, only the dissociation of water and carbon dioxide are considered. The product species of Dutch natural gas for stoichiometric conditions was found from Eq.11. Employing the same values for $\alpha, \beta \; and \; \gamma$ that was used to determine the stoichiometric fuel to air ratio, the products species at combustion of DNG were obtained. The product of DNG at stoichiometry was found to be $0.9CO_2$ and $1.74H_2O$. For the computation process the reader is referred to Appendix A.

For the case of DNG the dissociation reaction can then be written as:

$$0.9CO_2 \leftrightarrow 0.9CO + 0.45O_2 \tag{49}$$

$$1.74H_2O \leftrightarrow 1.74H_2 + 0.87O_2 \tag{50}$$

The effect of the dissociation on the temperature and subsequently the laminar flame speed can be explained by using the first law of thermodynamics for species. From the first law of thermodynamics the enthalpy of the reaction is found to be [80]:

$$Q - W = \sum_{i}^{products} v_i\left[h_i(T) - h_i(T_0) + \Delta h_{fi}^0(T_0)\right] - \sum_{j}^{reactants} v_j\left[h_j(T) - h_j(T_0) + \Delta h_{fi}^0(T_0)\right] \tag{51}$$

In this equation Q is the heat release of the system in J/s, W is the work done by the system in J/s, v_i is number of moles of the species i/j, $h_i(T)$ is the species enthalpy in J/kg at temperature T in Kelvin, $h_i(T_0)$ is the enthalpy of species in J/kg at the initial temperature T_0 in Kelvin and $\Delta h_{fi}^0(T_0)$ is the enthalpy in J/kg of formation at initial temperature T_0 in Kelvin.

If the system performs no work $W = 0$ the equation for the first law of thermodynamics becomes:

$$Q = \sum_{i}^{products} v_i\left[h_i(T) - h_i(T_0) + \Delta h_{fi}^0(T_0)\right] - \sum_{j}^{reactants} v_j\left[h_j(T) - h_j(T_0) + \Delta h_{fi}^0(T_0)\right] \tag{52}$$

The equation for stoichiometry for methane allowing for incomplete combustion is given by the equation [80]:

$$C_\alpha H_\beta O_\gamma + \left(\alpha + \frac{\beta}{4} - \frac{\gamma}{2}\right)(O_2 + 3.76N_2) \rightarrow (\alpha - x)CO_2 + xCO + \left(\frac{\beta}{2} - y\right)H_2O + yH_2 + \left(\frac{x}{2} + \frac{y}{2}\right)O_2 + 3.76\left(\alpha + \frac{\beta}{4} - \frac{\gamma}{2}\right)N_2 \quad (53)$$

In this reaction, x and y are values for the number of moles of the present diatomic species due to dissociation. The values of x and y are typically found numerically. Note that the value of x and y for the case of DNG is within the interval:

$$0 \leq x \leq 0.9$$

$$0 \leq y \leq 1.74$$

This indicates the range from complete combustion (x=0, y=0) to fully incomplete combustion (x=0.9, y=1.74).

The dissociation of the molecules occurs almost simultaneously when the products are generated at high temperatures. The reaction equilibrium for DNG that allows for incomplete combustion is given by:

$$C_{0.9}H_{3.478}O_{0.0018} + 1.761(O_2 + 3.76N_2) \rightarrow (0.9 - x)CO_2 + CO + (1.74 - y)H_2O + yH_2 + \left(\frac{x}{2} + \frac{y}{2}\right)O_2 + 6.619N_2 \quad (54)$$

In here the values $\alpha = 0.9$, $\beta = 3.478$ and $\gamma = 0.0018$ were used.

From this chemical equilibrium reaction the number of moles of each species is obtained, with the exception for the exact number of diatomic species due to dissociation. Using the first law of thermodynamics, with the number of moles obtained from the chemical equilibrium reaction, the following expression is obtained:

$$Q = (F + I) + (J + K) + (L + M) \quad (55)$$

With:

$$F = 0.9[h(T) - h(T_0)]_{CO_2} + 1.74[h(T) - h(T_0)]_{H_2O} + 6.619[h(T) - h(T_0)]_{N_2}$$

$$I = 0.9\Delta h^0_{f_{CO_2}}(T_0) + 1.74\Delta h^0_{f_{H_2O}} - \Delta h^0_{f_{C_{0.9}H_{3,478}O_{0.0018}}}(T_0) - 1.761\Delta h^0_{f_{O_2}}(T_0)$$

$$J = -x\left\{[h(T) - h(T_0)]_{CO_2} - [h(T) - h(T_0)]_{CO} - \frac{1}{2}[h(T) - h(T_0)]_{O_2}\right\}$$

$$K = -x\left[\Delta h^0_{f_{CO_2}}(T_0) - \Delta h^0_{fCO}(T_0) - \frac{1}{2}\Delta h^0_{f_{O_2}}(T_0)\right]$$

$$L = -y\left\{[h(T) - h(T_0)]_{H_2O} - [h(T) - h(T_0)]_{H_2} - \frac{1}{2}[h(T) - h(T_0)]_{O_2}\right\}$$

$$M = -y[\Delta h^0_{f_{H_2O}} - \Delta h^0_{f_{H_2}}(T_0) - \frac{1}{2}\Delta h^0_{f_{O_2}}(T_0)$$

This equation shows that $F + I$ and $J + K$is the enthalpy release of the complete combustion, while $I + J$ and $L + M$ are the enthalpy of the dissociation reaction for CO_2 and H_2O respectively. If no dissociation reactions occurs then x and y are zero. However, if dissociation occurs then x and y are larger than zero, which shows that the enthalpy of the reaction is reduced subsequently resulting in a lower heat release Q. The reduction in the heat release corresponds to a lower flame temperature at stoichiometry compared to the theoretic maximum. This can be schematically shown in a Potential energy (U)-Temperature (T) diagram depicted in Fig.4.9.

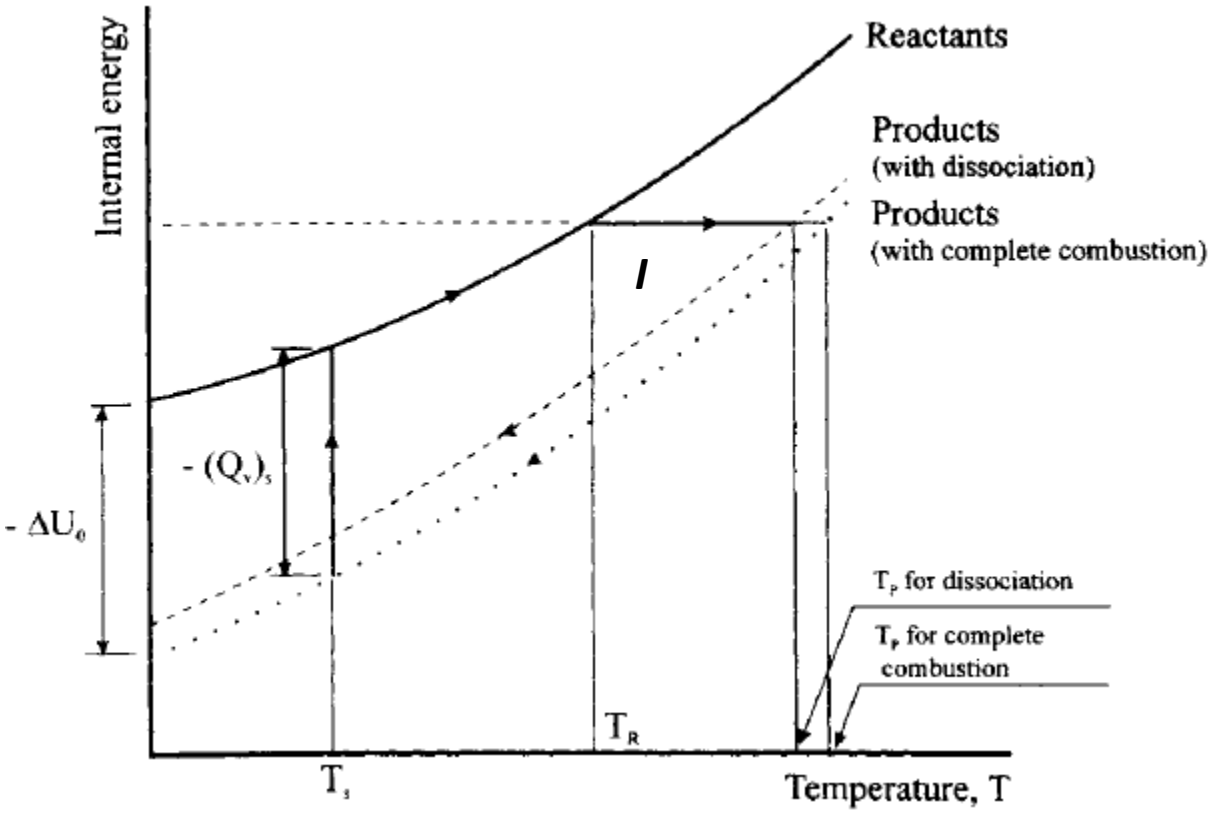

Fig. 4.9: Potential energy –Temperature diagram [79].

In this figure T_S indicates the starting temperature, T_R is the reactant temperature and T_P is the temperature of the products after combustion. This diagram is for a typical combustion engine, for this discussion only the region where the combustion occurs is of interest. This region is given by *(I)*. If dissociation occurs then the heat release was shown to be lower than the theoretical maximum. This corresponds to a smaller area between T_R and T_P which indicates a lower product temperature.

This phenomenon can be interpreted as the enthalpy release of the fuel is partially used to trigger the dissociation effect [26]. This causes a reduction in the net enthalpy release compared to the theoretical maximum at stoichiometry. Once dissociation is triggered, the local concentration of species changes. This dissociation of products causes the available oxygen compared to fuel locally to be higher. This indicates that the local fuel to air ratio is lower than stoichiometry. This causes an incomplete local combustion which in turn reduces the flame temperature.

The laminar flame speed and temperature are correlated according to the relation proposed by Mallard and Le'Chatalier given by Eq.5. Since the temperature at stoichiometry is lower than theoretical maximum, then the magnitude of the laminar flame speed is also reduced. This indicates, that in order to achieve a higher laminar flame speed additional fuel must be added. This causes the maximum to be shifted slightly to the right at a higher equivalence ratio than stoichiometry or a more rich mixture. For DNG, it is found to be at $\phi \approx 1.1$. This indicates that to reach the maximum laminar flame speed of DNG, 10% more fuel than stoichiometric FAR was required.

4.3.2 Tip opening phenomena

It is not until $\phi = 1.50$ that the flame tip opening was observed. This phenomenon is shown Fig.4.10. This is caused by the presence of large flame curvature and negative flame stretch. This curvature and flame stretch, changes the alignment of the direction vector (gradient) of the thermal and mass diffusivity qualitatively shown in Fig.4.11. This miss-alignment causes a difference at the rate of mass diffusivity and thermal diffusivity at the curved flame front which in turn increases the reaction time. With the increase of the mass diffusion, the mixture is diffused before combustion can take place. This leads to a local extinction of the flame if the strain of the flame becomes too high. Indeed this can be shown using the definition of the Lewis number given as:

$$L_e = \frac{\alpha}{D} = \frac{\lambda}{\rho D c_p} \tag{56}$$

In this α is the thermal diffusivity given by $\alpha = \lambda/\rho c_P$ and *D* indicating the mass diffusivity constant of the mixture. Several studies observed that the tip opening phenomenon occurred for premixed Bunsen flames when the local Lewis number was smaller than unity $(L_e < 1)$ [81] [82] [83]. The preheat zone was found to be thicker at the flame tip compared to the Bunsen flame sides. This thickening of the preheat zone enhances the mass diffusivity. The increase of the mass diffusivity at the flame tip is caused by the diffusional stratification of the mixture in the preheat zone. Diffusional stratification is when the density of the mixture varies the closer the mixture approaches the reaction zone. It was shown by Kozlovsky et al. [83] that the dominant contributor to tip opening for a premixed flame is caused by this phenomenon.

Vu et al. [82] conducted an investigation on the relation of the tip opening and the local Karlovitz number. The local Karlovitz number for a premixed Bunsen burner flame is found to be [82]:

$$K_{a_L} = \frac{\alpha}{\overline{U}R} = \frac{\alpha}{\overline{U}}\kappa \tag{57}$$

In this expression $\overline{U}$ is the average bulk flow velocity, *R* is the radius of the flame tip and κ is the curvature defined as $\kappa = 1/R$. It can be seen that this relation is based on the geometric shape of the flame front; relating the thermal diffusivity to the local flame curvature. If the flame radius goes to infinity which means one obtains a flat flame, then the K_{α_L} becomes zero. The local Karlovitz number is generally more accessible than the Lewis number since it relates the thermal diffusivity with the geometric flame curvature. Moreover the local Karlovitz number is independent on the bulk velocity and has been shown to be a more universal parameter to explain the tip opening phenomenon of a

premixed Bunsen flame [82]. The local Karlovitz number does however, vary with the equivalence ratio. It was shown by Vu et al. [82] that the local Karlovitz number reduces with increasing or decreasing the equivalence ratio beyond stoichiometry. It was found that the tip opening occurs at an interval between $\phi = 1.4$ and $\phi = 1.5$, indicating that a critical Karlovitz number exists where tip opening occurs. The critical Karlovitz number for a premixed flame is found to be equal to unity [82] [84]. This indicates that tip opening occurs when the chemical reaction time is somewhat equal to the physical flow time.

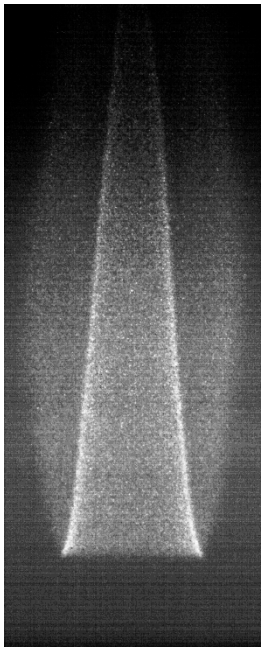

Fig. 4.10: Tip opening observed at $\phi = 1.50$.

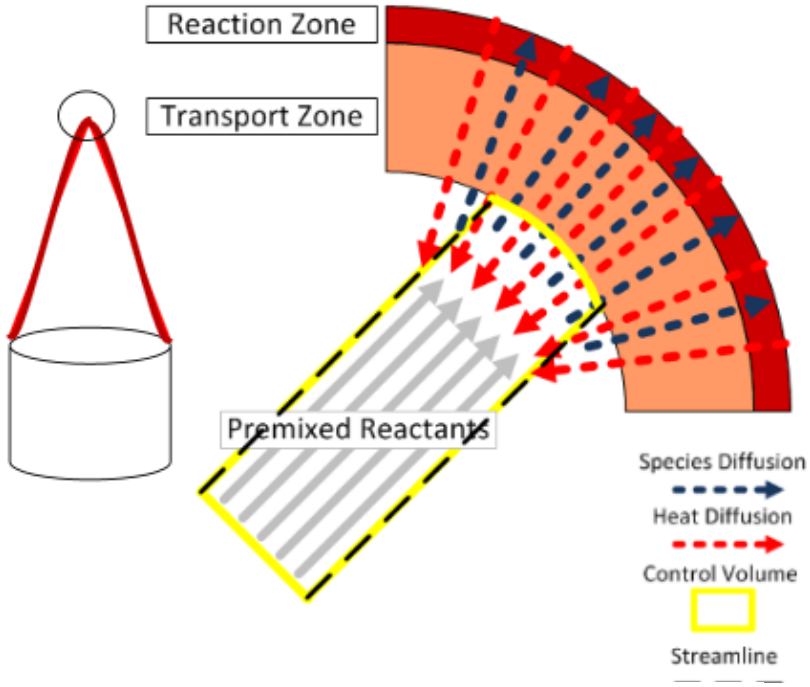

Fig. 4.11: Qualitative description on the tip opening phenomena [86].

The tip opening phenomenon introduces a problem to the mass conservation method used to determine the laminar flame speed. This is due to the criteria that all the unburned mass passes through the reaction zone. When tip opening is present these criteria are no longer satisfied. Since not all the mass flow of the unburned mixture passes through the reaction zone. This causes the mass conservation method to appear unsuitable to determine the laminar flame speed in such a situation. However, according to the investigation of Kozlovsky and Sivashinsky [83] on this case, concluded that the unburned mixture is usually fully consumed for a low Lewis number flame, despite the tip opening phenomenon. Nevertheless, the laminar flame speed of a tip opened Bunsen flame, is reported similarly to the methods used for a closed tip Bunsen flame by obtaining the flame area of a truncated flame in this situation [29]. However, the laminar flame speed is overestimated in this case and should be considered with care. In this research these are the values for the laminar flame speed at $\phi = 1.50, 1.53$ and $\phi = 1.55$. The laminar flame speed at these equivalence ratios requires a more sophisticated experimental setup in which the laminar flame speed is directly measured such as Laser Doppler Velocimetry (LDV), Particle Image Velocimetry (PIV) etc. since the possible mixture loss is difficult to evaluate with the current employed methods [85].

4.4 Volumetric flow rate influence on the laminar flame speed

The variation of the laminar flame speed with the increase of the bulk flow has been investigated. The Bulk flow has been increased by 50% and 80% from the initial values used to obtain the laminar flame speed for $\phi = 1.06 \pm 0.01$. The laminar flame speed has been computed using the mass conservation method and the semi-cone angle method. The change of the Bunsen flame with increasing the volumetric flow rate is shown in Fig.4.12. This figure shows that the increase in the unburned gas velocity results in an increase in the flame height. The effect of the variation of the volumetric flow rate on the laminar flame speed is shown in Fig 4.13.

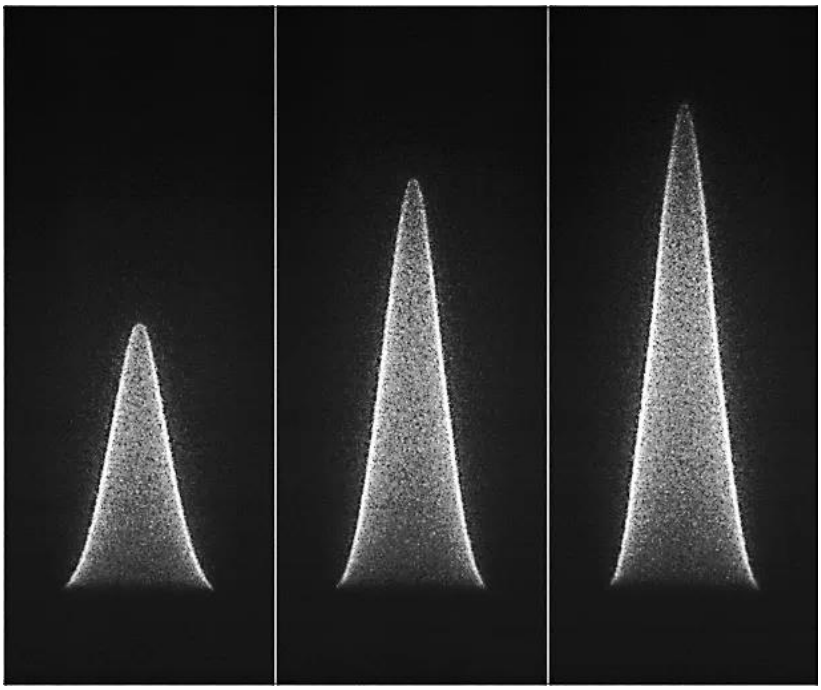

Fig. 4.12: The change in the Bunsen flame with increasing volumetric flow rate from left to right.

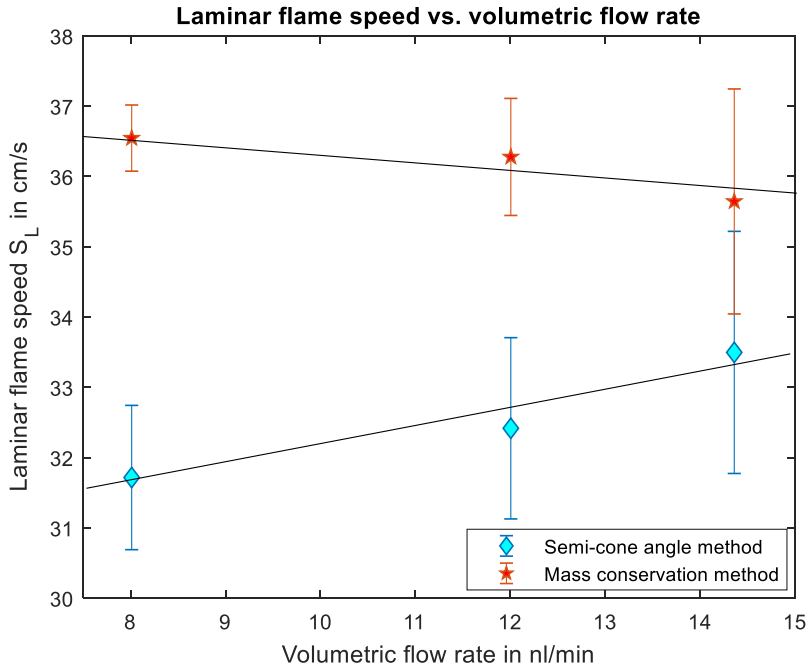

Fig. 4.13: The laminar flame speed variation with the total volumetric flow rate increase.

Observing this figure, it shows that the laminar flame speed reduces slightly with increasing the bulk flow rate. The behavior is seen to be decreasing linearly with increasing the total volumetric flow rate for this equivalence ratio. This rate is found to be at:

$$\frac{dS_L^{mc}}{d(\dot{V}_{tot}/A_e)} = -0.01$$

The superscript *mc* indicates the laminar flame speed obtained from the mass conservation method. The reduction rate is approximately 1% for a volumetric flow rate increase of 80%. It is worth noting that the increase in the bulk flow has been done consequently by ensuring the Reynolds number in the tube, is well within the limit to maintain a laminar flow

However, the results obtained using the semi-cone angle method is different. It shows a

linear increase with increasing the volumetric flow rate. The rate of change of the laminar flame speed obtained from the semi-cone angle method w.r.t. the volumetric flow rate is found to be:

$$\frac{dS_L^{sca}}{d(\dot{V}_{tot}/A_e)} = 0.02$$

In here the superscript *sca* indicates the laminar flame speed obtained from the semi-cone angle method. The increase in the laminar flame speed using the semi-cone angle method is found to be 2%. This variation is 1% higher than the laminar flame speed obtained from the mass conservation method in the absolute sense. This indicates that the mass conservation method is less sensitive to increasing the volumetric flow rate which shows that this method is more robust compared to the semi-cone angle method. Moreover, it shows that the semi-cone angle α of the flame does not change significantly with increasing the bulk flow velocity. Therefore the laminar flame speed using the semi-cone angle method shows an increasing trend. For the mass conservation method the opposite is true, increasing the unburned mixture velocity causes a slightly larger increase in the flame area. This results in a laminar flame speed that reduces with increasing the mixture velocity. Additionally, it can be deduced that the flame area increases approximately linearly with the increase in the bulk flow velocity. Similarly this can be stated for the semi-cone angle method in which the flame cone varies linearly with the volumetric flow rate.

Notice that the increase in the volumetric flow rate causes an increase in the flame height. This was shown to lead to a slight increase in the laminar flame speed estimation using the semi-cone angle method. From Fig.4.13 it shows that the laminar flame speed obtained from the two methods is converging. Indicating that increasing the flame height reduces the effect of flame curvature on the laminar flame speed estimated with the semi-cone angle method. Fig.4.12 shows that a flame height to burner diameter ratio of approximately 3 results in a more accurate result in the laminar flame speed measurement using the semi-cone angle method, based on the laminar flame speed measurement using the mass conservation method. Therefore it is recommended to use a volumetric flow rates that results in a flame height that is approximately larger than 3 times the burner diameter to reduce the effect of the flame curvature on the laminar flame speed estimation using the semi-cone angle method.

The value of the laminar flame speed in this investigation is shown in Table 21 for the mass conservation method and in Table 22 for the semi-cone angle method, including the volumetric flow rates and relative errors of the measurements.

Table 21: Detailed values of the variation of the laminar flame speed using the mass conservation method

$\dot{V}_{total}$ nl/min	8.01	12.00	14.36
$\frac{\Delta\dot{V}_{tot}}{\dot{V}_{tot}}$ in %	1.13	0.90	0.82
S_L^{mc} in cm/s	36.54	36.28	35.64
S.E. $\frac{\Delta S_{L_{SEM}}^{mc}}{S_L^{mc}}$ in %	0.08	0.14	0.28
Uncertainty $\frac{\Delta SL^{mc}}{S_L^{mc}}$ in %	1.29	2.29	4.49

Table 22: Detailed values of the variation of the laminar flame speed using the semi-cone angle method

$\dot{V}_{total}$ in nl/min	8.01	12.00	14.36
R.E $\frac{\Delta\dot{V}_{tot}}{\dot{V}_{tot}}$ in %	1.13	0.90	0.82
S_L^{sca} in cm/s	31.71	32.42	33.49
S.E. $\frac{\Delta S_{L_{SEM}}^{sca}}{S_L^{sca}}$ in %	0.20	0.25	0.32
Uncertainty $\frac{\Delta SL^{sca}}{S_L^{sca}}$ in %	3.24	3.98	5.14

Ch.5 Probability Density Function & source of uncertainty

The uncertainty of a measurement is determined by systematic errors and random errors. The systematic errors are inherited by the used hardware to measure the parameters during the experiment. In this case the systematic errors were due to the flow controllers. These errors are present every time the experiment is repeated. The stochastic or random errors occur during the experiment due to random disturbances. These errors are typically quantified by repeating the measurements multiple times and using statistical techniques [87]. The measurement of the laminar flame speed in this research is determined from the average of a series of measurements, by analyzing a large batch of images taken in a short time instance. However, any series of measurements can lead to an average value. The question in this case is:" to what measurement distribution the computed average laminar flame speed belongs to?" The answer to this question indicates the reproducibility of the reported data and hence measurement precision.

It was discussed earlier that the average laminar flame speed is determined with a 95% confidence level. This was performed by stating that the measurements spread will assume a Gaussian distribution which allowed the use of the table given in Appendix B in order to determine the value for Z in Eq.37. This assumption is verified here by deriving the probability density function (PDF) for the laminar flame speed of DNG for each equivalence ratio. For this analysis only the laminar flame speed obtained using the mass conservation method is considered. This was shown earlier to agree better with the laminar flame speed of methane. Therefore it can be assumed that the result obtained from the mass conservation method is more accurate compared to the semi-cone angle method.

Recall that in this experiment the OH chemiluminescence of the Bunsen burner flame has been recorded at 1000 FPS. This is equivalent to repeating the same measurement a 1000 times. From this sampling rate the uncertainty in the experiment is quantified by obtaining the STD of the measurements. From this data a PDF is derived to obtain the distribution of the measurements. This PDF will therefore indicate the range of measurements and the probability of the magnitude of the laminar flame speed, which can be obtained by repeating the experiment.

The source of this random uncertainty is attempted to be identified by means of transforming the laminar flame speed variation in time, to the frequency domain. This will result in the Eigen mode of the variation of the laminar flame speed, which may be traced back to the performance of the experimental hardware during the recording of the images.

5.1 Probability Density Function

The uncertainty of the laminar flame speed is determined by observing the time variation of this parameter. This has been performed by using the same MATLAB algorithm that was used to determine the laminar flame speeds over their respective equivalence ratios. The numbers of images for each

equivalence ratio is equal to the sample size which in this case is equal to 1000 images. Using this data, one can derive a probability density function. The PDF of the laminar flame speed of each equivalence ratio is determined by first creating bins or classes.

Bins are a collection of measurements within a certain range. This term is commonly used in statistics to indicate a certain measurement intervals in which number of occurrence of the observation are sorted. This categorizes the measurements by the magnitude of the laminar flame speed. Bins are typically used in the construction of a histogram. Therefore the method used to determine the bins for a histogram is used here to determine the probability density function.

There are no actual theoretical methods in which one can obtain the optimal number of bins for the sample size [88]. Some proposals exist such as those found in literature [89] [90] [91] in which the optimal number of bins is determined by assuming a reference standard deviation of the measurement. These methods are typically useful for small data sets to estimate the PDF. However all of the proposed techniques are determined by assuming the STD of the sample or by assuming a smoothening function for the data set [89]. Instead of employing these methods, the number of bins or bin size is usually determined using certain rule of thumb techniques [88]. The number of bins can for instance be determined by means of taking the square root of the number of observation. This is mathematically written as [92]:

$$n = \sqrt{N} \tag{58}$$

In this *N* is the number of samples and *n* is the number of bins. This is known as the square root rule. Other techniques exist in obtaining the "optimal" number of bins for a certain measurement such as the Inter Quartile Range (IQR) method described by Freedman et al. [93]. The IQR of a data set is determined from the difference between the median of the second half and the median of the first half of the data set. This method gives the width of the bin from the expression [93]:

$$W = 2(IQR)N^{-\frac{1}{3}} \tag{59}$$

In this expression *W* is the bin width. The number of bins can then be simply determined by dividing the sample size by this bin width. This is given mathematically by:

$$n = \frac{N}{W} \tag{60}$$

The number of bins suggested by the IQR method and the commonly employed square root method suggest 33 bins for this case. For more on the determination of the bin size the reader is referred to reference [89].

The PDF of the measurements can then be obtained by taking the center of these bins. The number of occurrence is then normalized using the total sample size. From this, a curve is fitted between these points to obtain the distribution of the observations. In this case all of the observations tend to follow a first order Gaussian distribution of the form:

$$P = ae^{-\left(\frac{(S_L-b)^2}{2c^2}\right)} \tag{61}$$

The values of these constants are given in Table 23. The value for the constant *a* is the maximum of the PDF, *b* is the average of the laminar flame speed and *c* is the standard deviation of the measurement. The time variation of the laminar flame speed for each equivalence ratio and their respective PDF's are shown in Fig.5a and Fig.5b. Observe that the PDF of each case is shown to have a normal distribution. This confirms the initial assumption that the variation of the laminar flame speed follows a Gaussian distribution. This concludes that the method to determine the confidence level for the average laminar flame speed measurement was appropriate.

Table 23: The value of the constants in Eq.61

ϕ	0.80	0.88	0.93	1.00	1.06	1.15	1.20	1.36	1.41	1.45	1.50	1.53	1.55
a	0.08	0.14	0.11	0.12	0.16	0.14	0.13	0.08	0.08	0.15	0.11	0.10	0.09
b	29.12	30.6	33.47	35.61	36.54	36.65	34.53	23.07	18.91	15.85	14.64	13.58	13.63
c	0.81	0.68	0.61	0.57	0.47	0.52	0.47	0.69	0.29	0.45	0.29	0.44	0.46

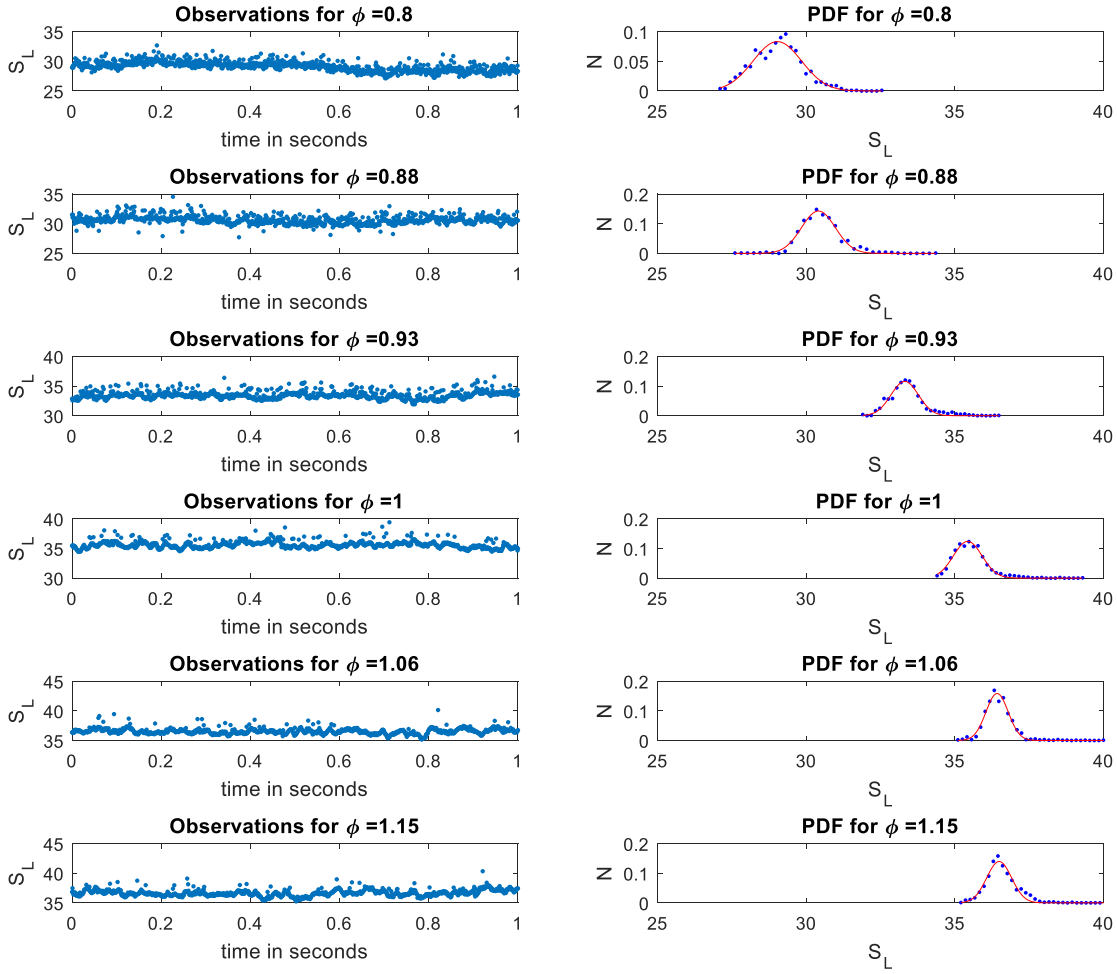

Fig. 5a: The time variation of the laminar flame speed from the lean to stoichiometry region with their corresponding probability densitv function.

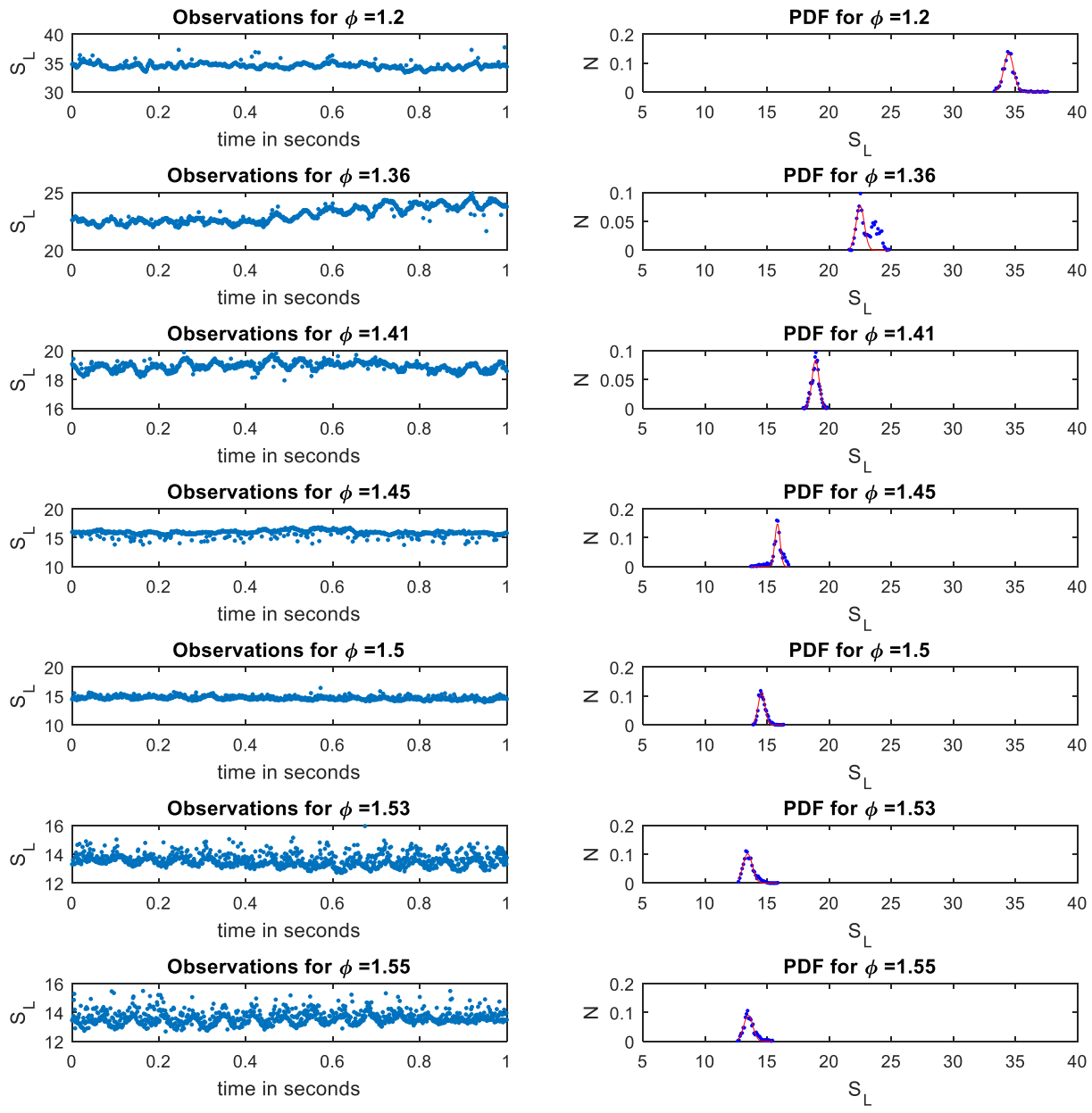

Fig. 5b: The time variation of the laminar flame speed for post stoichiometry condition up to far rich region with their corresponding PDFs.

Observing the time variation of the laminar flame speed it can be noticed that it is constant for most of the equivalence ratios. This is as expected, since the Burner was designed to maintain a steady flame. However, further observation shows that some experimental results depict an oscillation about the average. It shows that a noise is present in addition to a typical sinusoid. This is clearly apparent for $\phi = 1.36, 1.41, 1.45, 1.50, 1.53\ and\ 1.55$. Moreover the PDF of the laminar flame speed at $\phi = 1.36$ shows a double peak. This phenomenon is apparent in this experiment due to the high acquisition rate of the camera.

The cause of the sinusoid is assumed to be from the fluctuation in the air and fuel valves in the experiment. By observing these equivalence ratios, it shows that this phenomenon occurs in the rich region of the flame. This indicates that the volumetric flow rate for air is reduced closer to the lower limit of the flow control valve. This causes the valve to become less accurate in its control resulting in the observed fluctuations.

5.1.1 Volumetric flow rate and sampling duration influence on the PDF

The same analysis is performed by conducting an additional measurement on the nearest stoichiometric mixture quality in the used equivalence ratio span which is $\phi = 1.06 \pm 0.01$. However, the volumetric flow rate has been increased by 50% and 80%. Moreover the sampling duration has been increased to 6.5 seconds. The number of bins in the PDF for this session has been increased accordingly to 81. The result is shown in Fig.5.1. Note that the number of occurrence *(N)* in the PDF is normalized w.r.t. the total sample size.

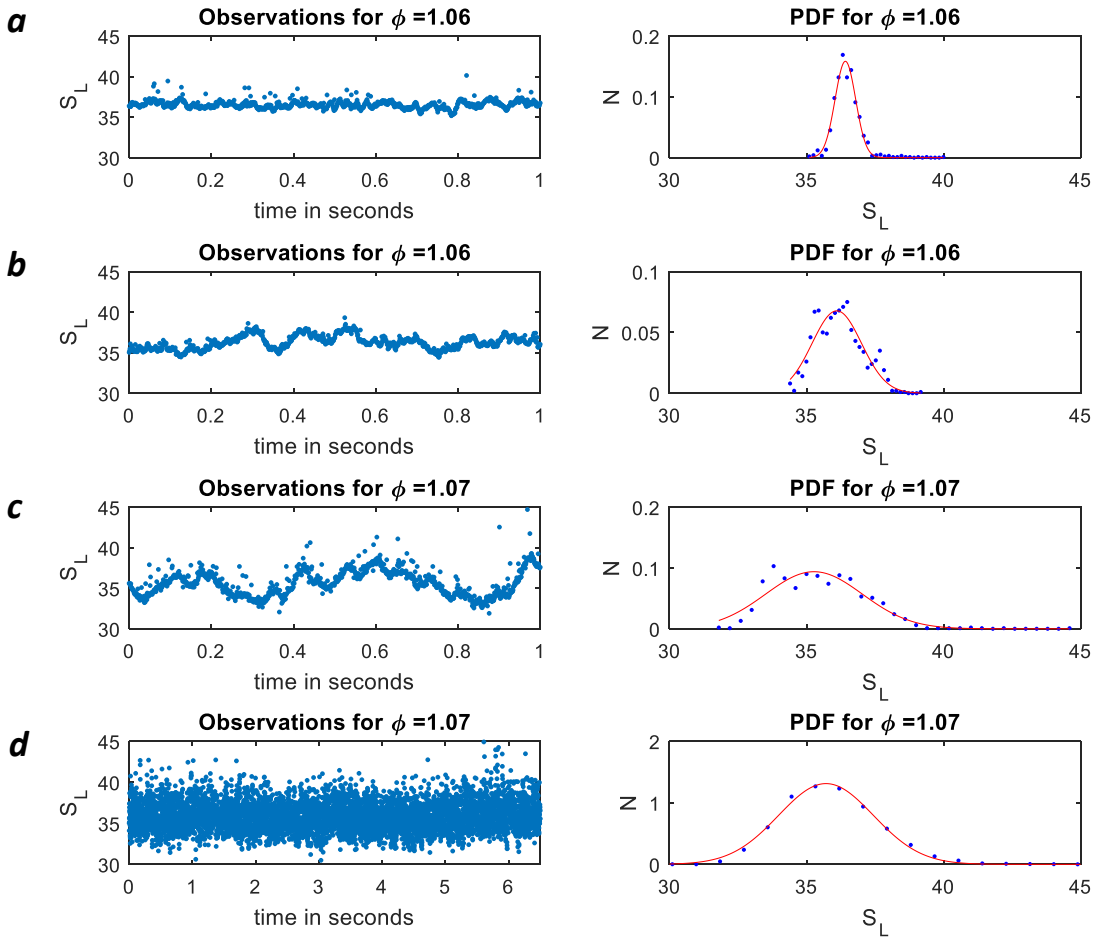

Fig. 5.1a, b, c, d: in 5.1a the laminar flame speed variation and PDF for a flow rate of 8nl/min is shown, in 5.1b the laminar flame speed variation and PDF for a flow rate of 12 nl/min is shown, in 5,1c the laminar flame speed variation and PDF for a flow rate of 14.36 nl/min is depicted and in 5.1d the sampling duration was increased to 6.5 seconds for a flow rate of 14.36 nl/min.

Comparing the PDF of Fig.5.1b to Fig.5.1a shows that the effect of increasing the volumetric flow rate by 50% to 12nl/min increases the width of the PDF at half amplitude. Further increase in the volumetric flow rate to 14.36nl/min. shows a larger magnitude in the variation of the laminar flame speed, resulting in a further increase in the width of the PDF as shown in Fig.5.1c.This indicates that the increase in volumetric flow rate increases the uncertainty of the measurement. Recall that the increase in volumetric flow rate increases the flame height. This increase in the flame height causes the flame to be more susceptible to uncertainties due to the increase in unsteadiness [69].

The effect of increasing the sampling rate in combination with increasing the volumetric flow on the PDF is shown in Fig.5.1d. This shows a clear Gaussian distribution of the measurement compared to the PDF in Fig.5.1c. This indicates that a longer sampling duration improves the distribution of the measurements, depicted by the converging of the PDF to a Gaussian distribution. This in turn allows for a more accurate probability analysis of the laminar flame speed estimation.

5.2 Frequency domain analysis of the laminar flame speed

It was shown earlier that the time variation of the laminar flame speed shows an oscillation about its average which appears to be periodic. This indicates that an Eigen mode or a fundamental frequency is present in the measurement. To distinguish the main frequencies within the measurement, one can gain an in depth knowledge on the origin of this periodic oscillation. Indeed, one can view the measurements in the frequency domain. Note that in this section the signal refers to the variation of the laminar flame speed in time.

The transformation of a signal in time domain to the frequency domain is performed by Fourier transforming the signal. According to the Fourier transformation theorem, any function that is a periodic/aperiodic in time $x(t)$can be transformed into its respective frequency domain, this results in the frequency domain representation of the signal $X(f)$ [94]. This is given by the definition of the Fourier transformation [94]:

$$X(f) = \int_{-\infty}^{\infty} x(t)\, e^{-2\pi i F t} dt \tag{62}$$

In this expression *F* is the fundamental frequency in Hz, *t* is time in seconds and *j* is an imaginary number.

The Fourier transform of the variation of the laminar flame speed is therefore employed here in this analysis. It is clear that the laminar flame speed is a function of time $S_L(t)$. The variation of the laminar flame speed in time can therefore be expressed in frequency domain by Fourier transforming this function $\mathcal{F}\big(S_L(t)\big) = S_L(f)$. This leads to the following expression in terms of the laminar flame speed variation in time:

$$S_L(f) = \int_{-\infty}^{\infty} S_L(t)\, e^{-2\pi i F t} dt \tag{63}$$

This allows for a clear distinction to the (if present) fundamental frequency of the laminar flame speed measurement. Note that the integral has to be evaluated from $-\infty$ to ∞ which indicates that the variation of the laminar flame speed must be continues in time.

In practice however, the signal cannot be continuously measured. Instead, the signal is typically sampled at a certain sampling frequency f_s. This results in a discrete set of data points. To determine high order frequencies in a discrete data set, the sampling frequency must be at least twice the highest frequency present in a signal according to Nyquist theorem. The Fourier transformation of a discrete function can then be conducted by applying the discrete Fourier transformation (DFT) of the data set. The DFT of an n^{th} sampled data value x_n is given by the expression [94]:

$$X_k = \sum_{n=0}^{N} x_n \, e^{-2\pi i \frac{kn}{N}} \qquad k = 1, 2, 3, \dots N \tag{64}$$

Note that in this expression k/N represents the frequency in which, N is the total sample size of the measurement. For this case the laminar flame speed is sampled at an acquisition rate of 1 kHz for the duration of 1 second. This will results in a total sample size $N = 1000$ which can be Fourier transformed using the DFT expression given in Eq.64. This results in the following equation for the DFT of the variation of the laminar flame speed in time:

$$S_{L_k} = \sum_{n=0}^{1000} S_{L_n} \, e^{-2\pi i \frac{kn}{1000}} \qquad k = 1, 2, 3, \dots, 1000 \tag{65}$$

The DFT of the signal is evaluated here by means of Fast Fourier Transformation (FFT). The principle of the FFT and its algorithm is not discussed here. However, if the reader is interested this information can be found in reference [94]. The FFT is a method to evaluate the DFT given in Eq.65 although it is computationally significantly less expensive than evaluating Eq.65 directly. MATLAB has this algorithm already pre-programmed in its package which is used in this analysis. Note that the laminar flame speed has an average value larger than zero, which indicates that the amplitude of the 0^{th} order term in the frequency domain will be significantly larger than the amplitude of the fluctuations. For the computation, the average or the zero order term of the signal has been removed in order to observe only the fluctuations around the average signal value. Moreover, only half the frequency spectrum is used since the second half is the mirror image and is therefore redundant. The results of the Fourier transformation of the signal are shown in Fig.5.2a and Fig.5.2b.

Observing the frequency domain of the signal, shows that there is a high fundamental frequency present in only the laminar flame speed measurements at equivalence ratios $\phi > 1.15$. This fundamental frequency is seen to be at approximately 15Hz to 16Hz. Further observation of the figures shows that a second low fundamental frequency is present. This low fundamental frequency is found to be 1Hz to 3Hz which vanishes with increasing equivalence ratio.

This gives an indication on one of the sources of the unsteadiness of the flame. This further supports the hypothesis that the variation in the laminar flame speed is due to the oscillation of the flow control

valves, if the flow rates are close to the limit of the flow control units. This can be observed from both Fig.5.2a and Fig.5.2b, it shows that the fundamental frequency of 1-3Hz is present from $\phi = 0.80$ up to $\phi = 1.45$. This trend states that this fundamental frequency exists when a fuel lean mixture is used up to a rich mixture $\phi = 1.45$. This indicates that this fundamental frequency is present when the fuel flow rate is close to the limit of the fuel control unit, which suggests that the low fundamental frequency is the oscillation of the fuel flow control unit. Similarly, it is shown in the figures that the fundamental frequency of 15-16 Hz is present when the equivalence ratio increases. This indicates that the high fundamental frequency occurs when the air flow is closer to the limit of the air flow control unit. This suggests that this high fundamental frequency is the oscillation of the air flow control unit. It should be noted that the fundamental frequency is not clearly visible for the case of $\phi = 1.06$ due to noise therefore this hypothesis requires further investigation.

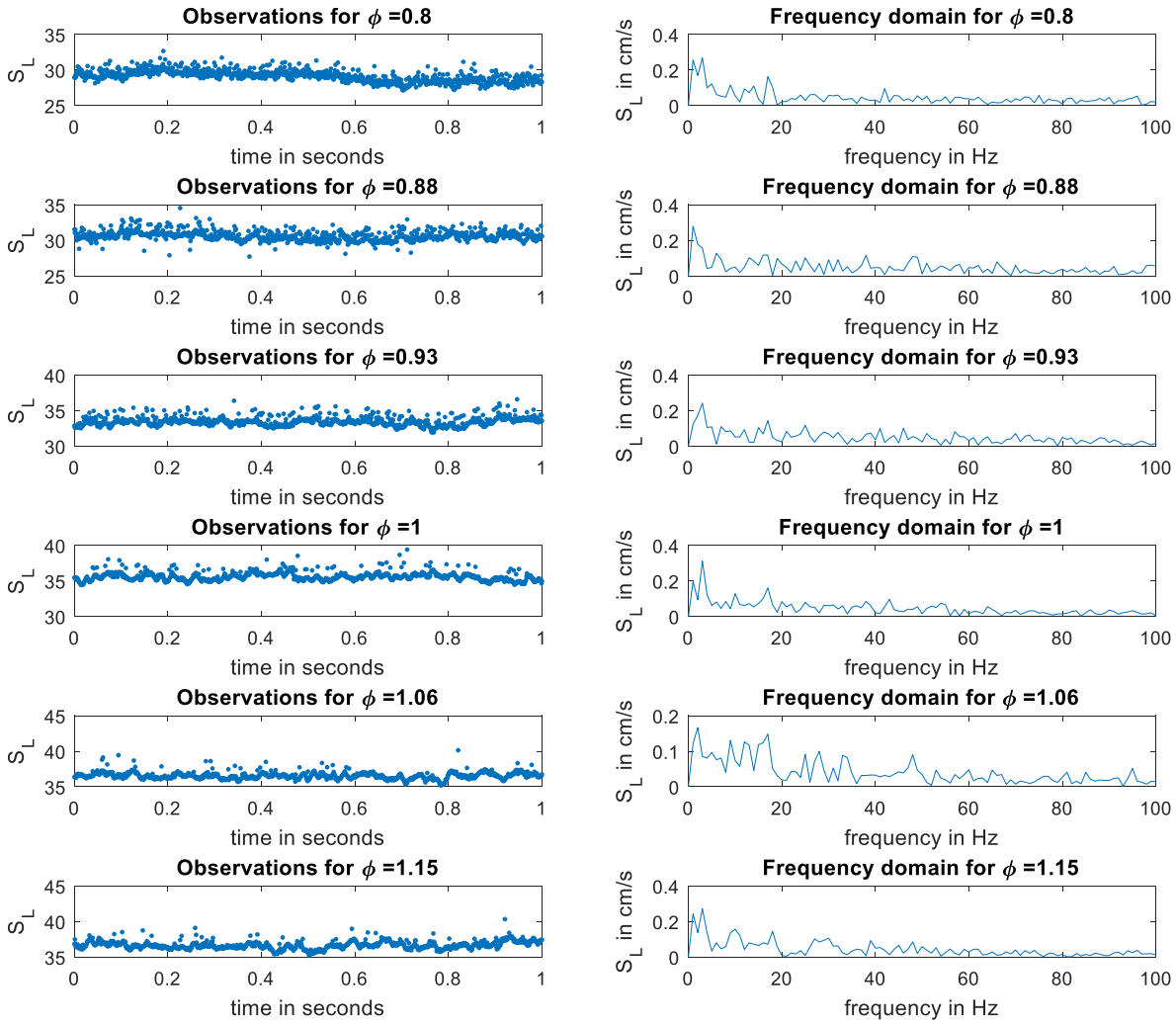

Fig. 5.2a: The Frequency domain analysis of the laminar flame speed variation in time.

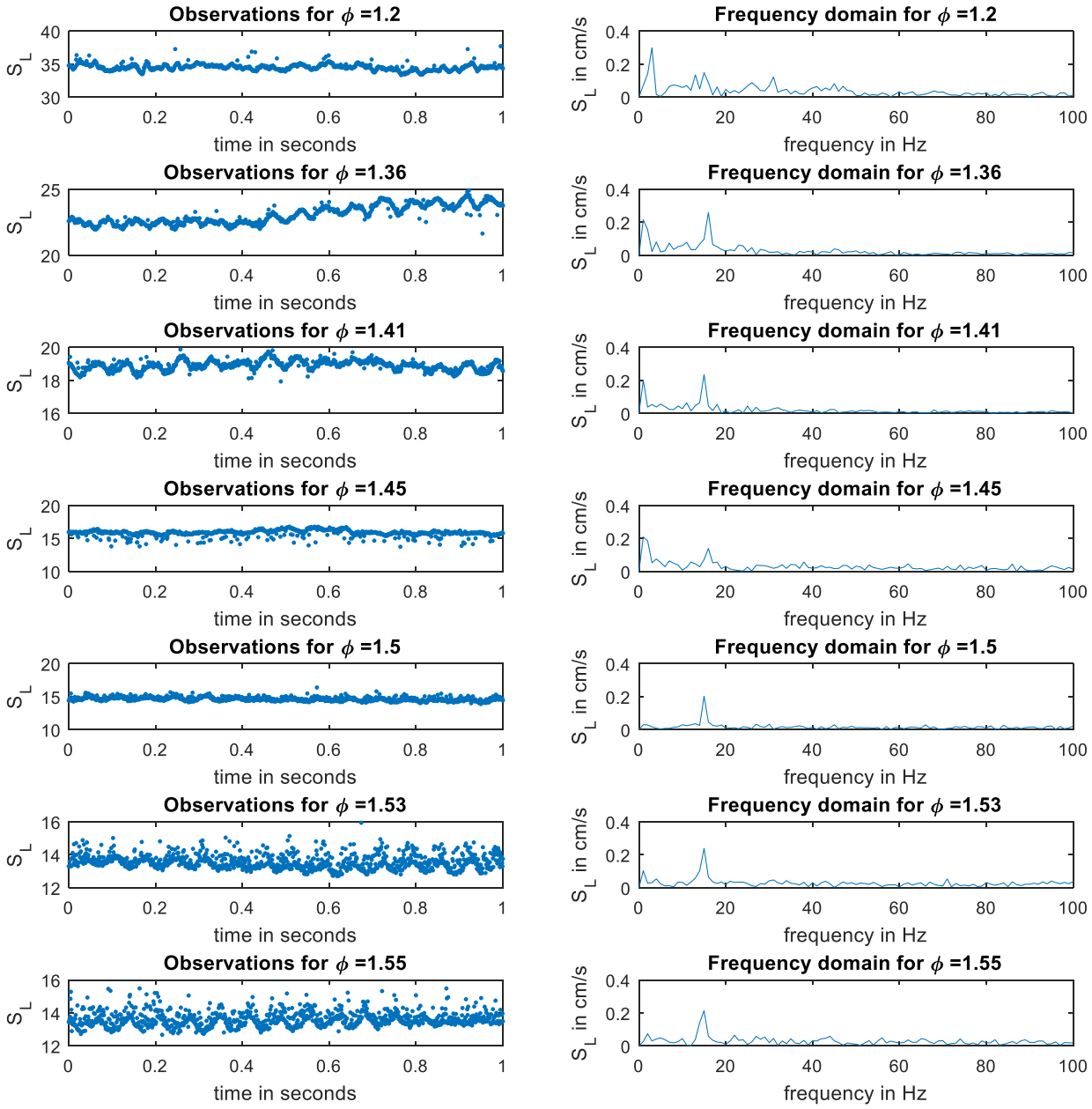

Fig. 5.2b: The Frequency domain analysis of the laminar flame speed variation in time.

Ch.6 Conclusion and future work

6.1 Conclusion

In this research the laminar flame speed of Dutch natural gas was measured by using OH chemiluminescence technique to visualize the reaction zone of a Bunsen flame. The laminar flame speed was estimated using both the semi-cone angle method and the mass conservation method. The results were compared to the laminar flame speeds of the natural gas of other regions and with pure methane. The random uncertainty of this experiment was quantified by means of a Probability Density function (PDF). Additionally, an attempt was made to identify the source of the uncertainty by evaluating the variation of the laminar flame speed in the frequency domain. From this investigation the following can be concluded:

- From the results it was found that the semi-cone angle method underestimated the laminar flame speed compared to the mass conservation method. The maximum difference was found to be 34.81% compared to the mass conservation method for $\phi = 1.20$. This discrepancy was due to the non-uniformity of the bulk flow. The semi-cone angle method is therefore more suitable for an aerodynamically tailored Nozzle burner in which a uniform flow is achieved at the burner exit. However, to lower the discrepancy of the semi-cone angle method compared to the mass conservation method, a correction was introduced in order to account for this non-uniformity of the bulk flow. For this correction the bulk flow was assumed to have a Poiseuille flow distribution. This correction showed a better estimation to the laminar flame speed although, this was still underestimated by a maximum of 13.95% compared to the semi-cone angle method at near stoichiometric conditions. This discrepancy is thought to be due to the flame stretch. It is therefore recommended to use the mass conservation method to estimate the laminar flame speed of tube type Bunsen burner flames.
- Comparison of the laminar flame speed of DNG to the gas of Pittsburgh and Abu Dhabi showed that the difference between the laminar flame speeds of the two natural gas compositions at stoichiometry $\phi = 1.00$ was lower by 5.32%. The comparison of the laminar flame speed of DNG to natural gas from Indonesia showed to be lower by 3.63% at stoichiometric conditions $\phi = 1.00$. Dutch natural gas consistently showed to have an overall lower laminar flame speed compared to gas of Pittsburgh, Abu Dhabi and Indonesia at stoichiometry and rich mixtures. This is thought to be due to high inert gas content in the DNG which was shown to be significantly higher compared to natural gas from Indonesia, Abu Dhabi and Pittsburgh. However, the laminar flame speed of DNG at lean conditions was shown to be comparable or slightly higher than the natural gas from Pittsburgh and Abu Dhabi.
- The laminar flame speed of DNG that was obtained using the corrected semi-cone angle method and mass conservation method was compared with the laminar flame speed of pure methane. The laminar flame speeds of pure methane used for this comparison were obtained from expanding sphere method. This comparison showed that the laminar flame speed of DNG using the mass conservation method, leads to an overall higher magnitude compared to the laminar flame speed of methane until $\phi > 1.00$. At rich regions the laminar flame speed of DNG is

shown to be lower this suggests that the high inert gas content in DNG reduces the flame speed at near stoichiometric and rich mixtures. A similar comparison with the laminar flame speed of DNG using the corrected semi-cone angle method shows an overall, lower laminar flame speed compared to pure methane. However both methods are shown to be within the spectrum of laminar flame speed values obtained through previous experiments. Although, the laminar flame speed obtained from the mass conservation method appears to give more accurate indication of the burning velocity of DNG.

- The variation of the volumetric flow rate effect on the laminar flame speed was investigated. It was observed that increasing the volumetric flow rate, causes a slight decrease in the laminar flame speed estimation using the mass conservation method while the opposite was true for the results of the semi-cone angle method. Moreover increasing the volumetric flow rate was shown to be beneficial to the accuracy of laminar flame speed estimation using the semi-cone angle method. It is therefore recommended to use a volumetric flow rate that results in a Bunsen flame height that is approximately 3 times larger than the burner exit diameter.
- From the uncertainty analysis it was found that the laminar flame speed using the mass conservation method showed a lower overall uncertainty compared to the mass-conservation method. Indicating that the mass-conservation method is more reliable to measure the laminar flame speed from a tube type Bunsen burner flame. The maximum uncertainty in the mass conservation method was found to be 3.39% compared to the 10.63% from the semi-cone angle method.
- The frequency domain analysis of the variation of the laminar flame speed in time showed that a low and high fundamental frequency were present. These fundamental frequencies were hypothesized to be the oscillation of the flow control valves for air and fuel. A low fundamental frequency of 2to 3Hz was observed which vanished as the equivalence ratio increased. This fundamental frequency is therefore assumed to be of the fuel control valve fluctuations. Since the increase in equivalence ratio indicates a higher fuel flow rate, which is further away from the minimum limit of the fuel flow controller. Similarly it was observed that a high fundamental frequency is present when the equivalence ratio is increased. Indicating that the high fundamental frequency may be related to the oscillation of the air control valve. This observation was possible due to the high camera acquisition rate used in this experiment.

6.2 Future work

6.2.1 Improvement to the experimental setup

Some suggestions are given here to improve the experimental setup and the experimental method as a whole. From the investigation several factors were apparent which can be improved if the same experimental setup is used. For instance, the tip of the Bunsen burner flame can be recorded better if a knife edge was used at the burner base in order to suppress the light from the flame base. This method was suggested in the literature to improve image quality and recording of the chemiluminescence emission of the Bunsen flame. It was also documented that the location of the knife edge w.r.t. the flame base affects its influence on the clarity of the flame tip. The light from the flame base is

suppressed while the OH* emission of the flame tip remains unchanged. The ideal location should be determined by trial during the experiment. Additionally the camera shutter speed should be increased.

During the experiment the Bunsen flame was found to blow off at equivalence ratio's below $\phi = 0.8$. The reason of this blow off is not clear if it is the burning limit of DNG or related to the Bunsen burner design. However, a possible improvement to the Bunsen burner can be achieved by introducing a co-flow with the Bunsen burner flame. The co-flow will add momentum to the products of the Bunsen flame which improves burner stability. This may allow for an investigation of the laminar flame speed at lower equivalence ratios. Additionally to eliminate a factor of uncertainty to the fluctuations of the Bunsen burner flame due to drafts in the environment, it is beneficial to shroud the Bunsen flame. A schematic to improve the experimental setup is shown in Fig.6.

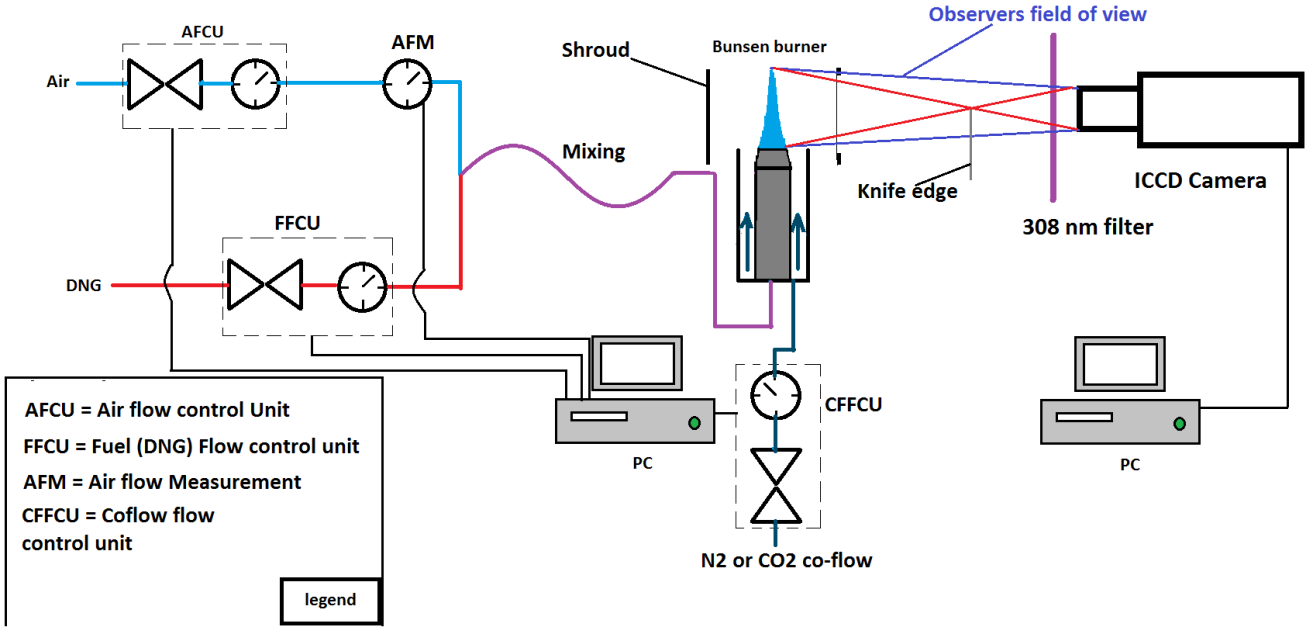

Fig. 6: Proposed improvement to the used experimental setup.

6.2.2 Topics for future research

The results obtained from this experiment were obtained using the OH chemiluminescence technique. The laminar flame speed was then quantified from the flame geometry. The results could be compared to the laminar flame speed obtained using a different measurement technique such as PIV or LDV. One may also consider measuring the adiabatic flame speed using the heat flux method or using a flat flame burner to compare with the results presented in this report. However, the experiment should be considered to be repeated using a nozzle burner for the determination of the laminar burning velocity using the semi-cone angle method.

The Bunsen burner flame was shown to have a tip opening at the equivalence ratio $\phi = 1.50$. The effect of this tip opening on the measurement of the laminar flame speed using the mass conservation method is unknown. The literature suggests that the tip opening of the Bunsen flame should be simulated. However, to verify the simulation experimental data is required. The laminar flame speed obtained

using the methods in this investigation should be verified by means of direct measurement techniques such as PIV and LDV. From this investigation the OH chemiluminescence method to determine the laminar flame speed of a tip opened Bunsen flame can be justified.

The characteristics of DNG mixed with other fuels such as hydrogen or methane should be investigated. The influence of these additional fuels on the characteristics of DNG should be quantified. One may also extend this further by investigating the burning characteristics of DNG mixed with increased dilution using CO_2 or N_2.

From literature it was found that the laminar flame speed changes with the ambient pressure and temperature. This topic was outside the scope of this research. However, one may investigate the influence of the ambient temperature and pressure on the laminar flame speed of DNG using a Bunsen burner. In practice the combustion process usually occurs at elevated temperature and pressure. This topic will therefore approach the practical application more closely. However, it should be noted that the Bunsen flame is unsuitable if high pressure effects on the laminar flame speed is investigated. For high pressure effects on the laminar flame speed different flame geometry or measurement technique should be considered.

From the frequency domain analysis of the laminar flame speed variation in time it was found that a fundamental frequency is present. This was clearly shown at high equivalence ratios beyond stoichiometry. From this observation a hypothesis was presented in which this oscillation of the laminar flame speed was related to the fluctuations of the air and fuel control units in this experiment.

To prove this hypothesis an additional experiment should be conducted using the same flow control units for air and DNG. In the experiment the emphasis should be place in the rich spectrum of the equivalence ratio $\phi > 1.20$. Subsequently the volumetric flow rate should be increased and the OH* emission of the Bunsen flame should be recorded. For this experiment changing the burner diameter may allow the increase of the volumetric flow rate well beyond the lower limit of the flow controllers and avoid flame blow off. The laminar flame speed variation should then be analyzed in the frequency domain for these equivalence ratios in order to investigate the presence of the fundamental frequencies at increased flow rates.

To relate the oscillation of the measurement to the flow controllers, a hotwire setup should be used at the burner exit in order to measure the variation of the flow rate in time. The fundamental frequency of the flow rate measured with the hot wire should then be compared to the fundamental frequency determined from the variation of the laminar flame speed in time. Moreover, higher order frequencies may be present which was not detected due to the acquisition rate employed in this experiment. To identify the higher order frequencies a higher acquisition rate should be used. This acquisition rate should be at least twice the highest frequency expected in the signal (Nyquist sampling theorem).

Appendix A: Derivations of equations

The derivation of the absolute error in the equivalence ratio in section 2.3.1

Given the equation:

$$\Delta\phi = \sqrt{\left[\left(\frac{\partial\phi}{\partial\dot{V}_{DNG}}\Delta\dot{V}_{DNG}\right)^2 + \left(\frac{\partial\phi}{\partial\dot{V}_{air}}\Delta\dot{V}_{air}\right)^2\right]} \qquad (a)$$

The terms within the square root of this expression are determined from the definition of the equivalence ratio. This gives results in the following:

$$\phi = \frac{1}{FAR_{stoich}}\frac{\dot{V}_{DNG}}{\dot{V}_{air}}$$

$$\frac{\partial\phi}{\partial\dot{V}_{DNG}} = \frac{1}{FAR_{stoich}}\frac{1}{\dot{V}_{air}} \qquad (b)$$

$$\frac{\partial\phi}{\partial\dot{V}_{air}} = \frac{-1}{FAR_{stoich}}\frac{\dot{V}_{DNG}}{\dot{V}_{air}^2} \qquad (c)$$

Substitution of *b* and *c* in *a* results in the following expression:

$$\Delta\phi = \sqrt{\left[\left(\frac{1}{FAR_{stoich}}\frac{1}{\dot{V}_{air}}\Delta\dot{V}_{DNG}\right)^2 + \left(\frac{-1}{FAR_{stoich}}\frac{\dot{V}_{DNG}}{\dot{V}_{air}^2}\Delta\dot{V}_{air}\right)^2\right]}$$

This can be further simplified to the final result:

$$\Delta\phi = \frac{1}{FAR_{stoich}}\sqrt{\left[\left(\frac{1}{\dot{V}_{air}}\Delta\dot{V}_{DNG}\right)^2 + \left(\frac{\dot{V}_{DNG}}{\dot{V}_{air}^2}\Delta\dot{V}_{air}\right)^2\right]}$$

The derivation of the moles of air required for complete combustion in section 3.1 and product species in 4.3.1

The number of moles air required for complete combustion of DNG is obtained by employing the chemical equilibrium equation for hydro carbons given by:

$$C_\alpha H_\beta O_\gamma + \left(\alpha + \frac{\beta}{4} - \frac{\gamma}{2}\right)(O_2 + 3.76N_2) \rightarrow \alpha CO_2 + \frac{\beta}{2}H_2O + 3.76\left(\alpha + \frac{\beta}{4} - \frac{\gamma}{2}\right)N_2$$

For the number of moles are required for complete combustion the values for α, β and γ must be determined. These are equivalent to the number of moles of carbon, hydrogen and oxygen present in the fuel. For DNG the species that contain carbon, hydrogen and or oxygen are found to be CH_4, C_2H_6 ,

$C_3H_8,\ i-C_4H_{10}\ and\ CO_2$. The amount of each of these species present in 1 unit volume DNG is given in percent. This is used to solve for the total number of carbon, hydrogen and oxygen in 1 unit volume of DNG. The values for α, β and γ can then be found as follows:

$$\alpha = (0.813 + 2 * 0.029 + 3 * 0.004 + 4 * 0.002 + 1 * 0.009) = 0.9$$

$$\beta = (0.813 * 4 + 6 * 0.029 + 8 * 0.004 + 10 * 0.002) = 3.478$$

$$\gamma = (2 * 0.009) = 0.018$$

Substitution of these values in the chemical equilibrium equation for hydro carbons results in:

$$C_{0.9}H_{3.478}O_{0.018} + \left(0.9 + \frac{3.478}{4} - \frac{0.018}{2}\right)(O_2 + 3.76N_2) \rightarrow 0.9CO_2 + \frac{3.478}{2}H_2O + 3.76\left(0.9 + \frac{3.478}{4} - \frac{0.018}{2}\right)N_2$$

In which the number of moles of air for stoichiometric combustion of DNG is given by:

$$n_{air} = \left(0.9 + \frac{3.478}{4} - \frac{0.018}{2}\right) * (1 + 3.76) = 8.38$$

The computation of the correction factor for the non-uniformity of the flow in section 4.1.1

Given the relation for the average velocity of a Poiseuille flow:

$$\overline{u(r)} = \frac{1}{b-a}\int_a^b u(r)\,dr$$

This is fully written as:

$$\overline{u(r)} = \frac{1}{b-a}\int_a^b 2U_0\left(1 - \left(\frac{r}{R}\right)^2\right)dr$$

The limits of integration are corresponding with the radius of the burner exit with its center the zero point. This results in:

$$\overline{u(r)} = \frac{1}{6-(-6)}\int_{-6}^{6} 2U_0\left(1 - \left(\frac{r}{6}\right)^2\right)dr$$

Solving the integral gives the solution:

$$\overline{u(r)} = \frac{1}{12}\,2U_0\left[\left(r - \frac{1}{3}\frac{r^3}{6^2}\right)\right]_{-6}^{6}$$

$$\overline{u(r)} = \frac{1}{6}U_0\left[\left(6 - \frac{1}{3}\frac{6^3}{6^2}\right) - \left(-6 - \frac{1}{3}\frac{(-6)^3}{6^2}\right)\right]$$

$$\overline{u(r)} = U_0 \left[\left(1 - \frac{1}{3}\right) - \left(-1 + \frac{1}{3}\right)\right]$$

$$\overline{u(r)} = U_0 \left[2 - \frac{2}{3}\right]$$

$$\overline{u(r)} = U_0 \left[\frac{6}{3} - \frac{2}{3}\right]$$

$$\overline{u(r)} = U_0 \left[\frac{4}{3}\right] = \frac{4}{3} U_0$$

Appendix B: Normal distribution table

The standard normal probability distribution table as given by
http://www.stat.ufl.edu/~athienit/Tables/Ztable.pdf

For a 95% confidence interval the value of z can be determined by first dividing the confidence interval by 2 which gives 47.5% to the left and to the right of mean. Hence the area of the PDF to the left of the mean is given by $0.5 + 0.475 = 0.975$.

This value is indicated in this table which shows that the value for z is equal to 1.96 for a 95% confidence interval.

Standard Normal Probabilities

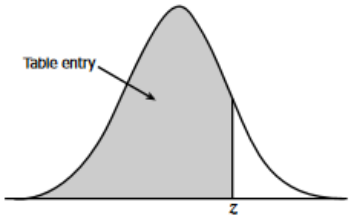

Table entry for z is the area under the standard normal curve to the left of z.

z	.00	.01	.02	.03	.04	.05	.06	.07	.08	.09
0.0	.5000	.5040	.5080	.5120	.5160	.5199	.5239	.5279	.5319	.5359
0.1	.5398	.5438	.5478	.5517	.5557	.5596	.5636	.5675	.5714	.5753
0.2	.5793	.5832	.5871	.5910	.5948	.5987	.6026	.6064	.6103	.6141
0.3	.6179	.6217	.6255	.6293	.6331	.6368	.6406	.6443	.6480	.6517
0.4	.6554	.6591	.6628	.6664	.6700	.6736	.6772	.6808	.6844	.6879
0.5	.6915	.6950	.6985	.7019	.7054	.7088	.7123	.7157	.7190	.7224
0.6	.7257	.7291	.7324	.7357	.7389	.7422	.7454	.7486	.7517	.7549
0.7	.7580	.7611	.7642	.7673	.7704	.7734	.7764	.7794	.7823	.7852
0.8	.7881	.7910	.7939	.7967	.7995	.8023	.8051	.8078	.8106	.8133
0.9	.8159	.8186	.8212	.8238	.8264	.8289	.8315	.8340	.8365	.8389
1.0	.8413	.8438	.8461	.8485	.8508	.8531	.8554	.8577	.8599	.8621
1.1	.8643	.8665	.8686	.8708	.8729	.8749	.8770	.8790	.8810	.8830
1.2	.8849	.8869	.8888	.8907	.8925	.8944	.8962	.8980	.8997	.9015
1.3	.9032	.9049	.9066	.9082	.9099	.9115	.9131	.9147	.9162	.9177
1.4	.9192	.9207	.9222	.9236	.9251	.9265	.9279	.9292	.9306	.9319
1.5	.9332	.9345	.9357	.9370	.9382	.9394	.9406	.9418	.9429	.9441
1.6	.9452	.9463	.9474	.9484	.9495	.9505	.9515	.9525	.9535	.9545
1.7	.9554	.9564	.9573	.9582	.9591	.9599	.9608	.9616	.9625	.9633
1.8	.9641	.9649	.9656	.9664	.9671	.9678	.9686	.9693	.9699	.9706
1.9	.9713	.9719	.9726	.9732	.9738	.9744	.9750	.9756	.9761	.9767
2.0	.9772	.9778	.9783	.9788	.9793	.9798	.9803	.9808	.9812	.9817
2.1	.9821	.9826	.9830	.9834	.9838	.9842	.9846	.9850	.9854	.9857
2.2	.9861	.9864	.9868	.9871	.9875	.9878	.9881	.9884	.9887	.9890
2.3	.9893	.9896	.9898	.9901	.9904	.9906	.9909	.9911	.9913	.9916
2.4	.9918	.9920	.9922	.9925	.9927	.9929	.9931	.9932	.9934	.9936
2.5	.9938	.9940	.9941	.9943	.9945	.9946	.9948	.9949	.9951	.9952
2.6	.9953	.9955	.9956	.9957	.9959	.9960	.9961	.9962	.9963	.9964
2.7	.9965	.9966	.9967	.9968	.9969	.9970	.9971	.9972	.9973	.9974
2.8	.9974	.9975	.9976	.9977	.9977	.9978	.9979	.9979	.9980	.9981
2.9	.9981	.9982	.9982	.9983	.9984	.9984	.9985	.9985	.9986	.9986
3.0	.9987	.9987	.9987	.9988	.9988	.9989	.9989	.9989	.9990	.9990
3.1	.9990	.9991	.9991	.9991	.9992	.9992	.9992	.9992	.9993	.9993
3.2	.9993	.9993	.9994	.9994	.9994	.9994	.9994	.9995	.9995	.9995
3.3	.9995	.9995	.9995	.9996	.9996	.9996	.9996	.9996	.9996	.9997
3.4	.9997	.9997	.9997	.9997	.9997	.9997	.9997	.9997	.9997	.9998

Bibliography

[1] Dirrenberger, Patricia, et al. "Measurements of laminar flame velocity for components of natural gas." *Energy & fuels* 25.9 (2011): 3875-3884.

[2] Huang, Zuohua, et al. "Measurements of laminar burning velocities for natural gas–hydrogen–air mixtures." *Combustion and Flame* 146.1 (2006): 302-311.

[3] Black, James. "Cost and performance baseline for fossil energy plants volume 1: Bituminous coal and natural gas to electricity." *National Energy Technology Laboratory: Washington, DC, USA* (2010).

[4] Daggett, D., R. Hendricks, and R. Walther. "Alternative fuels and their potential impact on aviation." (2006).

[5] Lim, E., and Cees Bil. "Liquefied natural gas aircraft: a life cycle costing perspective." *52nd AIAA Aerospace Sciences Meeting*. American Institute of Aeronautics and Astronautics, 2014.

[6] Economides, Michael J., and David A. Wood. "The state of natural gas." *Journal of Natural Gas Science and Engineering* 1.1-2 (2009): 1-13.

[7] Agentschap NL ministerie van economische zaken, "*Gas Composition Transition Agency Report 2013*". (2013)

[8] https://www.oxfordenergy.org/wpcms/wp-content/uploads/2017/05/The-Dutch-Gas-Market-trials-tribulations-and-trends-NG-118.pdf

[9] Barend J.Botter " GAS in the NETHERLANDS: The VITAL COMBINATION of MANY SMALL FIELDS and a GLOBAL GIANT" *AAPG European Region Annual Conference, Paris-Malmaison, France 23-24 November 2009*

[10] Correljé, Aad, Coby Van der Linde, and Theo Westerwoudt. "Natural gas in the Netherlands. From cooperation to competition?." (2003).

[11] Poinsot, Thierry, and Denis Veynante. *Theoretical and numerical combustion*. RT Edwards, Inc., 2005.

[12] Wu, Yi. *Experimental investigation of laminar flame speeds of kerosene fuel and second generation biofuels in elevated conditions of pressure and preheat temperature*. Diss. Rouen, INSA, 2016.

[13] Selle, Laurent, Thierry Poinsot, and Bernard Ferret. "Experimental and numerical study of the accuracy of flame-speed measurements for methane/air combustion in a slot burner." *Combustion and Flame* 158.1 (2011): 146-154.

[14] Poinsot, T. J., and D. P. Veynante. "Combustion." *Encyclopedia of Computational Mechanics*.

[15] Rallis, Costa John, and Ashton Martin Garforth. "The determination of laminar burning velocity." *Progress in Energy and Combustion Science* 6.4 (1980): 303-329.

[16] Westenberg, A. A., and R. M. Fristrom. "Methane-oxygen flame structure. IV. Chemical kinetic considerations." *The Journal of Physical Chemistry* 65.4 (1961): 591-601.

[17] Fristrom, Robert Maurice, and Arthur Ayer Westenberg. *Flame structure*. McGraw-Hill, 1965.

[18] Lewis, Bernard, and Guenther Von Elbe. "Theory of flame propagation." *Proceedings of the Symposium on Combustion*. Vol. 1. Elsevier, 1948.

[19] Law, C. K. "Dynamics of stretched flames." *Symposium (International) on Combustion*. Vol. 22. No. 1. Elsevier, 1989.

[20] Candel, Sebastien M., and Thierry J. Poinsot. "Flame stretch and the balance equation for the flame area." *Combustion Science and Technology* 70.1-3 (1990): 1-15.

[21] Law, Chung K. *Combustion physics*. Cambridge university press, 2010.

[22] Choi, Chun W., and Ishwar K. Puri. "Contribution of curvature to flame-stretch effects on premixed flames." *Combustion and flame* 126.3 (2001): 1640-1654.

[23] Chen, Zheng, Michael P. Burke, and Yiguang Ju. "Effects of Lewis number and ignition energy on the determination of laminar flame speed using propagating spherical flames." *Proceedings of the Combustion Institute* 32.1 (2009): 1253-1260.

[24] Lamoureux, N., N. Djebaıli-Chaumeix, and C-E. Paillard. "Laminar flame velocity determination for H2–air–He–CO2 mixtures using the spherical bomb method." *Experimental Thermal and Fluid Science* 27.4 (2003): 385-393.

[25] McAllister, Sara, Jyh-Yuan Chen, and A. Carlos Fernandez-Pello. "Thermodynamics of Combustion." *Fundamentals of Combustion Processes*. Springer New York, 2011. 15-47.

[26] Moran, Michael J., et al. *Fundamentals of engineering thermodynamics*. John Wiley & Sons, 2010.

[27] https://www.britannica.com/science/combustion/History-of-the-study-of-combustion

[28] Lewis, Bernard, and Guenther Von Elbe. "Determination of the speed of flames and the temperature distribution in a spherical bomb from time-pressure explosion records." *The Journal of Chemical Physics* 2.5 (1934): 283-290.

[29] Bouvet, N., et al. "Characterization of syngas laminar flames using the Bunsen burner configuration." *International Journal of Hydrogen Energy* 36.1 (2011): 992-1005.

[30] Natarajan, Jayaprakash. *Experimental and numerical investigation of laminar flame speeds of $H_2/CO/CO_2/N_2$ mixtures*. Diss. Georgia Institute of Technology, 2008.

[31] F. N. Egolfopoulos, "laminar flame speed: what do we measure, what do we report, what do we learn how do we use," *New perspective for laminar burning velocity,* 2012.

[32] Zhang, Yang. *Propagation and Extinction Studies of Laminar Lean Premixed Syngas/Air Flames*. Springer, 2017.

[33] Natarajan, J., T. Lieuwen, and J. Seitzman. "Laminar flame speeds of H2/CO mixtures: effect of CO2 dilution, preheat temperature, and pressure." *Combustion and flame* 151.1-2 (2007): 104-119.

[34] Glassman, Irvin, Richard A. Yetter, and Nick G. Glumac. *Combustion*. Academic press, 2014.

[35] Zabetakis, Michael George. *Flammability characteristics of combustible gases and vapors*. No. BULL-627. Bureau of Mines Washington DC, 1965.

[36] Cheng, Robert K., Benoit Bédat, and Larry W. Kostiuk. "Effects of buoyancy on lean premixed V-flames Part I: laminar and turbulent flame structures." *Combustion and flame* 116.3 (1999): 360-375.

[37] Roda, Aldo. "A history of bioluminescence and chemiluminescence from ancient times to the present." *Chemiluminescence and Bioluminescence*. 2010. 1-50.

[38] Clark, T. *Studies of OH, CO, CH and C2 radiation from laminar and turbulent propane-air and ethylene-air flames-NACA Technical Note 4266*. Technical report, National Advisory Committee for Aeronautics, Lewis Flight Propulsion Laboratory Cleveland, Ohio, 1958.

[39] Nori, Venkata, and Jerry Seitzman. "Evaluation of chemiluminescence as a combustion diagnostic under varying operating conditions." *AIAA paper* 953 (2008).

[40] Cormier, Milton, ed. *Chemiluminescence and bioluminescence*. Springer Science & Business Media, 2013.

[41] Bozkurt, Metehan. *Shock-tube investigation of key reactions for chemiluminescence in various combustion systems*. Diss. Universität Duisburg-Essen, Fakultät für Ingenieurwissenschaften» Maschinenbau und Verfahrenstechnik» Institut für Verbrennung und Gasdynamik, 2013.

[42] Guyot, Daniel, et al. "CH*/OH* chemiluminescence response of an atmospheric premixed flame under varying operating conditions." *ASME Turbo Expo 2010: Power for Land, Sea, and Air*. American Society of Mechanical Engineers, 2010.

[43] Haber, L. C., and U. Vandsburger. "A global reaction model for OH* chemiluminescence applied to a laminar flat-flame burner." *Combustion Science and Technology* 175.10 (2003): 1859-1891.

[44] Mazas, A. N., et al. "Effects of water vapor addition on the laminar burning velocity of oxygen-enriched methane flames." *Combustion and Flame* 158.12 (2011): 2428-2440.

[45] Haber, L. C., et al. *An experimental examination of the relationship between chemiluminescent light emissions and heat-release rate under non-adiabatic conditions*. VIRGINIA POLYTECHNIC INST AND STATE UNIV BLACKSBURG DEPT OF MECHANICAL ENGINEERING, 2001.

[46] Ikeda, Yuji, Jun Kojima, and Tsuyoshi Nakajima. "Local chemiluminescence measurements of OH*, CH* and C2* at turbulent premixed flame-fronts." *Smart Control of Turbulent Combustion*. Springer, Tokyo, 2001. 12-27.

[47] Kojima, Jun, Yuji Ikeda, and Tsuyoshi Nakajima. "Basic aspects of OH (A), CH (A), and C 2 (d) chemiluminescence in the reaction zone of laminar methane–air premixed flames." *Combustion and Flame* 140.1 (2005): 34-45.

[48] Meier, Wolfgang, Xuru R. Duan, and Peter Weigand. "Reaction zone structures and mixing characteristics of partially premixed swirling CH 4/air flames in a gas turbine model combustor." *Proceedings of the Combustion institute* 30.1 (2005): 835-842.

[49] Oh, Jeongseog, and Dongsoon Noh. "Laminar burning velocity of oxy-methane flames in atmospheric condition." *Energy* 45.1 (2012): 669-675.

[50] Londoño, Luís Fernando, et al. "Determination of laminar flame speed of methane-air flames at subatmospheric conditions using the cone method and ch* emission." *Dyna* 80.180 (2013): 130-135.

[51] Natarajan, J., T. Lieuwen, and J. Seitzman. "Laminar flame speeds of H 2/CO mixtures: effect of CO 2 dilution, preheat temperature, and pressure." *Combustion and flame* 151.1 (2007): 104-119.

[52] Kojima, Jun, Yuji Ikeda, and Tsuyoshi Nakajima. "Spatially resolved measurement of OH*, CH*, and C2* chemiluminescence in the reaction zone of laminar methane/air premixed flames." *Proceedings of the Combustion institute* 28.2 (2000): 1757-1764.

[53] Roby, Richard J., James E. Reaney, and Erik L. Johnsson. *Detection of temperature and equivalence ratio in turbulent premixed flames using chemiluminescence*. Virginia Polytechnic Inst. and State Univ., Blacksburg (US), 1998.

[54] Muruganandam, T. M., et al. "Optical equivalence ratio sensors for gas turbine combustors." *Proceedings of the Combustion Institute* 30.1 (2005): 1601-1609.

[55] Higgins, Bryan, et al. "Systematic measurements of OH chemiluminescence for fuel-lean, high-pressure, premixed, laminar flames." *Fuel* 80.1 (2001): 67-74.

[56] McNaught, Alan D., and Alan D. McNaught. *Compendium of chemical terminology*. Vol. 1669. Oxford: Blackwell Science, 1997.

[57] White, Frank M., and Isla Corfield. *Viscous fluid flow*. Vol. 3. Boston: McGraw-Hill Higher Education, 2006.

[58] Nederlandse Gasunie.*"Physical Properties of natural gases" (1980)*

[59] Anderson Jr, John David. *Fundamentals of aerodynamics*. Tata McGraw-Hill Education, 2010.

[60] Hu, S., et al. "Assessment of uncertainties of laminar flame speed of premixed flames as determined using a Bunsen burner at varying pressures." *Applied Energy* (2017).

[61] Ishida, Hiroki. "Lift-off and blow-off of laminar jet premixed flame of flammable mixture with inert gas." *RESEARCH REPORTS* (2004): 25-28.

[62] Chen, Yung-cheng, et al. "Flame lift-off and stabilization mechanisms of nonpremixed jet flames on a bluff-body burner." *Combustion and flame* 115.1 (1998): 51-65

[63] http://ipl.physics.harvard.edu/wp-uploads/2013/03/PS3_Error_Propagation_sp13.pdf

[64] Brown, James Dean. "Shiken: JALT Testing & Evaluation, SIG Newsletter." (2011): 10-14.

[65] http://fluid.wme.pwr.wroc.pl/~spalanie/dydaktyka/combustion_MiBM/fund/Stoichiometry.pdf retrieved Oct-2017

[66] Souflas, Konstantinos, et al. "Determination of Laminar Flame Speeds Using Axisymmetric Bunsen Flames: Intricacies and Accuracy." *9th Mediterranean Combustion Symposium*. 2015.

[67] Stewart, James. *Single variable calculus: Early transcendentals*. Nelson Education, 2015.

[68] Wu, Yi, et al. "Effects of pressure and preheating temperature on the laminar flame speed of methane/air and acetone/air mixtures." *Fuel* 185 (2016): 577-588.

[69] Kochar, Yash N. *Laminar flame speed and stretch sensitivity of hydrocarbon fuels at high preheat, pressure and vitiation*. Diss. Georgia Institute of Technology, 2014.

[70] He, Yong, et al. "Investigation of laminar flame speeds of typical syngas using laser based Bunsen method and kinetic simulation." *Fuel* 95 (2012): 206-213.

[71] Neter, John, et al. *Applied linear statistical models*. Vol. 4. Chicago: Irwin, 1996.

[72] Guiberti, T. F., Daniel Durox, and Thierry Schuller. "Flame chemiluminescence from CO2-and N2-diluted laminar CH4/air premixed flames." *Combustion and Flame* 181 (2017): 110-122.

[73] Štigler, Jaroslav. "Analytical velocity profile in tube for laminar and turbulent flow." (2012).

[74] Halter, F., et al. "Characterization of the effects of pressure and hydrogen concentration on laminar burning velocities of methane–hydrogen–air mixtures." *Proceedings of the Combustion Institute* 30.1 (2005): 201-208.

[75] Hassan, M. I., K. T. Aung, and G. M. Faeth. "Measured and predicted properties of laminar premixed methane/air flames at various pressures." *Combustion and Flame* 115.4 (1998): 539-550.

[76] Beeckmann, J., L. Cai, and H. Pitsch. "Experimental investigation of the laminar burning velocities of methanol, ethanol, n-propanol, and n-butanol at high pressure." *Fuel* 117 (2014): 340-350.

[77] Varea, Emilien, et al. "Measurement of laminar burning velocity and Markstein length relative to fresh gases using a new postprocessing procedure: Application to laminar spherical flames for methane, ethanol and isooctane/air mixtures." *Combustion and Flame* 159.2 (2012): 577-590.

[78] Strehlow, Roger A. *Combustion fundamentals*. McGraw-Hill College, 1984

[79] Winterbone, Desmond, and Ali Turan. *Advanced thermodynamics for engineers*. Butterworth-Heinemann, 2015.

[80] Flagan, Richard C., and John H. Seinfeld. *Fundamentals of air pollution engineering*. Courier Corporation, 2012.

[81] Wang, Jinhua, et al. "Effects of stretch and preferential diffusion on tip opening of laminar premixed Bunsen flames of syngas/air mixtures." *Fuel* 148 (2015): 1-8.

[82] Vu, Tran Manh, et al. "Tip opening of premixed bunsen flames: Extinction with negative stretch and local Karlovitz number." *Combustion and Flame* 162.4 (2015): 1614-1621.

[83] Kozlovsky, G., and G. I. Sivashinsky. "On open and closed tips of Bunsen burner flames." *Theoretical and Computational Fluid Dynamics* 6.2-3 (1994): 181-192

[84] Chung, S. H., et al. "Local extinction Karlovitz number for premixed flames." *Combustion and flame* 106.4 (1996): 515-520.

[85] Bouvet, N., et al. "Flame speed characteristics of syngas (H2–CO) with straight burners for laminar premixed flames." *Third European Combustion Meeting*. 2007.

[86] http://seitzman.gatech.edu/classes/ae6766/FlameStretchSpeedMeasurements.pdf

[87] S L R Ellison and A Williams (Eds). Eurachem/CITAC guide: Quantifying Uncertainty in Analytical Measurement, Third edition, (2012) ISBN 978-0-948926-30-3. Available from www.eurachem.org.

[88] Birgé, Lucien, and Yves Rozenholc. "How many bins should be put in a regular histogram." *ESAIM: Probability and Statistics* 10 (2006): 24-45.

[89] Scott, David W. "On optimal and data-based histograms." *Biometrika* 66.3 (1979): 605-610.

[90] Terrell, George R. "The maximal smoothing principle in density estimation." *Journal of the American Statistical Association* 85.410 (1990): 470-477.

[91] Terrell, George R., and David W. Scott. "Oversmoothed nonparametric density estimates." *Journal of the American Statistical Association* 80.389 (1985): 209-214.

[92] http://cameron.econ.ucdavis.edu/excel/ex11histogram.html

[93] Freedman, David, and Persi Diaconis. "On the histogram as a density estimator: L 2 theory." *Zeitschrift für Wahrscheinlichkeitstheorie und verwandte Gebiete* 57.4 (1981): 453-476.

[94] Ziemer, Rodger E., William H. Tranter, and D. Ronald Fanin. *Signals and systems: Continuos and discrete*. Macmillan Publishing Company, 1993.